JAKOBSHAVN ISBRÆ: VELOCITY VARIATIONS FROM HOURLY TO DECADAL TIME SCALES AT GREENLAND'S FASTEST TIDEWATER GLACIER.

By

David Bryan Podrasky

RECOMMENDED:

Dr. Edward Bueler

Dr. Regine Hock

Dr. Christopher Larsen

Dr. Roman Mötyka

Dr. Martin Truffer
Advisory Committee Chair

Dr. Paul McCarthy
Chair, Department of Geology and Geophysics

APPROVED:

Dr. Paul Layer
Dean, College of Natural Science and Mathematics

Dr. John Eichelberger
Dean of the Graduate School

17 December 2013
Date

JAKOBSHAVN ISBRÆ: VELOCITY VARIATIONS FROM HOURLY TO DECADAL TIME SCALES AT GREENLAND'S FASTEST TIDEWATER GLACIER.

A

DISSERTATION

Presented to the Faculty

of the University of Alaska Fairbanks

in Partial Fulfillment of the Requirements

for the Degree of

DOCTOR OF PHILOSOPHY

By

David Bryan Podrasky, B.A.

Fairbanks, Alaska

December 2013

Abstract

Outlet glaciers in Greenland, and elsewhere, have recently shown large variations in terminus position and ice flux. One example is the tidewater retreat of Jakobshavn Isbræ, which began in the late 1990s with high thinning rates, acceleration and collapse of the floating glacier tongue. The retreat has continued to the present, with glacier speeds more than doubling in two decades' time.

A campaign of in-situ measurements was initiated in 2006 with the aim of determining the importance of short-term forcing as a control on the continuing evolution of the glacier. Three years of continuous GPS measurements along the centerline of Jakobshavn Isbræ reveal seasonal velocity variations due to seasonally varying terminus position. The relationship between glacier speed and surface melt is complex, with both speed-up and slowdown events in response to variations in the rate of surface melt. During a particularly long and intense melt season in 2007, a series of melt-driven slowdowns effectively reduced the mean ice flow over the whole year. On shorter timescales, the response to surface meltwater input is more predictable with diurnal velocity variations of 1–2 % that closely match changes in meltwater input.

The influence of iceberg calving and tidal forcing is restricted to the lower 10 km of the glacier, imposing an upper limit on longitudinal stress coupling length of a few ice thicknesses. The response to these forcings does not exceed 5 % of mean flow. This is consistent with a glacier operating under high driving stresses.

Ice sheet velocities as far as 120 km inland of the margin have responded to the continuing retreat with increases in speed. The flow has also rotated toward the centerline of the main channel. This speedup and channelization of flow are the result of evolving ice surface gradients as the glacier continues to respond to changes initiated at the periphery. This shows that ocean driven changes have led to increased ice flux far inland on the Greenland Ice Sheet, implying a continuing large-scale evolution of the Jakobshavn Isbræ drainage basin.

Table of Contents

Page

List of Figures

Page

List of Tables

Page

List of Appendices

Page

Acknowledgements

It is -30°F in Fairbanks as I sit and think of all the people who have helped me during my years in Alaska. While I certainly won't miss the bitter cold, I will miss the camaraderie and warm friendship I found at the Geophysical Institute and UAF in general. The GI truly is a unique collection of some of the world's best high-latitude minds. Coming from Montana, I found the culturally diverse community at the GI a mind opening experience. Disregarding the cold and the bugs, I am thankful for the opportunity to live in a part of the world that many only dream of visiting.

Alaska turned out to be a terribly distracting location to work on a graduate degree. There were many new things to do and try: burbot fishing, nordic skiing and dip-netting to name a few. And, northern summers are always too short to fit in all of the fun along with field work, data crunching and writing. In the end, old habits die hard and I will most fondly remember the many canoeing and fishing trips over the years. UAF offers a good education, but Alaska's Arctic Grayling are some of the best teachers around!

I consider myself lucky to have been a part of the glaciers group at the GI, which is a genuine community of excellent cryospheric scientists. When I contacted Martin Truffer about the possibility of a graduate assistantship he informed me that he would be out of the country on sabbatical the following year. He took me on as a student anyway, with the condition that I pursue a doctoral degree instead of the master's degree I had originally intended. This seemed fine to me and I was given a teaching assistantship in the physics department during the year he was away. As I got to know Martin better after his return to Alaska I learned to appreciate his effectiveness as an advisor. For one, he always managed to secure funding for students, no small feat while he had as many as four doctoral students to support! Martin also always made time for students, meeting to discuss ideas or promptly reading even the roughest of manuscripts. He gave me the freedom necessary to fully explore research possibilities and decide for myself which were worth pursuing.

The other members of my thesis committee worked in concert to keep me on track toward completion. Chris Larsen always had thoughtful questions that often redirected my thinking about ideas I presented to the committee. Ed Bueler frequently had excellent questions too, unfortunately they were often over my head. But, he also helped me learn to present equations and mathematical arguments in the clearest manner possible. Roman Motyka tried his best to help me meet deadlines and always provided the most thorough edits of manuscripts. Regine Hock was always on the lookout for trivial or mundane

writing in my manuscripts which helped me pare a bit of the excessively boring text from my writing. She is also a good friend, but a lousy canoe partner!

Mark Fahnestock was not on my committee, but he may as well have been for all of the useful advice and input he offered. He has a great sense of humor and I thoroughly enjoyed working with him in the field. Mark is absolutely full of great glaciological ideas, I just wish I was clever enough to wrap my head around one of his ideas before he moved on to the next.

Jason Amundson was a senior doctoral student when I arrived in Fairbanks and he was a great resource both during and after Martin's sabbatical. Jason taught me a great deal about processing GPS data, the linux operating system and survival in the far north. Regrettably, his politeness never did rub off on me. I enjoyed conversations with Valentina Radić and Laura LeBlanc who also helped me settle into the group. In addition to the excellent faculty, the glaciers group is lucky to have an active group of emeritus professors and I was fortunate to benefit from discussions with Carl Benson, Keith Echelmeyer, Will Harrison and Craig Lingle.

A year into my studies Martin took on two new doctoral students, Marijke Habermann and Barbara Trüssel. The three of us worked on very different projects, but I found their input and encouragement over the past five years most helpful. It was great to commiserate with Barbara and Marijke when the stresses of being a graduate student would pile up. I had a great time getting to know all of the other, many, glaciers graduate students in the group: Tim Bartholomous, Cody Beedlow, Christina Carr, Jenny Davis, Jason Geck, Austin Johnson, Joe Kennedy, Cristian Kienholz, Bob McNabb, Lee Peterson, and Joanna Young. Ronni Grapenthin wasn't a glaciers graduate student, but I know he always wanted to be! Thanks also to Sam Herreid, who isn't a graduate student, but works harder than one. I'm grateful to Andy Aschwanden who provided coffee, friendship and hours of free advice.

I made a great number of friends during my time in Alaska, many of whom are noted above. I would also like to acknowledge the amity of those who first befriended me in Fairbanks. Thanks to Carl, Vanessa and Daisy for all of the good times together. I certainly couldn't have completed my studies without the unwavering support of my family members who were so tolerant of the long distance and infrequent visits home. Finally, I wish to thank the two best girls in my life. Lu, who provided just the motivation I needed to finish my degree, even though she never slept long enough for me to get any work done at home. And, my wife, Agatha. Agatha let me drag her away from her home on an un-

known academic adventure in Alaska, and tolerated it for six long winters. She supported me all through my studies helping me to remember what is really important in life. I will never forget the memories we've made together.

"Writing is like the life of a glacier;
one eternal grind."

—John Muir

Chapter 1
Introduction

The application of satellite remote sensing methods for monitoring the cryosphere has revealed widespread retreat, thinning and acceleration of tidewater outlet glaciers draining the polar ice sheets in Antarctica and Greenland [Joughin and others, 2010; Pritchard and others, 2010]. Warmer air [Box and others, 2009] and warmer ocean water temperatures [Holland and others, 2008] are driving measurable contribution to sea level rise from the Greenland Ice Sheet directly, through increasingly negative surface mass balance [Hall and others, 2008], and indirectly, with increasing calving flux initiated by tidewater glacier retreat. Contribution to sea level rise from the Greenland Ice Sheet at a rate of 0.39 $\mathrm{mm\,a^{-1}}$ [Shepherd and others, 2012] is believed to be equally divided between surface mass balance and frontal ablation [van den Broeke and others, 2009].

Future change in surface mass balance of the polar ice sheets can be estimated using climate projection scenarios [Mernild and others, 2010], but rates of ice discharge from individual tidewater outlet glaciers are more difficult to predict. Large changes in ice flow of tidewater outlets can be initiated by sudden changes in glacier geometry. For example, the disintegration of the Larsen B ice shelf was followed by thinning and acceleration of the glaciers flowing into the embayment [Scambos, 2004]. The velocity response to large-scale ice-shelf retreat is very short, as little as one year for glaciers on the Antarctic Peninsula [Glasser and others, 2011]. Other examples of outlet glaciers quickly responding to forcing [Truffer and Fahnestock, 2007] call for a reassessment of traditional concepts of ice sheet response timescales [Nye, 1960].

The difficulty of predicting outlet glacier behavior arises from various nonlinear interactions (e.g. sliding and iceberg calving) occurring as part of the tidewater glacier cycle [Meier and Post, 1987]. While the retreat of a tidewater glacier can be initiated by climate, the evolution of the retreat phase is controlled primarily by the topography of the glacier channel [Vieli and others, 2001]. Results from regional models of four Greenland outlet glaciers, together draining 22 % of the ice sheet, affirm basal topography as the primary control on outlet glacier retreat under a range of climate projections [Nick and others, 2013]. While these regional modeling results indicate mass losses far below reasonable upper limits[Pfeffer and others, 2008], the future of ice-sheet wide contribution to sea level rise remains uncertain.

1.1 Jakobshavn Isbræ

Located on the west coast of Greenland, Jakobshavn Isbræ is one of the largest tidewater glaciers draining the Greenland Ice Sheet. The area of the drainage basin is nearly 10 000 km^2 and encompasses 6 % of the total ice sheet area [Rignot and Kanagaratnam, 2006]. North and south glacier tributaries terminate at the head of the 60 km long, 800 m deep Kangia Icefjord [Echelmeyer and others, 1991]. A shallow morainal shoal, the remnant of a maximum glacier extent from around 8 k a [Weidick and others, 1990], located at the mouth of Kangia Icefjord restricts the passage of large icebergs into Disko Bugt.

1.1.1 Historical observations

The first scientific observations of Jakobshavn Isbræ were made by H. J. Rink in 1851. Rink's estimate of terminus position indicates a calving front 40 km west of the present-day terminus [Rink, 1857]. Later measurements by R. R. J. Hammer point to a seasonally varying front position, specifically a winter advance of 1 km and summer retreat of 2 km in 1880 [Hammer, 1883]. Subsequent investigations by many others revealed a steady retreat from the 1851 terminus position, totaling 20 km over a century [Weidick and Bennike, 2007]. By the 1950s, a wealth of aerial photographs followed by satellite imagery documented terminus positions varying $\sim$2.5 km about a stable mean position until the end of the 1990s [Sohn and others, 1998].

The first attempts at measuring the rate of ice motion were made by K. J. V. Steenstrup from 1879 to 1880 [Steenstrup, 1883]. Much later, photogrammetric measurements of surface speeds were made in 1957 and 1964, which also revealed the large volume of calve ice entering Kangia Icefjord [Carbonell and Bauer, 1968]. Despite seasonal variations in surface meltwater production and terminus position, there was little evidence for seasonal variations in ice flow up until the late 1990s [Hammer, 1883; Echelmeyer and Harrison, 1990]. The importance of Jakobshavn Isbræ as one of Greenland's most important outlet glaciers was cemented with seismic measurements of the surprisingly deep, 1500 m below sea level, U-shaped fjord extending 70 km inland [Clarke and Echelmeyer, 1996].

Large ice thickness and steep surface slopes along the deep channel result in large driving stresses on the southern tributary of Jakobshavn Isbræ [Echelmeyer and others, 1991]. Measurements of englacial temperatures indicate the presence of a temperate layer at the base of the glacier margins [Iken and others, 1993]. Additionally, borehole conductivity measurements show a layer sourced from glacier ice deposited during the Wisconsin age

[Lüthi and others, 2002], and tilt sensor measurements showed that this layer deforms more readily under simple shear than stiffer Holocene ice. The effect of a converging bedrock channel vertically stretches these two layers of easily deformable ice as ice flows in from the surrounding ice sheet [Funk and others, 1994]. The result is a thick layer of soft ice at the bottom of the glacier which allows for large rates of vertical shear, concentrated near the bed. Over much of the southern tributary of Jakobshavn Isbræ the large driving stresses can be accommodated by internal deformation and basal motion in approximately equal proportion [Truffer and Echelmeyer, 2003].

1.1.2 21st century scientific investigations of Jakobshavn Isbræ

By 1995 the mean terminus position of Jakobshavn Isbræ was still stable, but synthetic aperture radar (SAR) measurements showed seasonal velocity variations amounting to 12 % of background flow [Luckman and Murray, 2005]. Two years later, airborne topographic measurements showed glacier thinning [Thomas and others, 2003], while yearly-mean speed increased by 5 $\mathrm{km\,a^{-1}}$ to 20 $\mathrm{km\,a^{-1}}$ [Luckman and Murray, 2005]. Thinning of the glacier continued, commensurate with thinning of the glacier tongue primarily due to increased rates of sub-shelf melting [Motyka and others, 2011], driven by warm ocean water from Disko Bugt passing over the marine shoal at the mouth of Kangia Icefjord [Holland and others, 2008]. Thinning of the floating ice culminated in the catastrophic collapse of the tongue and a retreat of 12 km in under three years' time [Podlech and Weidick, 2004].

Following the breakup of the floating tongue by 2003, both terminus position and surface velocities varied seasonally. Large seasonal fluctuations of 5 km in terminus position [Cassotto, 2011] after the early 2000s have been attributed to seasonal calving behavior. During this time, the glacier calved large, full-thickness icebergs in summer, whereas in winter calving was limited [Amundson and others, 2010]. Seasonal variations in terminus position have been identified as the primary mechanism driving seasonal velocity variations upstream of the grounding line [Joughin and others, 2008].

Continued monitoring of surface speeds on Jakobshavn Isbræ has revealed a nearly constant speedup of 5 % $\mathrm{a^{-1}}$, resulting in doubling of speeds along the lower 20 km of the southern tributary. Efforts to model ice flow, constrained by the SAR velocities show that the interannual acceleration observed along the length of the southern tributary can be attributed to a progressive steepening of glacier ice as thinning and retreat continue [Joughin and others, 2012]. Basal stress, infered from SAR velocities, has decreased along

the lower reach of the glacier due to lower effective pressure, a result of the thinning that began in the late 1990s [Habermann and others, 2013].

1.2 Time variation of ice flow of Greenland outlet glaciers

On timescales shorter than years and decades, measurements of glacier motion at Helheim Glacier, another of Greenland's tidewater outlet glaciers, suggest that sensitivities to ocean tidal forcing [De Juan and others, 2010] and iceberg calving [Nettles and others, 2008] are limited to a few ice thicknesses in distance from glacier termini. Prior measurements of near-terminus ice flow during calving events at Jakobshavn Isbræ show a step-change in velocity in response to calving [Amundson and others, 2008] followed by a transient deceleration reaching pre-calving speeds within a few days [Rosenau and others, 2013]. However, these previous studies do not provide an indication of the length of glacier influenced by calving or tides.

Other forcing on the same timescale as ocean tides and calving includes surface meltwater forcing and surpraglacial lake drainage. Global positioning system (GPS) measurements at Swiss camp sites [Steffen and Box, 2001], north of the Jakobshavn Isbræ drainage, indicate a short-term increase in ice sheet flow speed in response to surface meltwater input [Zwally and others, 2002]. The episodic drainage of supraglacial lakes also temporarily increases speeds on the ice sheet, but the response is localized [Hoffman and others, 2011]. On seasonal timescales the relation between surface melt and ice-sheet flow is not as simple, with evidence for slower than average speeds near the end of the melt season [Sundal and others, 2011]. On interannual timescales there seems to be little evidence to support the hypothesis that increased surface melting leads to faster ice-sheet flow, in fact data from sites along the K-transect, south of Jakobshavn Isbræ, show a trend of slower flow over almost two decades during which rates of surface melt increased [van de Wal and others, 2008].

Greenland's outlet glaciers also respond to surface meltwater forcing on seasonal and diurnal timescales, but the faster surface speeds tend to obscure the relatively small diurnal variations. GPS measurements from Helheim Glacier indicate diurnal velocity variations $\sim 5\,\%$ of background with delays between surface meltwater forcing and velocity response of 12–36 hrs [Andersen and others, 2010], much longer than at ice sheet locations.

1.3 Thesis objectives

It is clear that the fast flow speeds and large discharge of Jakobshavn Isbræ are due to the large ice thickness and relatively steep surface slopes resulting in high driving stresses along the southern tributary [Echelmeyer and others, 1991]. This thesis studies the relative importance of various modes of forcing in affecting variations in ice flow away from mean values. The largest and most far reaching of these deviations has come in response to the catastrophic breakup and retreat of the floating tongue in the early 2000s. To better understand the important mechanisms controlling the continuing retreat, a multi-year campaign of in-situ measurements was initiated in 2006. The main glacier and surrounding adjacent ice was monitored with GPS, optical theodolite surveys, passive seismometers and time-lapse photography as well as satellite remote sensing data sets.

In chapter 2 of the thesis, analysis of three years of GPS position data reveals details about velocity variations over a wide range of timescales. The rate of interannual acceleration is discussed along with seasonal velocity variations, both of which are closely related to terminus position and geometry. On shorter timescales, the response to surface meltwater forcing and supraglacial lake drainage are examined with results indicating a complex relationship between glacier speed and meltwater input. As lead author of this paper I processed and analyzed GPS data, interpreted the results and drafted the manuscript. I worked closely with M. Truffer to develop the conceptual model for glacier response to seasonal calving behavior. R. Cassotto generated the terminus position data set and J. Amundson provided the catalog of calving events. I. Joughin supplied synthetic aperuture radar velocity fields. J. Brown, M. Fahnestock, M. Lüthi and R. Motyka helped with data collection and logistics and contributed helpful discussions.

Variability over much shorter timescales is investigated in chapter 3 with an emphasis on the response to forcing applied at the glacier terminus. Two-week long time series of near-terminus glacier speeds are decomposed with a suite of models in order to quantify the response to large calving events and ocean tidal forcing. I was lead author on this paper, working with M. Truffer and M. Fahnestock to design and implement the observational campaign, and collected and processed GPS data. Theodolite data collection and processing was performed by M. Lüthi, who also contributed to the interpretation of results. I was responsible for drafting and submitting the manuscript for publication.

Chapter 4 presents results from a basin-wide examination of the decadal-scale evolution of surface velocities at Jakobshavn Isbræ. Since the mid 1980s not only have surface

speeds increased, but the direction of surface velocities have consistently rotated toward the fast-flowing southern tributary. These changes in surface velocity are documented as far as 120 km inland of the ice-sheet margin indicating an inland response to changes initiated at the periphery of the ice sheet within two decades. Combined with an examination of changes in ice thickness from 1985 to 2008 the evolution of surface velocities are explained primarily by changes in the ice surface gradient. M. Fahnestock, R. Motyka and M. Truffer helped me develop the concept for this chapter. R. Motyka provided the DEM data sets and I. Joughin provided sythetic aperture radar velocity data sets. R. Cassotto, D. Dellagiustina, M. Fahnestock and M. Truffer helped collect GPS data. I worked with M. Fahnestock to generate the 1985 velocity data set. I synthesized the various data sets and performed the analysis, working with M. Truffer to interpret the results. I wrote the manuscript and M. Truffer provided helpful discussions and editorial comments.

A summary of the findings presented in the main chapters of the thesis are provided in chapter 5.

References

Amundson, J. M., M. Truffer, M. P. Lüthi, M. A. Fahnestock, M. West and R. J. Motyka, 2008. Glacier, fjord, and seismic response to recent large calving events, Jakobshavn Isbræ, Greenland, *Geophys. Res. Lett.*, **35**(22), L22501.

Amundson, J., M. Fahnestock, M. Truffer, J. Brown, R. Motyka and M. Lüthi, 2010. Ice mélange dynamics and implications for terminus stability, Jakobshavn Isbræ, Greenland. *J. Geophys. Res.*, **115**(F1), F01005 (doi: 10.1029/2009JF001405).

Andersen, M. L., T. B. Larsen, M. Nettles, P. Elosegui, D. van As, G. S. Hamilton, L. A. Stearns, J. L. Davis, A. P. Ahlstrøm, J. de Juan, G.Ekström, L. Stenseng, S. A. Khan, R. Forsberg and D. Dahl-Jensen, 2010. Spatial and temporal melt variability at Helheim Glacier, East Greenland, and its effect on ice dynamics, *J. Geophys. Res.*, **115**(F4), 1–18.

Box, J. E., L. Yang, D. H. Bromwich and L. S. Bai, 2009. Greenland Ice Sheet Surface Air Temperature Variability:1840–2007, *J. Clim.*, **22**(14), 4029–4049.

van den Broeke, M., J. L. Bamber, J. Ettema, E. Rignot, E. Schrama, W. J. van de Berg, E. van Meijgaard, I. Velicogna and B. Wouters, 2009. Partitioning recent Greenland mass loss., *Science*, **326**(5955), 984–6.

Cassotto, R. K., 2011. Implications of chang in winter fjord ice mélanges for Greenland outlet glacier dynamics, (M.S. thesis, University of New Hampshire).

Carbonell, M. and Bauer, A., 1968. Exploitation des couvertures photographiques aériennes répétées du front des galciers vélant dans Disko Bugt et Umanak Fjord, juin-juillet 1964, *Meddelelser om Grønland*, **173**(5), 1–78.

Clarke, T. S. and K. A. Echelmeyer, 1996. Seismic-reflection evidence for a deep subglacial trough beneath Jakobshavns Isbrae West Greenland, *J. Glaciol.*, **42**(141), 219–232.

De Juan, J., P. Elósegui, M. Nettles, T. B. Larsen, J. L. Davis, G. S. Hamilton, L. A. Stearns, M. L. Andersen, G. Ekström, A. P. Ahlstrøm, L. Stenseng, S. A. Khan and R. Forsberg, 2010. Sudden increase in tidal response linked to calving and acceleration at a large Greenland outlet glacier, *Geophys. Res. Lett.*, **37**(12), 1–5.

Echelmeyer, K. A., T. S. Clarke and W. D. Harrison, 1991. Surficial glaciology of Jakobshavns Isbræ, West Greenland: Part 1. Surface morphology, *J. Glaciol.*, **37**(127), 368–382.

Echelmeyer, K. A. and W. D. Harrison, 1990. Jakobshavn Isbræ, West Greenland: Seasonal varitations in velocity—or lack thereof, *J. Glaciol.*, **36**(122), 82–88.

Funk, M., K. A. Echelmeyer and A. Iken, 1994. Mechanisms of fast flow in Jakobshavns Isbræ, West Greenland: Part II. Modeling of englacial temperatures, *J. Glaciol.*, **40**(136), 569–585.

Glasser, N. F., T. A. Scambos, J. Bohlander, M. Truffer, E. Pettit and B. J. Davies, 2011. From ice-shelf tributary to tidewater glacier: continued rapid recession, acceleration and thinning of Röhss Glacier following the 1995 collapse of the Prince Gustav Ice Shelf, Antarctic Peninsula, **57**(203), 397–406.

Habermann, M., M. Truffer and D. Maxwell, 2013. Changing basal conditions during the speed-up of Jakobshavn Isbræ, Greenland, *Cryosphere Disc.*, **7**, 1–38.

Hall, D. K., R. S. Williams, S. B. Luthcke and N. E. Digirolamo, 2008. Greenland ice sheet surface temperature, melt and mass loss: 2000–06, *J. Glaciol.*, **54**(184), 81–93.

Hammer, R. R. J., 1883. Undersøgelser ved Jakobshavns Isfjord of nærmeste Omegn i Vinteren 1879–1880, *Meddelelser om Grønland*, **4**, 1–68.

Hoffman, M. J., G. A. Catania, T. A. Neumann, L. C. Andrews and J. A. Rumrill, 2011. Links between acceleration, melting, and supraglacial lake drainage of the western Greenland Ice Sheet, *J. Geophys. Res.*, **116**(F4), 1–16.

Holland, D. M., R. H. Thomas, B. de Young, M. H. Ribergaard and B. Lyberth, 2008. Acceleration of Jakobshavn Isbræ triggered by warm subsurface ocean waters, *Nature Geosci.*, **1**(10), 659–664.

Iken, A., K. A. Echelmeyer, W. D. Harrison and M. Funk, 1993. Mechanisms of fast flow in Jakobshavns Isbræ, West Greenland: Part I. Measurements of temperature and water level in deep boreholes, *J. Glaciol.*, **39**(131), 15–25.

Joughin, I., B. E. Smith and W. Abdalati, 2010. Glaciological advances made with interferometric synthetic aperture radar, *J. Glaciol.*, **56**(200), 1026–1042.

Joughin, I., B. E. Smith, I. M. Howat, D. Floricioiu, R. B. Alley, M. Truffer and M. A. Fahnestock, 2012. Seasonal to decadal scale variations in the surface velocity of Jakobshavn Isbræ, Greenland: Observation and model-based analysis, *J. Geophys. Res.*, **117**(F2), 1–20.

Joughin, I., I. M. Howat, M. A. Fahnestock, B. E. Smith, W. Krabill, R. B. Alley, H. Stern and M. Truffer, 2008. Continued evolution of Jakobshavn Isbræ following its rapid speedup, *J. Geophys. Res.*, **113**(F4).

Lüthi, M. P., M. Funk and A. Iken, 2002. Mechanisms of fast flow in Jakobshavn Isbræ, West Greenland: Part III. Measurements of ice deformation, temperature and cross-borehole conductivity in boreholes to the bedrock, *J. Glaciol.*, **48**(162), 369–385.

Luckman, A. and T. Murray, 2005. Seasonal variation in velocity before retreat of Jakobshavn Isbræ, Greenland, *Geophys. Res. Lett.*, **32**(8), 1–4.

Meier, M. F. and A. Post, 1987. Fast Tidewater Glaciers, *J. Geophys. Res.*, **92**(B9), 9051–9058.

Mernild, S. H., G. E. Liston, C. A. Hiemstra and J. H. Christensen, 2010. Greenland Ice Sheet surface mass-balance modeling in a 131-yr perspective, 1950–2080, *J. Hydromet.*, **11**(1), 3–25.

Motyka, R. J., M. Truffer, M. A. Fahnestock, J. Mortensen, S. Rysgaard and I. Howat, 2011. Submarine melting of the 1985 Jakobshavn Isbræ floating tongue and the triggering of the current retreat, *J. Geophys. Res.*, **116**(F1), 1–17.

Nettles, M., T. B. Larsen, P. Elósegui, G. S. Hamilton, L. A. Stearns, A. P. Ahlstrøm, J. L. Davis, M. L. Andersen, J. de Juan, S. A. Khan, L. Stenseng, G. Ekström and R. Forsberg, 2008. Step-wise changes in glacier flow speed coincide with calving and glacial earthquakes at Helheim Glacier, Greenland, *Geophys. Res. Lett.*, **35**(24), 1–5.

Nick, F. M., A. Vieli, M. L. Andersen, I. Joughin, A. Payne, T. L. Edwards, F. Pattyn and R. S. W. van de Wal, 2013. Future sea-level rise from Greenland's main outlet glaciers in a warming climate, *Nature*, **497**(7448), 235–238.

Nye, J. F., 1960. The response of glaciers and ice-sheets to seasonal and climatic changes, *Proc. R. Soc. London, Ser. A*, **256**(1287), 559–584.

Pfeffer, W. T., J. T. Harper and S. O'Neel, 2008. Kinematic constraints on glacier contributions to 21st-century sea-level rise., *Science*, **321**(5894), 1340–3.

Podlech, S. and A. Weidick, 2004. A catastrophic break-up of the front of Jakobshavn Isbræ, West Greenland, 2002/03, *J. Glaciol.*, **50**(168), 153–154.

Pritchard, H. D., S. B. Luthcke and A. H. Fleming, 2010. Understanding ice-sheet mass balance: progress in satellite altimetry and gravimetry, *J. Glaciol.*, **56**(200), 1151–1161.

Rink, H. J. 1857. Grønland, geografisk of satistisk beskrevet, **1**: *Det nordre Inspectorat*, 420 pp., København: Andreas Frederik Høst.

Rignot, E. and P. Kanagaratnam, 2006. Changes in the velocity structure of the Greenland Ice Sheet., *Science*, **311**(5763), 986–90.

Rosenau, R., E. Schwalbe, H. G. Maas, M. Baessler and R. Dietrich, 2013. Grounding line migration and high-resolution calving dynamics of Jakobshavn Isbræ, West Greenland, *J. Geophys. Res.*, **118**, 1–14.

Scambos, T. A., 2004. Glacier acceleration and thinning after ice shelf collapse in the Larsen B embayment, Antarctica, *Geophys. Res. Lett.*, **31**(18), L18402.

Shepherd, A., and 46 others, 2012. A reconciled estimate of ice-sheet mass balance., *Science*, **338**(6111), 1183–9.

Sohn, H. G., K. C. Jezek and C. J. van der Veen, 1998. Jakobshavn Glacier, west Greenland: 30 years of spaceborne observations, *Geophys. Res. Lett.*, **25**(14), 2699.

Steenstrup, K. J. V., 1883. Bidrag til Kjendskab til Bræerne of Bræ-Isen i Nordgrønland, *Meddelelser om Grønland*, **4**, 69–112.

Steffen, K. and J. Box, 2001. Surface climatology of the Greenland ice sheet: Greenland Climate Network 1995Ð1999, *J. Geophys. Res.*, **106**(D24), 33951–33964.

Sundal, A. V., A. Shepherd, P. Nienow, E. Hanna, S. Palmer and P. Huybrechts, 2011. Melt-induced speed-up of Greenland ice sheet offset by efficient subglacial drainage, *Nature*, **469**(7331), 521–524.

Thomas, R. H., W. Abdalati, E. Frederick, W. B. Krabill, S. Manizade, K. Steffen, 2003. Investigation of surface melting and dynamic thinning on Jakobshavn Isbræ, Greenland, *J. Glaciol.*, **49**(165), 231–239.

Truffer, M. and K. A. Echelmeyer, 2003. Of isbræ and ice streams, *Ann. Glaciol.*, **36**(1), 66–72.

Truffer, M. and M. A. Fahnestock, 2007. Climate change. Rethinking ice sheet time scales., *Science*, **315**(5818), 1508–10.

Vieli, A., M. Funk and H. Blatter, 2001. Flow dynamics of tidewater glaciers: a numerical modelling approach, *J. Glaciol.*, **47**(159), 595–606.

van de Wal, R. S. W., W. Boot, M. R. van den Broeke, C. J. P. P. Smeets, C. H. Reijmer, J. J. A. Donker and J. Oerlemans, 2008. Large and rapid melt-induced velocity changes in the ablation zone of the Greenland Ice Sheet., *Science*, **321**(5885), 111–3.

Weidick, A. and O. Bennike, 2007. Quaternary glaciation history and glaciology of Jakobshavn Isbræ and the Disko Bugt region, West Greenland: a review, *Geol. Surv. Den. Green. Bull.*, (14).

Weidick, A., H. Oerter, N. Reeh, H. H. Thomson and L. Thorning, 1990. The recession of the Inland Ice margin during the Holocene climatic optimum in the Jakobshavn Isfjord area of West Greenland, *Palaeogeogr. Palaeocl.*, **82**, 389–399.

Zwally, H. J., W. Abdalati, T. Herring, K. Larson, J. Saba and K. Steffen, 2002. Surface melt-induced acceleration of Greenland ice-sheet flow., *Science*, **297**(5579), 218–22.

Chapter 2
Outlet glacier response to forcing over hourly to inter-annual time scales, Jakobshavn Isbræ, Greenland [1]

Abstract

The loss of the floating ice tongue on Jakobshavn Isbræ in the early 2000s has been concurrent with a pattern of thinning, retreat and acceleration leading to enhanced contribution to global sea level. These changes on decadal time scales have been well documented. Here we identify how the glacier responds to forcings on shorter time scales—such as from variations in surface melt, the drainage of supraglacial lakes and seasonal fluctuations in terminus position. Ice motion and surface melt were monitored intermittently from 2006 to 2008. Dual frequency GPS were deployed 20–50 km upstream of the terminus along the glacier centerline. Gaps in surface melt measurements were filled using a temperature index model of ablation driven by surface air temperatures recorded during the same time period. Our results corroborate the premise that the primary factors controlling speeds on Jakobshavn Isbræ are terminus position and geometry. We also observe that surface speeds demonstrate a complex relationship with meltwater input: On diurnal time scales, velocities closely match changes in water input; however, on seasonal time scales a longer, more intense melt season was observed to effectively reduce the overall ice flow of the glacier for the whole year.

2.1 Introduction

During the last decade many Greenland outlet glaciers have exhibited dramatic calving retreats coincident with increasing flow speed and rates of thinning not explained by surface melt alone [Rignot and Kanagaratnam, 2006; Moon and Joughin, 2008; Thomas and others, 2009]. Ice discharge into the ocean from Greenland outlet glaciers constitutes a large fraction of mass wastage for the ice sheet [Rignot and Kanagaratnam, 2006; van den Broeke and others, 2009]. Therefore, an understanding of processes controlling outlet glacier dynamics is essential for estimating future contributions to sea level rise from the Greenland

[1] Published as Podrasky, D., M. Truffer, M. Fahnestock, J. Amundson, R. Cassotto, and I. Joughin, 2012. Outlet glacier response to forcing over hourly to inter-annual time scales, Jakobshavn Isbræ, Greenland. *J. Glaciol.*, *58*(212), doi:10.3189/2012JoG12J065.

Ice Sheet. While the triggering of recent changes in Greenland is most likely attributable to climate change, the relative importance of various components (atmospheric and oceanographic changes) of climate forcing remains unclear. Greater surface melt due to higher air temperatures is resulting in increasing contributions to sea level rise [Box, 2005; Hanna and others, 2008]. Recent studies and oceanographic data suggest that warming oceans are also having an impact on eustatic sea level rise contributions through increased calving and thinning of Greenland outlet glaciers [Holland and others, 2008; Motyka and others, 2011]. Interactions between warm ocean water and marine terminating outlet glaciers and the effects of glacier dynamics have the potential to dominate contributions to sea level rise from the ice sheet.

During the late 20th century the terminus position of Jakobshavn Isbræ—on the west coast of Greenland—was stable, relative to current behavior, with a seasonal fluctuation in terminus position of about 2.5 km and a persistent floating tongue [Sohn and others, 1998]. Surface speeds, measured by Echelmeyer and Harrison [1990] in the mid 1980s, indicated almost no seasonal variation in flow. In the early 2000s the floating ice tongue began a pattern of break-up and the glacier retreated by more than 12 km from a fairly stable position [Podlech and Weidick, 2004]. Concurrent with the retreat, measurements of ice motion began to show seasonal velocity variations [Luckman and Murray, 2005] and flow speeds doubled [Joughin and others, 2004]. This resulted in a draw-down of upstream ice and thinning of the glacier by tens of meters per year [Krabill and others, 2004]. During the retreat the year-round floating tongue disintegrated and only re-formed each winter upon the cessation of calving [Joughin and others, 2008a; Amundson and others, 2010]. The seasonal floating tongue has played an important role in reducing flow during the winter and slowing the rate of retreat [Joughin and others, 2008a]. As the retreat progresses, surface speeds continue to increase and the terminus is moving into a much deeper part of the fjord with a reverse bed slope [Plummer and others, 2008]. This configuration causes an unstable front position [Vieli and others, 2001; Schoof, 2007] and has been observed to result in dramatic retreat rates in other glacier systems [Meier and Post, 1987]. The drainage basin of Jakobshavn Isbræ encompasses approximately 5%, or 9.2×10^4 km^2, of the areal extent of the Greenland Ice Sheet [Rignot and Kanagaratnam, 2006] and continued retreat and thinning have the potential to affect the discharge of a large portion of the ice sheet.

During its retreat, surface speeds on Jakobshavn Isbræ have been documented with remote sensing techniques [Joughin and others, 2004; Luckman and Murray, 2005; Joughin

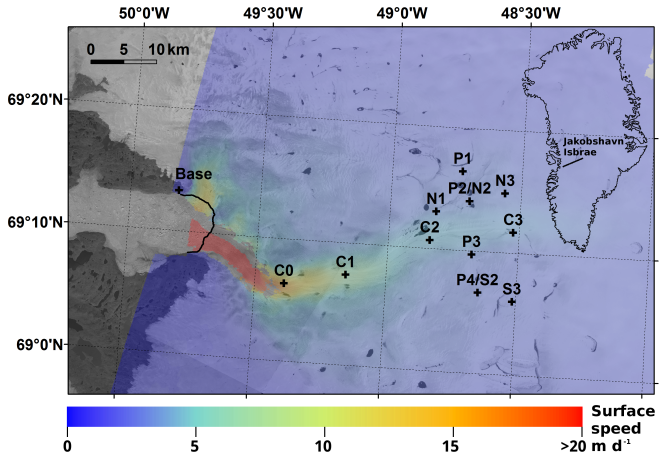

Figure 2.1: Map of Jakobshavn Isbræ study area with glacier sites C0, C1, C2, C3; ice sheet sites N1, N2, N3, S2, S3, P1, P2, P3, P4; and GPS base station. Color coded surface speeds derived from SAR (Radarsat) in 2006 are overlaid on a 2004 ASTER scene. Solid black curve indicates 2004 terminus position.

and others, 2008a]. While these techniques are able to map seasonal and inter-annual changes in velocity, the timing and rates of these variations are obscured by low temporal resolution. Our study complements the remote sensing record with measurements from Global Positioning System (GPS) receivers, allowing resolution of ice motion on sub-diurnal time scales.

By observing ice motion on short time scales we can better constrain the nature and timing of the reaction of Greenland's outlet glaciers to surface meltwater input. Variability of surface melt supply has been suggested as one mechanism for forcing ice sheet acceleration [Zwally and others, 2002; Parizek and Alley, 2004]. On the other hand, sufficiently large melt rates can lead to more efficient drainage of basal water [Schoof, 2010]. In this case, the impact of increased melt can have the opposite effect and ice motion can experience deceleration. This paper focuses on the details of velocity variations on short time scales on Jakobshavn Isbræ at locations along a center line approximately 20–50 km from the terminus. Combined with estimates of surface melt and timing of supraglacial lake drainages, we present results demonstrating the complex response of ice motion to meltwater input as well as the seasonal and inter-annual response of flow to changes in glacier geometry.

2.2 Methods

2.2.1 Ice motion

GPS observations were conducted on Jakobshavn Isbræ at three continuously occupied sites and one temporary site, along an approximate glacier center line (Fig. 2.1). Measurements were taken from May 2006 to September 2008 at the three continuously occupied sites: C1, C2 and C3. The lower-most site, C1, was placed approximately 20 km upstream of the 2006 terminus followed by sites C2 at 30 km and C3 at 40 km. During summer of 2007, an additional GPS site, C0, was temporarily occupied approximately 4 km downstream from C1. GPS measurements were also recorded from June to August 2007 at four sites along a transect perpendicular to the direction of glacier flow, situated between sites C2 and C3. Sites P1 and P2 were located to the north of the glacier, P3 and P4 to the south. Additional data were recorded May to August 2008 at five sites situated along flow lines north and south of the glacier (Fig. 2.1 and Table 2.1). Sites N1, N2 and N3 were located along the north margin with sites S2 and S3 along the southern margin. We used dual frequency GPS receivers (either Trimble 5700, Trimble NetRS or Topcon GB-1000) at all sites. GPS antennas were mounted atop a triangular arrangement of one-inch steel poles drilled vertically into the ice. On-ice GPS data were processed against a base station located on bedrock with baseline distances of 20–40 km. We determined the coordinates of the base station using the Auto-GIPSY static GPS processing service (now APPS `http://apps.gdgps.net`). Position solutions for the on-ice sites were produced every 15 seconds using the differential kinematic processing tool *Track* (version 1.22), a component of the Massachusetts Institute of Technology GAMIT/GLOBK GPS processing software suite (`http://www-gpsg.mit.edu/simon/gtgk/index.htm`).

Position time series data were manually inspected to identify obvious processing errors. These errors were most commonly a step-wise change in position followed by a step-wise return lasting a few hundred to thousand epochs (one epoch is 15 seconds). Such errors appear as very rapid accelerations immediately followed by deceleration in velocity time series. Once identified, the erroneous data segments were removed before further processing. There were also periods of missing data due to insufficient power for the GPS receivers.

GPS position time series for all sites were smoothed using a smoothing spline interpolation method implemented in the Matlab (version 7.7) software package. This method

Table 2.1: Data coverage for glacier sites (C1–3 and C0) and ice sheet sites (P1–4, N1–3 and S2–3) given in day of year. Numbers in parentheses indicate the final day of hour-long daily acquisitions during winter where applicable.

Site	2006	2007	2008
C0	—	149–225	—
C1	150–240(365)	142–235(495)	131–205
C2	151–227(359)	146–193(507)	131–219(591)
C3	147–240(294)	143–194(497)	133–207(593)
P1	—	153–214	—
P2	—	150–210	—
P3	—	153–213	—
P4	—	153–206	—
N1	—	—	133–208
N2	—	—	133–205
N3	—	—	133–207
S2	—	—	132–219
S3	—	—	132–219

resulted in a level of smoothing comparable to a 12-hour local linear regression scheme. Smoothing was applied to horizontal and vertical data separately. Horizontal ice surface velocities were derived from the smoothed position time series data. Each spring we retrieved and re-installed the glacier GPS receivers (C1, C2 and C3) as close as possible to the starting position of the previous year with the goal of having the GPS units track the same Eulerian coordinates from year to year. This allowed for the secular evolution of surface flow to be observed. Due to the rough, broken surface of the lower glacier, we were unable to re-position the GPS receivers in exactly the same starting location from one year to the next. Due to the high strain rates and the difference in starting position in subsequent years, it was necessary to correct the velocity time series for differences in starting position.

We used strain rates derived from 2007 Synthetic Aperture Radar (SAR) surface velocity data [Joughin and others, 2008a] to apply a constant velocity correction, δu_ξ, to each

year of glacier velocity data. The correction is a function of the local longitudinal strain rate, $\dot{\varepsilon}_\xi$, and the difference in starting positions, along a local flow line coordinate ξ. We define ξ_1 as the initial position in the first year and ξ_2 as the initial position in subsequent years. We applied infinitesimal strain theory as the velocity corrections are small compared with overall ice motion. Accounting for this velocity difference allows for accurate comparisons of the surface speed in one location from one year to the next

$$\delta u_\xi = \dot{\varepsilon}_\xi(\xi_2 - \xi_1). \tag{2.1}$$

In order to identify seasonal trends in surface speeds, daily-average position data for glacier sites were detrended to remove the components of motion associated with the large surface speeds and longitudinal strain rates at Jakobshavn Isbræ. Initial velocities, u_0, at time, t_0, from GPS were used to calculate the expected motion influenced by a constant relative acceleration, α, defined as

$$\alpha = \frac{1}{u}\frac{\partial u}{\partial t}, \tag{2.2}$$

and a time dependent longitudinal strain rate, $\dot{\varepsilon}_\xi$, which deviates from an initial strain rate, $\dot{\varepsilon}_{\xi,0}$, due to constant relative acceleration

$$\dot{\varepsilon}_\xi(t) = \dot{\varepsilon}_{\xi,0}\, e^{\alpha(t-t_0)}. \tag{2.3}$$

If relative acceleration is small such that $\alpha(t - t_0) \ll 1$, then the expected position, $\dot{\varepsilon}_\xi$, can be approximated by

$$\xi_{\text{exp}}(t) = \xi_0 + \frac{u_0}{\gamma}\left(e^{\gamma(t-t_0)} - 1\right), \tag{2.4}$$

where γ is a combined acceleration term due to a constant relative acceleration and a nearly constant strain rate:

$$\gamma = \alpha + \dot{\varepsilon}_{\xi,0}. \tag{2.5}$$

A more thorough treatment of the derivation of Equation (2.4) can be found in the appendix. Initial velocities are calculated by finding the best fitting rate of change over the first twenty days of measured position data. During each of these twenty day periods, there was no evidence of speed-ups or any other rapid variability. A non-linear least squares routine is used to determine the combined acceleration term, γ, for each time series. The expected motion can then be subtracted from the measured motion, ξ_{meas}, leaving residual positions, ξ_{res}:

$$\xi_{\text{res}} = \xi_{\text{meas}} - \xi_{\text{exp}}. \tag{2.6}$$

This analysis is similar to the technique employed by Amundson and others [2008] for removing the effects of large strain rates from short time series (not subject to significant inter-annual acceleration) of GPS data near the terminus of Jakobshavn Isbræ. When applied to year-long time series, this method efficiently removes long-term trends due to inter-annual acceleration and longitudinal strain rates. However, the assumption that the relative acceleration term is constant and small does not allow for any distinction between the effects of inter-annual acceleration and longitudinal strain rates.

To examine glacier velocity variations on shorter time scales, continuous velocity time series were derived from the smoothed GPS position data. These continuous velocities were used to determine the amount of diurnal variability through the melt season. The amplitude of diurnal variations was analyzed using a Gabor transformation,

$$G(t,f) = \int_{-\infty}^{\infty} e^{\frac{-(t'-t)^2}{2\sigma^2}} e^{-2\pi i f t'} u(t') dt', \tag{2.7}$$

a moving Fourier transform (FFT) with a Gaussian window [Gabor, 1946]. Continuous velocity data were detrended and then multiplied by a Gaussian function with maximum amplitude of one and sigma of two days. The windowed velocities were then transformed with the FFT to determine spectral coefficients of the diurnal frequency. We define diurnal strength as the square of the norm of G for f equal to $1\,\mathrm{d}^{-1}$ and it represents the variability due to diurnal frequencies of velocity data centered within the Gaussian window. This calculation was performed every six hours resulting in a time series of the diurnal strength of velocity variations. To classify diurnal strength, a threshold of $2 \times 10^5\,\mathrm{m}^2\,\mathrm{d}^{-2}$ was used to determine the presence or absence of significant diurnal variations in speeds.

2.2.2 Terminus position

We used Landsat images to document the continued retreat of Jakobshavn Isbræ. Mean terminus positions were determined using available cloud-free panchromatic Landsat 7 scenes. For each image, the glacier terminus was digitized and a mean front position was calculated across a 3 km swath perpendicular to the glacier centerline [Cassotto, 2011]. Data coverage is lacking during winter months due to lack of solar illumination, making it difficult to determine the exact maximum extent of the glacier each year; however, the minimum position of the terminus is generally well defined.

The timing of large calving events—in the manner of capsizing, full-glacier-thickness icebergs described by Amundson and others [2008]—was determined with a catalog of

Table 2.2: Data sources for melt at sites C1 and C2 for years 2006 to 2008. T_{base}, T_{C1} and T_{C2} are surface temperatures at the base station, C1 and C2 respectively. M_{C1} and M_{C2} refer to surface melt (measured or modeled) at C1 and C2. PDD(T_{base}) means that the melt was derived with the temperature-index model using lapse-rate corrected surface temperature from the base station. PDD indicates melt was modeled using in-situ surface temperatures.

Year	T_{base}	T_{C1}	T_{C2}	M_{C1}	M_{C2}
2006	meas.	N/A	N/A	PDD (T_{base})	PDD (T_{base})
2007	meas.	meas.	meas.	PDD	meas.
2008	meas.	meas.	meas.	meas.	meas.

calving events on Jakobshavn Isbræ compiled by Amundson and others [2012] using broadband seismic, time-lapse photographic and remote sensing (MODIS) data.

2.2.3 Surface melt

Air temperatures at sites C1 and C2 were recorded every 15 minutes. In order to estimate surface melt, ablation was measured at the same sites during the 2007 and 2008 melt seasons. Surface ablation data were recorded every hour using the pressure sensor method described by Bøggild and others [2004]. Data gaps in our temperature and ablation records prevented consistent, year to year measurements of melt (Table 2.2). In order to produce continuous melt estimates for both sites each year, we used available temperature records combined with ablation measurements from sites C1 and C2 to construct a temperature-index melt model. For 2006, we use daily-average temperature data from the GPS base station (Fig. 2.2) to infer temperatures at sites C1 and C2. Temperature lapse rates were calculated between the base station (150 m_{asl}) and sites C1 (700 m_{asl}) and C2 (970 m_{asl}) using data from years 2007 and 2008. The lapse rates were applied to the base station temperature data and these corrected temperatures were used as input to the temperature-index model for sites C1 and C2 during 2006. To estimate 2007 melt at site C1, we used in-situ temperatures as input to the temperature-index model.

We calculated degree day factors (DDFs) using daily-average temperature and melt data for C1 and C2 in 2008. This calculation follows Equation (2.8), taking the ratio of

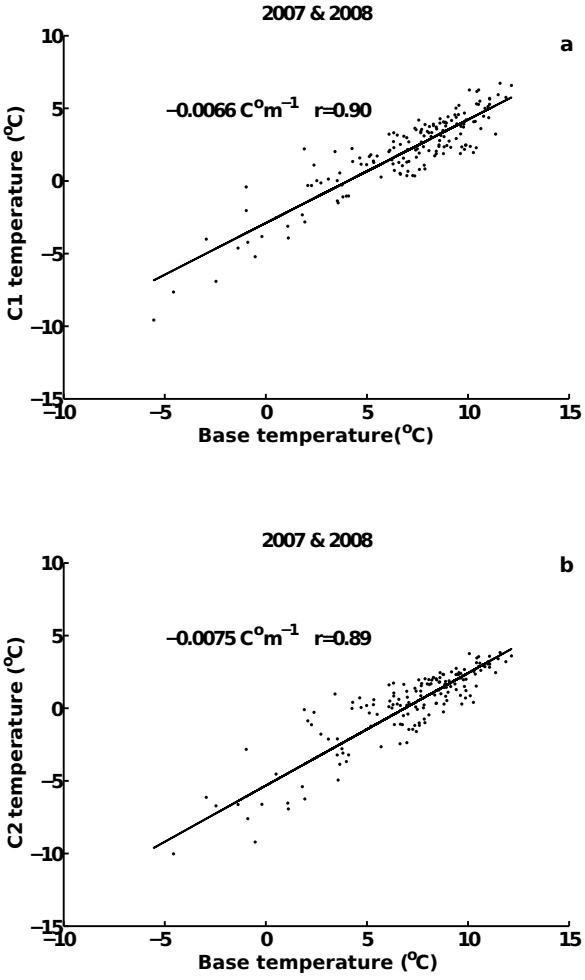

Figure 2.2: Temperature-temperature regression plots with lapse rates between Base and on-ice sites C1 (a) and C2 (b).

measured melt, M, over the sum of positive degree days, T^+, at intervals, Δt, of one day.

$$\sum_{i=1}^{n} M = DDF \sum_{i=1}^{n} T^+ \Delta t \tag{2.8}$$

These DDFs were then applied to estimated (2006, C1 and C2) and measured (2007, C1) temperatures to provide estimates of surface melt where direct measurements were unavailable. Direct measurements of surface ablation were recorded in 2008 at site C1 and also during 2007 and 2008 at site C2.

2.2.4 Supra-glacial lakes

We used Landsat 7 panchromatic scenes to manually identify time intervals when supra-glacial lakes drained each melt season. The timing of drainage for individual lakes, or groups of lakes, was subsequently refined using Moderate Resolution Imaging Spectro-radiometer (MODIS) 250 m granules. When lakes were identified as full in one MODIS frame and empty in the next we assumed a drainage event had occurred during the time period between observations. The areal extents of full lakes that would later drain were digitized. For this study we only considered lake drainage events within approximately 30 km of the nearest GPS station. We identified lake drainage events during each melt season of 2006, 2007 and 2008.

This method only constrains the timing of lake drainage, but does not indicate whether the water is routed along the surface, englacially, or subglacially. This has implications, because only subglacial events have the potential to affect ice motion.

2.3 Results

2.3.1 Ice motion

GPS records were successfully processed during years 2006 to 2008 for sites C1, C2 and C3; during 2007 for site C0; during summer 2007 for sites P1, P2, P3, and P4; and during summer 2008 for sites N1, N2, N3, S2, and S3. We estimate an uncertainty of 6 mm in horizontal position and 2 cm in vertical position at the beginning of each season by examining position noise during periods of otherwise steady motion. Though, these values are likely higher at later dates when a greater length of the antenna pole is exposed above the ice surface, resulting in larger errors due to motion of the antenna not associated with ice motion. To illustrate the evolution of surface speeds throughout the melt season, daily-average positions were used in calculating velocities. Daily-average velocities were then corrected for different starting positions using Equation (2.1) and strain rates (3×10^{-4} d^{-1} at site C1; 1×10^{-4} d^{-1} at site C2; and 7×10^{-5} d^{-1} at site C3) derived from Radarsat SAR data acquired during summer of 2007. Due to the robust statistics of daily-average positions, the uncertainty in daily-average position is small. Estimates of uncertainty for continuous velocity time series can be characterized based on time scales: velocity uncertainties over twenty-four hours, one hour and fifteen minutes are 0.1, 10 and 70 $\mathrm{mm\,d}^{-1}$, respectively. Velocity uncertainties are estimated by calculating the standard error of the

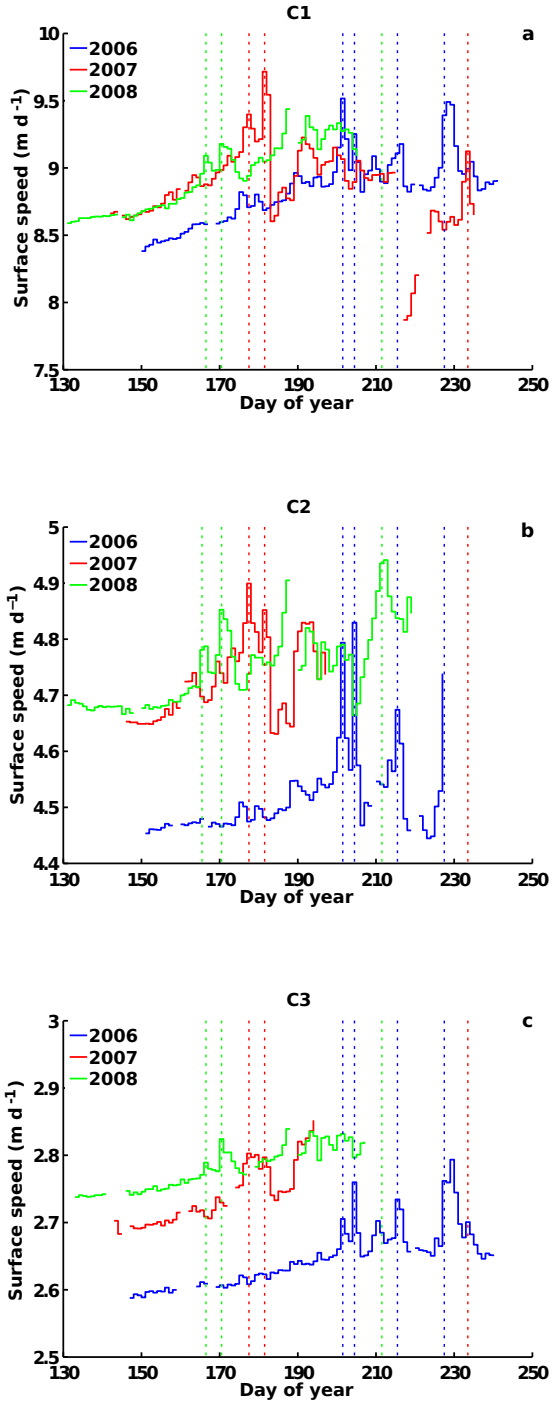

Figure 2.3: Surface velocities from continuous GPS records at glacier sites C1 (a), C2 (b) and C3 (c) from 2006–2008. Vertical dashed lines indicate the timing of short duration speed-up events described in the results section, following the same color coding as velocity curves.

mean for positions averaged over the above intervals and propagating this error through the time derivative of average positions.

Daily-average velocity time series for the glacier sites are shown in Figure 2.3 for melt seasons 2006 to 2008. Continuous velocity time series for ice sheet sites during 2007 are

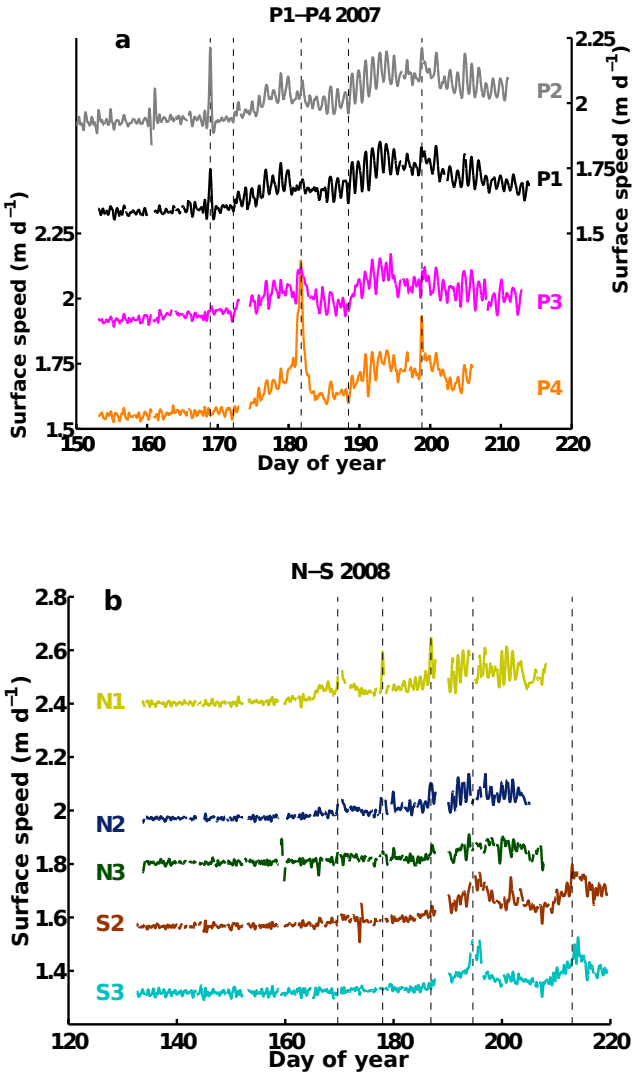

Figure 2.4: Surface speed from 2007 GPS records at ice sheet sites P1 and P2 (north); P3 and P4 (south) (a). Surface speed from 2008 GPS records at ice sheet sites N1, N2 and N3 (north); S2 and S3 (south) (b). Vertical dashed lines indicate the timing of short duration speed-up events described in the results section.

shown in Figure 2.4a and velocities at ice sheet sites during 2008 are shown in Figure 2.4b. Portions of the vertical data from glacier and ice sheet margin sites during 2006 and 2007 are presented later in Figure 2.8. Vertical position has not been corrected for variations in down-slope motion as horizontal speeds are exceptionally steady, varying less than 10%, and surface slopes are small (less than 2°), making such corrections negligible. As such, values of vertical position were simply detrended with respect to time and arbitrary additive constants were applied to improve clarity. Hereafter, we use the term uplift to refer to positive changes in the detrended vertical position. Dates of occupation for all GPS sites are presented in Table 2.1.

During each melt season, at the glacier sites, we see a steady spring acceleration followed by one or two brief speed-ups, each lasting one to three days (Fig. 2.3). After the first of the short speed-ups, the spring acceleration is interrupted and velocities are more variable (Fig. 2.5). At GPS sites located on the glacier the brief speed-ups are often followed by a period of slower flow, during which speeds are less than prior to the speed-up. We refer to these periods of slower flow as extra slow-down events [Meier and others, 1994] and discuss them in more detail in the Discussion section. The number, timing and magnitude of the short speed-up events and, when applicable, extra slow-downs is variable from one year to the next, but they occur simultaneously at all of the glacier sites, with no measurable delay.

In 2006 we identified as many as four short-lived speed-up events all occurring after day 200 (Fig. 2.3). Three of these speed-ups—beginning days 201, 215 and 227—coincide with periods of enhanced surface melt and uplift. The speed-up event on day 204 occurred during a time during which melt rates were falling (Fig. 2.5). These speed-up events are observed at sites C1 and C2 and, to a lesser degree, at C3. There were no GPS deployed at ice sheet sites in 2006, precluding any comparison in the timing and occurrence of speed-ups on the glacier versus the ice sheet.

During 2007, speed-up events were observed at ice sheet sites as well as on the glacier. At C1 there were speed-ups on days 177, 181, and 233. The first three speed-ups were also recorded at C0 and C2, but data gaps prevented the possibility of observing the day 233 event at these sites. There is evidence of enhanced surface melt associated with the day 177 event only. At ice sheet sites there was a speed-up event on day 169 at sites P1 and P2, both to the north of the main glacier, that was not reflected in the glacier data. On day 181 there is a notable speed-up of approximately 33% at site P4 and a much smaller speed up

at P3. Both P4 and P3 are situated south of the main glacier.

The temporal coverage of data from the glacier sites in 2008 was less extensive compared to previous years and, as a possible result, we identified fewer speed-up events in that year. We see two minor speed-ups on days 166 and 170 at C1, C2 and C3. There was also a speed up on day 211 that was only observed at site C2—the only glacier site recording data at the time. There is also some indication of a possible speed-up event around day 187 at the three sites, but the full timing and the magnitude of the event is obscured by data gaps. At the ice sheet sites we see a pattern in which the occurrence of a given speed-up is restricted to one side of the glacier or the other. At the northern sites we find speed-ups on days 164, 179 and 188 whereas at southern sites there were two speed ups: one on day 194 and another on day 212. Due to poor data coverage of continuous GPS data it is impossible to confirm any possible patterns of timing and distribution of speed-up events in 2008.

Velocities at the ice sheet sites in 2007 and 2008 showed steady speeds with little variability prior to an initial speed-up each year (Fig. 2.4). Following the early season period of steady flow, ice surface speeds at the ice sheet sites are generally greater and more variable; diurnal variations also become evident during this time. GPS sites on the same side of the glacier (north or south) tend to be very similar with a few exceptions. The timing of speed-up events and the amplitudes of diurnal variability are similar at sites P1 and P2 (north of the glacier) in 2007 and time series at P3 and P4 (south of the glacier) are alike except for two speeds-ups that occur at P4, but not P3, on days 182 and 199. During 2008, velocity time series at sites north of the glacier (N1, N2 and N3) and, likewise, at sites to the south (S2 and S3) share a similar shape, but the amplitude of diurnal variability is greater at sites further downstream, which are closer to the ice sheet margin.

The effect of ice motion subject to a constant relative acceleration was removed from the position data for the three glacier sites using Equations (2.4) and (2.6) with remote-sensing-derived strain rates. To examine the timing of changing glacier speeds as a response to seasonal forcings, such as surface meltwater forcing and seasonal calving behavior, velocity anomalies were determined for each year of data. These anomalies were calculated using the residual position data. Anomalies were derived from smoothed residual positions in order to suppress short-term effects. The velocity anomalies are defined as the difference between measured velocities and expected velocities calculated using the time-derivative of Equation (2.4). Positive values of velocity anomaly indicate times when the glacier is flowing faster than the mean year-long flow and conversely negative anomalies indicate

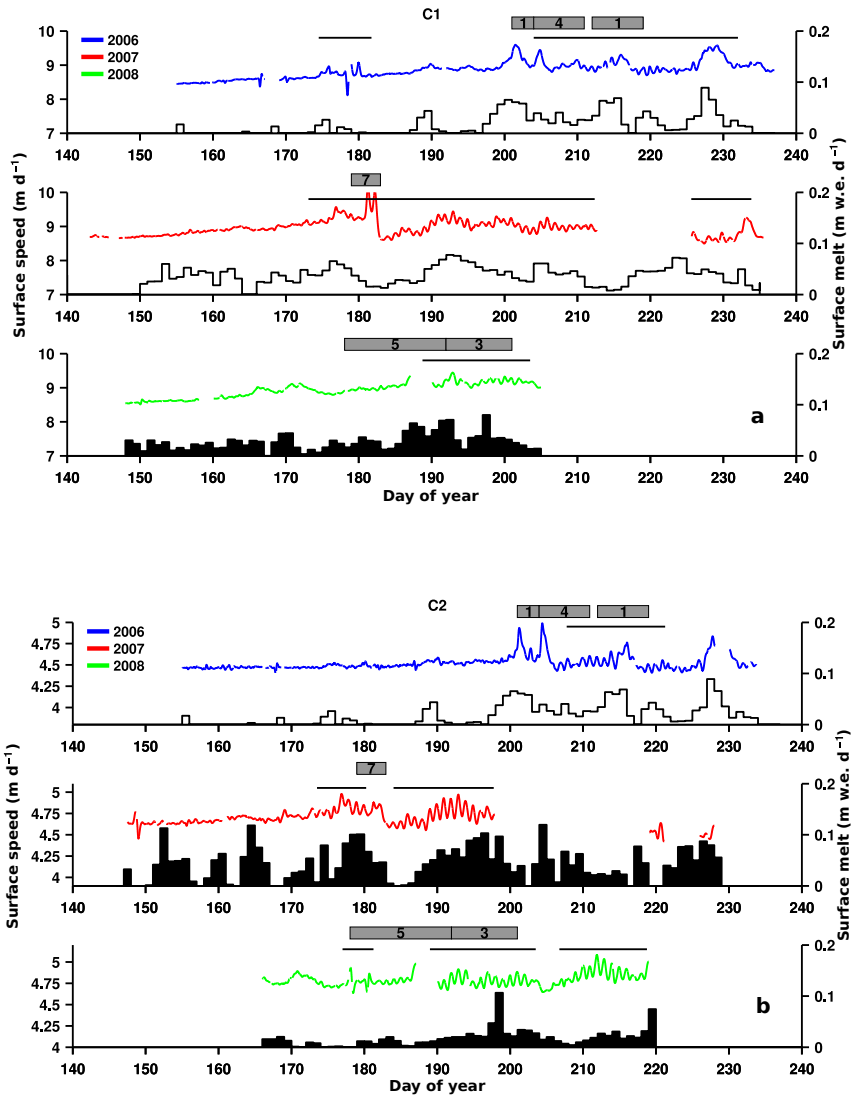

Figure 2.5: Surface velocities for glacier sites C1 (a) and C2 (b) are shown in blue (2006), red (2007), and green (2008); consistent with Figure 2.3. Surface melt is shown with black step-plots for C1 and C2: Filled bars indicate direct measurements of surface melt, unfilled bars are from the temperature-index model. In 2006, at both sites, surface melt was calculated using the temperature-index model with lapse rate-corrected temperatures recorded at the base station. Horizontal black lines above each time series denote periods during which diurnal velocity variations are present. Grey boxes above each velocity curve indicate lake drainage events, where the width of each box corresponds to the time interval over which the indicated number of lakes drained.

speeds less than mean flow.

2.3.2 Terminus position

The results of the Landsat terminus position mapping (Fig. 2.6) show the rapid retreat and high variability during the period of ice tongue break-up previously described by Podlech and Weidick [2004] and Luckman and Murray [2005]. During the years 2001 to 2005, the average rate of retreat was almost 3000 $\mathrm{m\,a^{-1}}$ and seasonal fluctuations were as much as 6 km. After 2005, the rate of retreat was slower, an average of 500 $\mathrm{m\,a^{-1}}$, and more steady. Every year from 2005 up to 2010, the glacier advanced during winter and formed a floating tongue that would then break-up in spring. Seasonal variations were particularly pronounced in years 2007 to 2009. Joughin and others [2008b] identified such fluctuations during 2004 to 2007 as a primary control on the seasonal evolution of ice flow on outlet glaciers in West Greenland. In the winter of 2009, this pattern did not continue; while the retreat rate has remained steady since 2005, there was no substantial floating tongue formed in winter 2009/2010 [Cassotto, 2011]. Iceberg calving continued through the winter of 2009 and spring 2010 preventing the terminus advance necessary for the formation of a floating tongue (Fig. 2.6).

2.3.3 Surface melt

In order to estimate daily surface melt, DDFs were calculated at sites C1 and C2 in 2008 following Equation (2.8). We calculated a DDF for site C1 of 1.2×10^{-2} $\mathrm{m_{w.e.}\,K^{-1}\,d^{-1}}$ and at C2 of 1.4×10^{-2} $\mathrm{m_{w.e.}\,K^{-1}\,d^{-1}}$. These values are within the range used by Fausto and others [2009] for cold and warm conditions on bare ice in Greenland. They were applied to the C1 and C2 temperatures determined from the lapse-rate corrected base station measurements. Between C1 and the base station we calculated a lapse rate of 6.6 $\mathrm{K\,km^{-1}}$ and between C2 and the base station we found a lapse rate of 7.5 $\mathrm{K\,km^{-1}}$. The same 2008 DDF was used with temperatures measured at C1 to calculate melt at C1 in 2007. The results of temperature-index melt calculations are presented in Figure 2.5.

Periods of significant diurnal velocity variations, identified with the Gabor transform method following Equation (2.7), were determined for sites C1 and C2 in 2006, 2007 and 2008 and are represented in Figure 2.5 as horizontal black lines above each velocity time series. During the spring acceleration, before the first speed-up, there is little or no diurnal

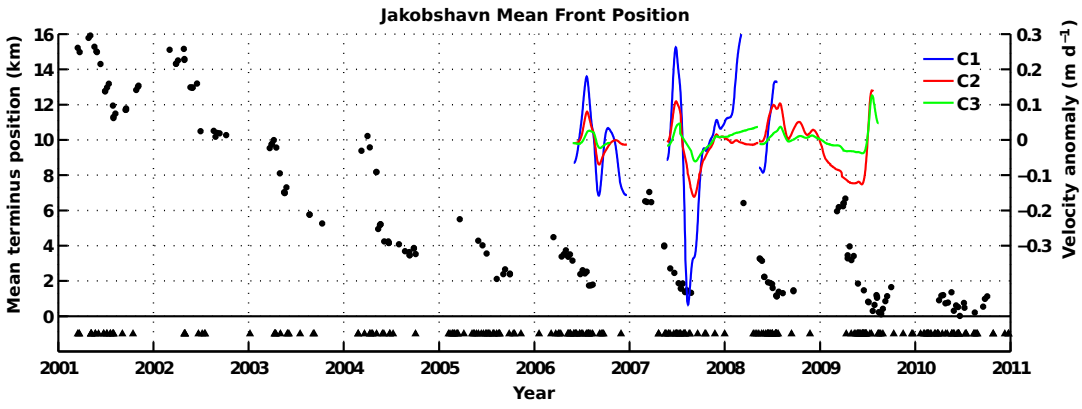

Figure 2.6: Landsat-derived mean terminus position (circles) with the timing of major calving events (triangles) cataloged from passive seismic measurements [Amundson and others, 2012], 2001 to 2011. Velocity anomalies of the glacier sites are shown in blue (C1), red (C2) and green (C3). Positive values of velocity anomaly indicate times when the glacier is flowing faster than the mean year-long flow and conversely, negative anomalies indicate speeds less than mean flow.

velocity variation at C1 and C2. Each year the onset of diurnal variation in surface speed follows the first speed-up—as identified in Figure 2.3 and described in the section on ice motion—when surface melt is sustained at elevated levels for several consecutive days. Following onset, the amplitude of the diurnal velocity variations is greatest during times with large positive degree days, corresponding to daily surface melt of approximately 0.05 $m_{w.e.}$ or greater.

In 2007, total surface melt was at least two times greater than in 2006 or 2008 when comparing cumulative melt rates during periods of overlapping data coverage. The anomalously high melt observed during 2007 is confirmed by modeling results [Mernild and others, 2010] and remote sensing observations [Mote, 2007] of West Greenland. The surface speeds at C1 and C2 also had the greatest amount of diurnal variability in 2007 and the onset of high diurnal strength appears related to the cumulative melt for the season. In years when surface melt begins earlier and is more intense, diurnals begin earlier and diurnal amplitudes are greater.

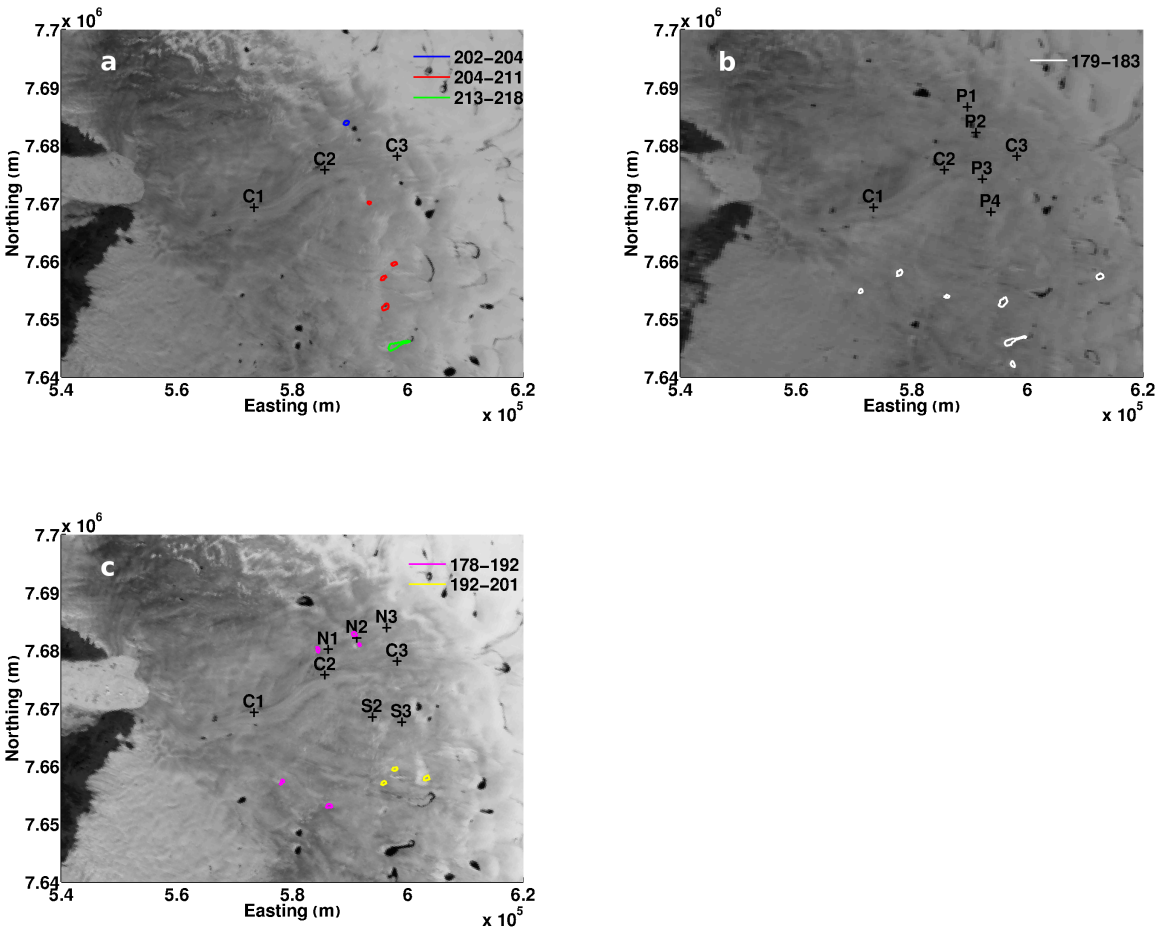

Figure 2.7: Outlines of supra-glacial lake drainage events were identified using MODIS 250 m scenes during melt seasons of 2006 (a), 2007 (b) and 2008 (c). The background image shows the ice surface after lakes have drained with the areal extent of full lakes color coded by the dates over which they drained. Most lake drainages occur to the south of the main glacier where a greater number of large lakes form each year.

2.3.4 Supra-glacial lake drainage events

The areal extent and timing of supra-glacial lake drainage events are depicted in Figure 2.7 for years 2006, 2007 and 2008. In general, we find that the majority of the lake drainage events occurred south of the glacier, where more lakes occur. During the summer of 2006 we identified three time periods with lake drainage events: days 202–204, days 204–211 and days 213–218. During 2007 there was only one time period with observed drainages:

Table 2.3: Inter-annual acceleration as a percentage per year of early spring surface speed (% per year).

Site	2006–2007	2007–2008
C1	6.0%	0.6%
C2	4.0%	1.0%
C3	4.0%	2.0%

days 179–183. In 2008 there were two lake drainage periods: days 178–192 and 192–201. In some cases, we observe the same lake(s) repeatedly draining each year; however, this is not always the case, and of 14 lakes, only 5 drained more than once in three years.

2.4 Discussion

2.4.1 Inter-annual velocity variations

The GPS-derived surface velocities on Jakobshavn Isbræ show a general pattern of increasing speed from one year to the next (Fig. 2.3). Joughin and others [2008a] have identified an approximate 5 $\%\,a^{-1}$ acceleration trend in SAR-derived surface velocities on the glacier from 2004 to 2007. Our GPS record confirms the general trend of steady acceleration between 2006 and 2007, but we observe a departure from this trend between 2007 and 2008 (Fig. 2.3 and Table 2.3). A smaller increase in speed (approximately half that during the previous year) was observed between 2007 and 2008 at the furthest upstream site C3, with even smaller increases for downstream sites C2 and C1.

Joughin and others [2008a] demonstrated that the inter-annual acceleration since the early 2000s has been driven by changes at the ice front. The deviation, from 2007 to 2008, from a steady inter-annual trend in the GPS speeds shows that sites closest to the terminus have the strongest response to changes in forcing; in this case to changes that resulted in less acceleration (Table 3 and Fig. 2.3). This suggests that both acceleration and deceleration are controlled at the ice front. From 2001 to 2005 the average rate of terminus retreat was nearly 2500 $m\,a^{-1}$, which is greater than the retreat rate during the time period from

1997 to 2001, when the onset of terminus retreat and increasing speeds occurred (approximately 1500 $\mathrm{m\,a^{-1}}$) [Luckman and Murray, 2005]. More recently, from 2005 to 2009, the average rate of terminus retreat was only about 500 $\mathrm{m\,a^{-1}}$ (Fig. 2.6). Despite these large variations in retreat rate, during the period from 1997 to 2009, the inter-annual acceleration was very steady with a relative acceleration of 5–8 $\mathrm{\%\,a^{-1}}$ [Joughin and others, 2008a]. In contrast, on shorter time scales surface speeds are more closely connected to seasonal terminus position.

2.4.2 Seasonal velocity variations

In the lower reaches of the glacier (approximately 10–20 km from the terminus) flow speeds are controlled by glacier geometry and terminus boundary conditions [Joughin and others, 2008a], with surface speeds greatest near the terminus. This type of tidewater behavior has also been confirmed by modeling results at Helheim Glacier in East Greenland [Nick and others, 2009]. In addition to an inter-annual acceleration in response to the decadal trend of decreasing glacier length, surface speeds are affected by seasonal variations in terminus position. Since 2000, the terminus position of Jakobshavn Isbræ has varied by as much as 5–8 km each year, primarily due to seasonality of calving (Fig. 2.6). As the rate of calving increases in the spring the glacier responds by speeding up (Fig. 2.6). We find that the lower glacier responds to changes in terminus position first, with response times increasingly delayed moving up-glacier. Based on the velocity anomaly data presented in Figure 2.6 we note a time delay in the velocity response to the start of calving and terminus retreat in spring. It is more difficult to identify a similar pattern in the fall as Landsat-derived terminus positions become unavailable due to a lack of solar illumination. However, SAR-derived terminus position and surface velocity data—continuous through a whole year—allow for a full examination of the seasonal response to variations in terminus position. Figure 4 in Joughin and others [2008b] presents SAR-derived surface speeds and terminus positions from 2005 to 2007 and these data show delays of approximately 40–50 days between the onset of seasonal terminus retreat and the beginning of the seasonal acceleration in spring. In fall seasons, there is a significantly shorter delay of 10–20 days between the onset of terminus advance and when the glacier begins to decelerate. The asymmetry of seasonal response to terminus position suggests separate glacier behavior in response to an advancing terminus versus a retreating terminus.

In early winter, the rates of ablation and calving both cease or are greatly reduced.

This leads to simultaneous glacier advance and thickening. We hypothesize that variations in glacier speed are primarily controlled by ice thickness through its influence on

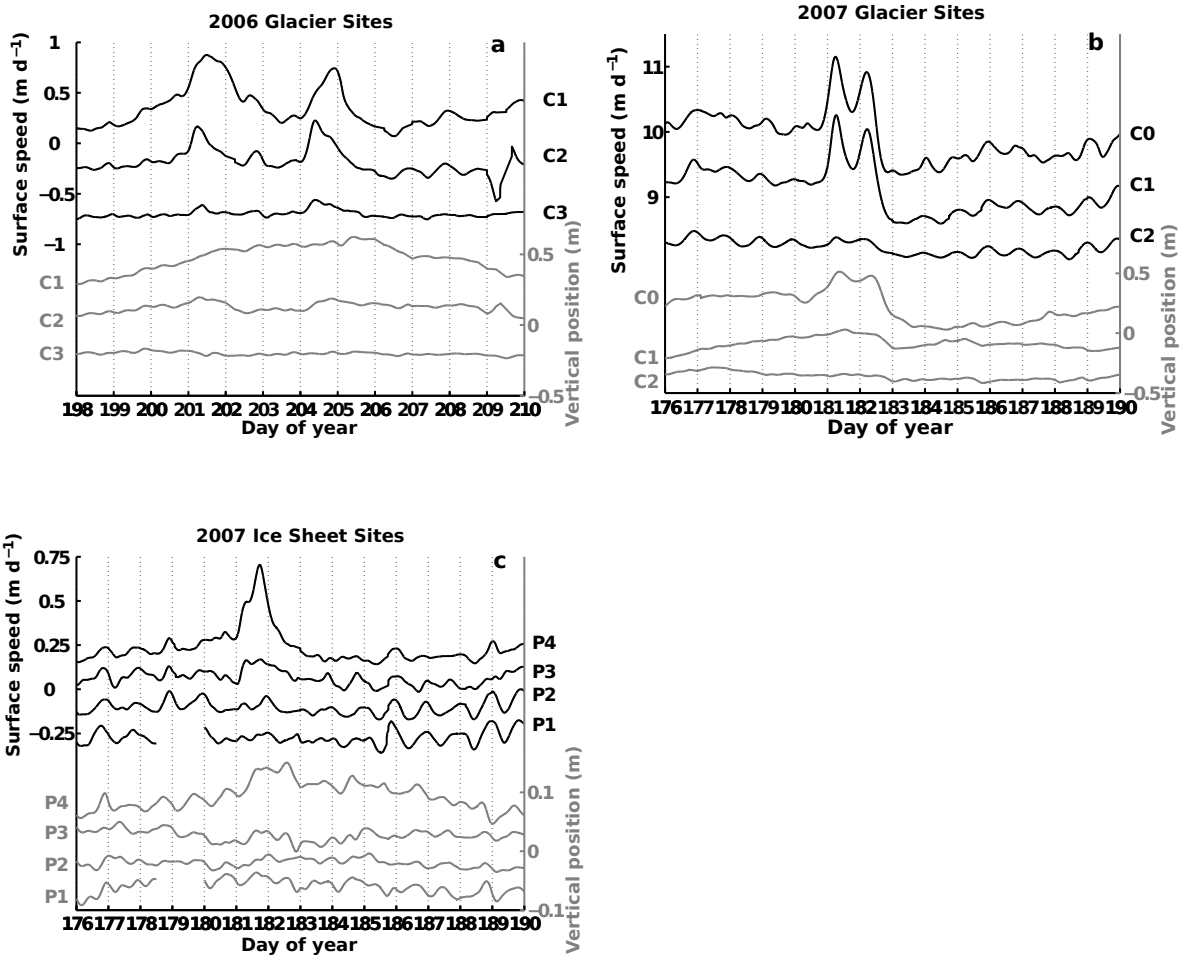

Figure 2.8: Surface speed (black) and vertical position (gray) of GPS sites C1, C2 and C3 (in 2006 there were no ice sheet GPS sites) during a speed-up event beginning day 201, 2006 (a). A speed-up event beginning day 181, 2007 was recorded at glacier sites C0, C1 and C2 (b); and margin sites P3 and P4 (c). Speed anomalies, shown in (a) and (c), are simply surface speeds shifted with arbitrary additive constants for clarity. Surface speeds presented in (b) are unmodified. Values of vertical position are from detrended vertical GPS position with arbitrary additive constants applied to offset the different curves for clarity.

effective basal pressure, and hence sliding, as also suggested by Joughin and others [2012]. In fall, the gradual advance of the glacier proceeds simultaneously with a gradual thickening of ice at the grounding zone, and velocity response is immediate over the lower glacier with large areas of the lower glacier gradually thickening and slowing at the same time. In spring, as the winter floating tongue disintegrates rapidly, the ice thickness response upstream of the grounding zone is delayed as increased flow at the calving front progressively thins the glacier. Speed response is delayed at up-glacier sites by the time required for thickness changes, and therefore sliding speed, initiated at the grounding zone to propagate upstream, similar to the suggestion by Pfeffer [2007] of upward propagation. So in fall, it is not necessary to propagate any changes in thickness, whereas in spring thickness changes are propagated up from the terminus. It is important to note that the spring speed-up coincides with the disintegration of the floating tongue, which sometimes happens well before the onset of surface melt [Joughin and others, 2008a]. It is therefore not comparable to spring speed-up events, as observed on alpine glaciers. Such events do exist, as we show below, but they are distinct from this seasonal evolution.

The pattern of seasonal velocity variations was interrupted dramatically in summer 2007, when all glacier GPS sites slowed down simultaneously in mid-summer. The onset of this slow-down was sudden (Fig. 2.3 and 2.5), and it significantly affected the average seasonal velocity. We discuss this event in more detail in the section on short-term velocity events.

2.4.3 Diurnal velocity variations

At all GPS sites the velocity response to surface melt is not constant through the melt season. We see no evidence for tidal modulation at diurnal or semi-diurnal frequencies at sites more than 10 km upstream of the terminus [Podrasky and others, 2010]. Furthermore, there is no evident shift in the timing of diurnal maxima throughout a tidal cycle as one would expect with the major tidal constituents which have periods not exactly equal to one solar day. We thus conclude that any diurnal variations in surface velocity at the sites in this study are due to surface melt. In spring seasons when the supply and variability of meltwater are low, we see a steady acceleration at the glacier sites with low diurnal variability. By the start of summer the spring acceleration is interrupted by rapid speed-up events synchronous across all glacier GPS sites (Fig. 2.3). Following the first speed-up we see evidence for diurnal variations, indicating that the glacier is able to respond to

surface meltwater input on short time scales (Fig. 2.5). The timing of diurnal maxima is approximately six hours after local noon at all sites with little change throughout the melt season. The amplitude of diurnal variations is greatest when surface melt is increasing at both glacier and ice sheet sites (for example, see Figure 2.5 during days 189–194 in 2007 and during days 190–195 in 2008). The velocity response of the ice sheet sites closely matches the estimates of surface melt; speeds are greater during periods of enhanced melt and are lower when there is less melt.

The absolute amplitude of diurnal variability is similar at both glacier and ice sheet sites and is as much as 10 $\mathrm{cm\,d^{-1}}$ during periods of strong diurnal variation (Figs. 2.4 and 2.5). While the amplitude of diurnals may be similar on the glacier and ice sheet, the amplitude of diurnals relative to background flow is smaller on the glacier compared to ice sheet sites. The relative amplitude of diurnal variability at glacier sites is approximately 1% to 2% and at ice sheet sites it is closer to 5%. We find a similar pattern regarding the expression of short-term velocity events at glacier versus ice sheet sites. On the ice sheet, the largest of the short-term velocity events represent approximately 30% increases in speed, whereas large events on the glacier amount to a speed increase of 5% to 10%.

2.4.4 Short-term velocity events

On seasonal and shorter time scales, summer speeds are influenced by the combination of an early season terminus retreat and surface meltwater forcing. During spring, at the beginning of each annual velocity record, short-term variations in surface speed are at a minimum (Figs. 2.4 and 2.5). During this period, there is low correlation between surface melt and velocity. We interpret this to mean that both quantity and variability of surface melt reaching the bed is low during spring. As rates of surface melt increase, the velocity time series are punctuated by brief velocity events of duration one to three days, as described in the Results section. These short-term velocity events consist of sudden speed-ups, lasting for only a few days (Figs. 2.3 and 2.4), and are distinct from the longer steady spring acceleration described in the previous section. The magnitudes of the speed-ups on Jakobshavn Isbræ, 5% to 10%, are similar to those observed at Helheim Glacier [Andersen and others, 2010] in East Greenland. Although, the magnitude of these speed-ups are small compared with other West Greenland outlet glaciers: Bartholomew and others [2010] observed speed-ups in excess of 200% at land-terminating Russell Glacier, and speed-ups as large as 33% have been reported on Kangiata Nunata Sermia [Sole and others, 2011]—a

tidewater outlet glacier 500 km south of Jakobshavn Isbræ. The relatively large speed-ups of marine-terminating Kangiata Nunata Sermia may be a consequence of where measurements were made rather than a difference in glacier behavior. The GPS measurements presented by Sole and others [2011] where made high on the glacier (35–70 km from the terminus) in a region where the glacier is bedded at or above sea level. Surface speeds at these sites are also significantly slower than speeds in the terminus region and as a result, the region of study at Kangiata Nunata Sermia may have a response to surface meltwater forcing that falls somewhere between a fast-flowing tidewater outlet and the surrounding ice sheet. While the percent speeds-ups observed at marine-terminating outlets are small, the absolute change in flux associated with a 5% increase in surface speed at Jakobshavn Isbræ or Helheim Glacier is large, due to the high ice velocity and large ice thickness.

Onset of the speed-ups is rapid, typically less than one day, and the duration of enhanced flow ranges from 2 to 5 d. At glacier sites, the speed-up is almost always followed by a drop in speed, or extra slow-down, where speeds are reduced to less than that before the onset of the event. Extra slow-down events were observed to occur multiple times in a single melt season. The largest of the extra slow-downs resulted in a 5% reduction in flow for two days at site C1 in summer of 2007 (Fig. 2.8b). At ice sheet sites, there are no extra slow-downs; at these sites speed-up events are followed by slow-downs which do not result in lower speeds than before the event. Extra slow-down events have been observed elsewhere in Greenland [Sole and others, 2011] and were first described by Meier and others [1994] on Columbia Glacier, Alaska.

Periods of reduced speed due to extra slow-down events were found to last on the order of eight days. We propose that the speed-up events due to rapid uplift were associated with the input of large amounts of surface water and we now examine whether the duration of the slow-down events can be understood in terms of creep closure of over-enlarged, low pressure subglacial drainage channels following the period of enhanced water input. Bartholomaus and others [2008] have suggested that the time scale for creep closure of subglacial conduits under ice sheets should be shorter than for valley glaciers due to the thick ice and potentially large effective stress found on ice sheets. But, in the case of marine-terminating glaciers, conduit closure is slowed due to necessarily high subglacial water pressure. For ice grounded below sea level the subglacial water pressure must be sufficiently high to generate positive gradients in pressure, necessary to route water to the terminus. That is, the water head upstream of the terminus must be greater than sea level in

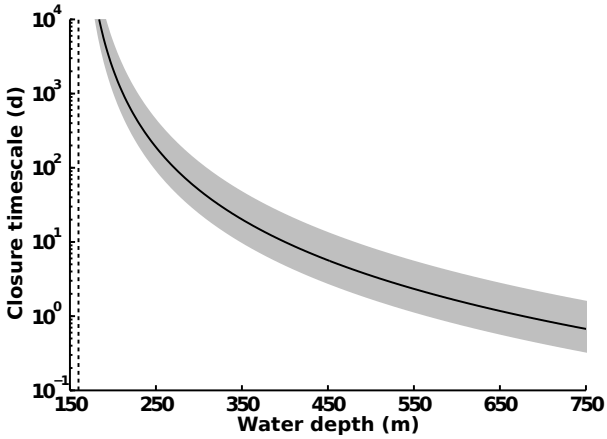

Figure 2.9: Characteristic time scale for conduit closure due to ice creep as a function of water depth—below ice surface. time scales were computed for a range (gray shading) of flow law parameters, 1×10^{-24} to 5×10^{-24} $s^{-1}\,Pa^{-3}$, as well as for a single value (black line) of 2.4×10^{-24} $s^{-1}\,Pa^{-3}$ [Cuffey and Paterson, 2010; Nye, 1953]. A flow law exponent of three was used in all calculations. Ice thickness was assumed 2000 m and the rate of conduit wall melt was assumed to be small compared to creep closure. Dashed line indicates water depth (160 m below ice surface) corresponding to zero effective pressure.

order to drive water flow. The minimum constraint on water head is independent of bed elevation, which implies that water pressures under over-deepened glacier beds will be greater than those beneath flat or forward-sloping glacier beds. Estimates of the ice thickness and bed elevation taken from Plummer and others [2008] are approximately 2000 m thick and 1500 m below sea level at C1 and 2000 m thick and 1000 m below sea level at C2. The sea level constraint on water pressure at the terminus dictates a minimum water pressure at C1 and C2 corresponding to a water level of 500 m and 1000 m below the ice surface at C1 and C2, respectively.

In general, the rate of creep closure of subglacial conduits is reduced in the presence of finite basal water pressure. In the case of tidewater systems, where ice is grounded below sea level, subglacial water pressures will be maintained at or above a minimum pressure dictated by bed topography. This means that, at the bed of tidewater glaciers, conduit closure via viscous creep will be slower than for conduits at atmospheric pressure. Following the description of Röthlisberger [1972], based on theory first presented by Nye [1953], we define conduit radius as r, a as the rate of wall melt due to viscous heating, A

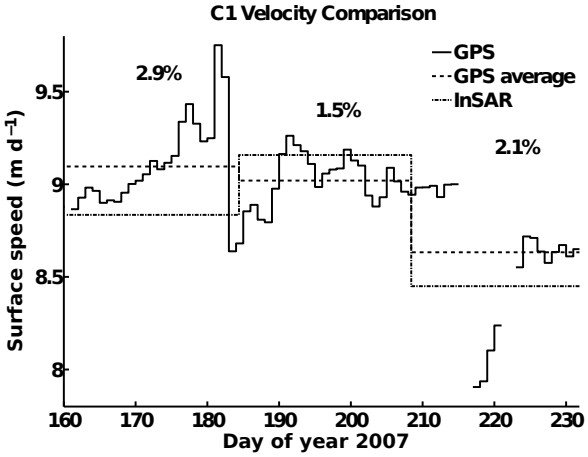

Figure 2.10: Comparison of RADARSAT-derived 24-day SAR velocities with GPS velocities at site C1, summer 2007. Percent difference between GPS average and SAR speeds is shown for each 24-day period.

as the flow law parameter, n as the flow law exponent, and N_{eff} as the effective pressure (difference between ice overburden and subglacial water pressure)

$$\frac{a}{r} - \frac{\dot{r}}{r} = A\left(\frac{N_{\text{eff}}}{n}\right)^{n}. \tag{2.9}$$

For this analysis we are interested in the maximum rate of conduit closure for a given effective pressure and so we assume that a is much smaller than $\dot{r}$ (non-zero values of a will have the effect of increasing closure times). Assuming a flow law exponent of three, the solution to Equation (2.9) for a conduit of initial radius, r_0, at time t_0, is

$$r(t) = r_0 e^{-A\left(\frac{N_{\text{eff}}}{3}\right)^{3}(t-t_0)} \tag{2.10}$$

and can be solved for a characteristic time scale, τ, over which the conduit radius has decreased to a value e^{-1} times r_0:

$$\tau = \frac{27}{AN_{\text{eff}}{}^{3}}. \tag{2.11}$$

Figure 2.9 shows conduit closure time scales as a function of englacial water depth for a range of flow law parameters (over a temperature range from 0 °C to -5 °C [Cuffey and Paterson, 2010] and from observations of creep closure of tunnels [Nye, 1953]) and an ice thickness of 2000 m. Closure time scales of one, eight and one-hundred days would require water levels of 670, 400 and 270 m (below the ice surface) respectively.

These response times are based on a very simple model, but they do suggest that the observed duration of extra slow-downs could be explained by the fact that conduits in regions where ice is grounded below sea level must remain pressurized at a minimum level. Because the rate of creep closure is greatly reduced by the low effective pressures below the glacier, any conduits enlarged by enhanced water flux would remain over-enlarged for days after water flux returns to normal levels. It is important to note this analysis neglects the influence of rapid basal motion for conduit destruction or disconnection [Kamb and others, 1994]. These processes related to high rates of basal motion would effectively reduce the characteristic time scale for conduit closure.

In most instances, the occurrence of the speed-up/extra slow-down pairs is closely related to the rate of surface melting; but, in a few cases the speed-ups do not appear to be related to temperature-index modeled surface melt. For instance, the record at site C1 in 2007 (Fig. 2.5) shows a speed-up around day 181 while rates of modeled surface melt are low and decreasing. However, Figure 2.8b clearly shows that the event is coincident with rapid uplift characteristic of a hydraulic jacking event [Iken and others, 1983]. During this event it seems that the temperature-index model is not accurately quantifying all of the sources of surface run off, such as supra-glacial lake drainages [Das and others, 2008; Hoffman and others, 2011] and enhanced surface melt due to high turbulent heat fluxes across the ice atmosphere interface [Hock, 2003].

During the days surrounding the speed-up event on day 181, 2007 a weather station near the GPS base station recorded air temperatures ranging from 2 to 5 $^{\circ}$C and sustained winds in excess of 5 $\mathrm{m\,s^{-1}}$ (Holland, pers. comm., 2009). Similar meteorological conditions, favoring high rates of atmospheric turbulent heat flux and enhanced rates of surface melt, were observed at Columbia Glacier in summer of 1987 [Meier and others, 1994]. In this case the timing of a short-lived speed-up event was best explained by an increase in the volume of stored water; with the subsequent extra slow-down occurring as the volume of stored water decreased. A second extra slow-down event, later in the same season on Columbia Glacier, coincided with heavy rainfall lasting two days. The inability to measure the meltwater discharge of Jakobshavn Isbræ makes it difficult to draw conclusions about the relation between basal motion and stored water. However, similarity to the extra slow-down events at Columbia Glacier and the characteristic vertical motion during events at Jakobshavn Isbræ suggest a common mechanism for the extra slow-downs of the two glaciers.

In addition to the enhanced surface melt in 2007—more than twice that in 2006 or 2008—there was also the occurrence of multiple lake drainage events. From day 179 to 183, seven lakes south of the glacier were observed to drain. This time period closely brackets the speed-up and subsequent extra slow-down events beginning on day 181. The high frequency of lake drainages during days 179 to 183 was the greatest within our study and is also large compared to an investigation of lake drainages by Hoffman and others [2011], who found typical lake drainage frequencies of one drainage per melt season or less. In this instance, supra-glacial lake drainage is another likely mechanism for rapid input of water to the glacier bed. As it was closest to the drained lakes and exhibited the largest velocity response, it seems likely that the speed-up and uplift event at southern-most site, P4, (Fig. 2.8c) is related to rapid input of surface water from supraglacial lakes draining to the bed. For the more distant ice sheet and glacier sites, it is more difficult to conclude whether the velocity response is due to lake drainage or surface melt. However, the lack of velocity response at the two ice sheet sites north of the glacier suggest that the velocity event on day 181 was primarily forced by lake drainage events rather than a region-wide surface melt event.

As discussed above, speed-up events are usually followed by a slow recovery to pre-speed up velocities. However, in summer 2007, two events led to large slow-downs that negated essentially the entire inter-annual acceleration for that year. A speed-up event on day 181 was followed by speeds below background speed for the next eight days (Fig. 2.3). Additionally, a second slow-down event (not fully captured in Figures 2.3 and 2.5 due to discontinuous GPS records) occurred around day 220. As a result of the data gap we cannot confirm that the day 220 slow-down was preceded by an initial speed-up. However, the day 220 slow-down, shown in Figure 2.3, led to an initial drop in velocity of 12% at C1 and affected the season-long average velocity. While slow-down events were also observed in 2006 (Fig. 2.8a), the magnitude of the 2007 events appear to be exceptional. The day 220 extra slow-down event is also captured in the SAR-derived data (Fig. 2.10), but the smaller magnitude events, such as on day 201 in 2006, are less obvious. Generally, a comparison between GPS and SAR speeds shows agreement of better than 3%. However, the GPS measurements are better suited for resolving the rapid nature and the amplitude of these speed-up/extra slow-down events (Fig. 2.10).

The 2007 melt season on Jakobshavn Isbræ was anomalous in timing and duration: It started earlier and was more intense than in the other years of our study (Fig. 2.5) as

well as many other years of the same decade [Mote, 2007; Mernild and others, 2010]. As a result of the longer melt season, the potential for extra slow-down events to influence ice motion was greater. It is possible that such long, intense melt seasons—such as in 2007—on Greenland outlet glaciers could act to moderate increasing flow speeds by offsetting melt-induced speed-ups with extra slow-downs. A similar process, through which seasonal speed-ups in the ablation area of the ice sheet are offset by more efficient drainage later in the season, has already been recognized over seasonal time scales [Colgan and others, 2011; Sundal and others, 2011]; and has been suggested as an important process over longer time scales as well [Truffer and Harrison, 2005; van de Wal and others, 2008].

2.5 Conclusions

We measured surface melt and ice motion for three melt seasons on Jakobshavn Isbræ and the adjacent ice sheet. While surface speeds on Jakobshavn Isbræ are remarkably steady, when compared to typical land-terminating glaciers, there are variations in glacier surface velocities over a wide range of time scales. On long time scales, three years of GPS measurements confirm that the glacier is still accelerating from year to year. However, there are indications that surface velocities deviate from a steady rate of acceleration in certain years. Between 2007 and 2008 there was very little (2% per year or less) inter-annual acceleration—a significant departure from the 4% to 8% per year observed in other years. The effect of these anomalies on glacier flow is strongest at sites nearest the terminus.

On seasonal time scales, the glacier experiences a steady spring acceleration—associated with the onset of glacier terminus retreat—with sites near the terminus speeding up first, followed by sites further upstream. Seasonal velocity variations rarely exceed 10% per year. This pattern of steady spring speed-up is interrupted each year by more variable flow with the beginning of the melt season. In the fall, after the end of the melt season, the glacier experiences a deceleration as the rate of calving slows and the terminus begins to gradually re-advance. The fall glacier deceleration happens uniformly on the lower glacier, which is possibly explained by thickening ice due to the cessation of ablation and calving and the influence of increased ice thickness on effective pressure, thereby reducing sliding. In spring, however, the floating tongue often breaks up rapidly and associated ice thickness changes on the glacier propagate upward from the terminus. The velocity response in spring is thus delayed and leads to an asymmetry in velocity response to changes in terminus position.

On even shorter time scales the seasonal evolution of surface speed is punctuated by brief speed-up events, with the largest events resulting in deviations of approximately 10% of background speed. After the steady spring speed-up, velocities on the glacier and ice sheet are more variable than in spring, and are closely related to the rate of surface melt. The presence of diurnal velocity variations during this time suggests that the glacier is able to respond to inputs of surface water on short time scales. Often, the speed-ups were followed by extra slow-down events, where the speeds following the event are lower than prior to the beginning of the event. This pattern of extra slow-downs following speed-ups was observed to occur multiple times in a given season.

While the duration of the speed-ups was typically short, the extra-slow downs resulted in periods of slower flow for as much as a week or longer. We attempt to partially explain the long duration of extra slow-downs with a simple model for the creep closure of a subglacial conduit. The large ice thickness of Jakobshavn Isbræ would be sufficient to collapse any subglacial channels within a matter of hours. However, the necessarily high basal water pressures imposed by the tidewater geometry decrease the rate of creep closure, thus favoring longer periods of increased effective pressure. The simple model explaining the duration of extra slow-down events is supported by the fact that there are no observed extra slow-downs at the ice sheet sites, where the bed topography is at or near sea level.

A likely mechanism responsible for generating pairs of speed-ups and extra slow-downs is the sudden input of large amounts of surface water, either from enhanced surface melt or the drainage of supraglacial lakes. This hypothesis is bolstered by observations made on Columbia Glacier in 1987 [Meier and others, 1994] where two extra slow-down events were explained by increases in stored water: in one instance from heightened rates of surface melt due to large atmospheric turbulent heat flux and in the second by a large rain event. Observations of similar extra slow-downs on Columbia Glacier, Kangiata Nunata Sermia [Sole and others, 2011] and on Jakobshavn Isbræ may suggest that this type of response to meltwater input is common on tidewater glacier systems.

In some cases, the long duration of extra slow-downs on Jakobshavn Isbræ suppressed glacier flow enough to cancel the enhanced flow resulting from the preceding speed-up. In summer of 2007 two particularly strong extra slow-downs exerted an influence on the mean flow for the entire season. The combined effect of these two events entirely cancelled the early spring speed-up in 2007 and is likely responsible for the negligible inter-annual acceleration from 2007 to 2008. The season-long influence of extra slow-downs on Jakob-

shavn Isbræ is identifiable in the remote sensing record, but in-situ observations of glacier flow are more suitable for investigating the underlying physical mechanisms responsible for the events. The use of a suite of complementary measurements providing wide spatial coverage and high temporal resolution is necessary for understanding how dynamic tidewater systems, like Jakobshavn Isbræ, will respond to future changes in climate.

Acknowledgements

Support for this project was provided by NASA's Cryospheric Sciences Program (NNG06GB49G). Logistical support was provided by CH2M Hill Polar Field Services and instrument support was provided by UNAVCO. We would like to thank J. Brown, M. Lüthi and R. J. Motyka for their help in the field. Thanks to S. Herried for his GIS wizardry. Helpful discussions with A. Aschwanden greatly improved the clarity of figures. Finally, we thank two anonymous reviewers for comments which greatly improved the clarity of the manuscript.

References

Amundson, J., M. Truffer, M. Lüthi, M. Fahnestock, M. West and R. Motyka, 2008. Glacier, fjord, and seismic response to recent large calving events, Jakobshavn Isbræ, Greenland. *Geophys. Res. Lett.*, **35**(22), L22501 (doi: 10.1029/2008GL035281).

Amundson, J., M. Fahnestock, M. Truffer, J. Brown, R. Motyka and M. Lüthi, 2010. Ice mélange dynamics and implications for terminus stability, Jakobshavn Isbræ, Greenland. *J. Geophys. Res.*, **115**(F1), F01005 (doi: 10.1029/2009JF001405).

Amundson, J., J. Clinton, M. Fahnestock, M. Truffer, R. Motyka and M. Lüthi, 2012. Observing calving-generated ocean waves with coastal broadband seismometers, Jakobshavn Isbræ, Greenland. *Ann. Glaciol.*, **53**(60), 79–84 (doi: 10.3189/2012/AoG60A200).

Andersen, M., T. Larsen, M. Nettles, P. Elosegui, D. van As, G. Hamilton, L. Stearns, J. Davis, A. Ahlstrøm, J. de Juan, G. Ekström, L. Stenseng, S. Khan, R. Forsberg and D. Dahl-Jensen, 2010. Spatial and temporal melt variability at Helheim Glacier, East Greenland, and its effect on ice dynamics. *J. Geophys. Res.*, **115**(F4), F04041 (doi: doi:10.1029/2010JF001760).

Bartholomaus, T., R. Anderson and S. Anderson, 2008. Response of glacier basal motion to transient water storage. *Nature Geosci.*, **1**(1), 33–37 (doi: 10.1038/ngeo.2007.52).

Bartholomew, I., P. Nienow, D. Mair, A. Hubbard, M. King and A. Sole, 2010. Seasonal evolution of subglacial drainage and acceleration in a Greenland outlet glacier. *Nature Geosci.*, **3**(6), 408–411 (doi: 10.1038/ngeo863).

Bøggild, C., O. Olesen, A. Ahlstrøm and P. Jørgensen, 2004. Automatic glacier ablation measurements using pressure transducers. *J. Glaciol.*, **50**(169), 303–304 (doi: 10.3189/172756504781830097).

Box, J., 2005. Greenland Ice Sheet surface mass-balance variability: 1991–2003. *Ann. Glaciol.*, **42**(1), 90–94 (doi: 10.3189/172756405781812772).

van den Broeke, M., J. Bamber, J. Ettema, E. Rignot, E. Schrama, W. van de Berg, E. van Meijgaard, I. Velicogna and B. Wouters, 2009. Partitioning recent Greenland mass loss. *Science*, **326**(5955), 984–986 (doi: 10.1126/science.1178176).

Cassotto, R., 2011. Implications of changing winter fjord ice mélanges for Greenland outlet glacier dynamics. (MS thesis, University of New Hampshire).

Colgan, W., H. Rajaram, R. Anderson, K. Steffen, T. Phillips, I. Joughin, H. Zwally and W. Abdalati, 2011. The annual glaciohydrology cycle in the ablation zone of the Greenland ice sheet: Part 1. Hydrology model, *J. Glaciol.*, **57**(204), 697–709 (doi: 10.3189/002214311797409668).

Cuffey, K. and W. Paterson, 2010. The Physics of Glaciers, Elsevier Ltd, 4th ed.

Das, S., I. Joughin, M. Behn, I. Howat, M. King, D. Lizarralde and M. Bhatia, 2008. Fracture propagation to the base of the Greenland Ice Sheet during supraglacial lake drainage. *Science*, **320**(5877), 778–781 (doi: 10.1126/science.1153360).

Echelmeyer, K. and W. Harrison, 1990. Jakobshavn Isbræ, West Greenland: Seasonal variations in velocity—or lack thereof. *J. Glaciol.*, **36**(122), 82–88.

Fausto, R., A. Ahlstrøm, D. van As, S. Johnsen, P. Langen and K. Steffen, 2009. Improving surface boundary conditions with focus on coupling snow densification and meltwater retention in large-scale ice-sheet models of Greenland. *Environ. Sci.*, **55**(193), 869–878 (doi: 10.3189/002214309790152537).

Gabor, D., 1946. Theory of communication. *J. Inst. Electr. Eng.*, **93**(26), 429–457.

Hanna, E., P. Huybrechts, K. Steffen, J. Cappelen, R. Huff, C. Shuman, T. Irvine-Fynn, S. Wise and M. Griffiths, 2008. Increased runoff from melt from the Greenland Ice Sheet: A response to global warming. *J. Clim.*, **21**(2), 331–341 (doi: 10.1175/2007JCLI1964.1).

Hock, R., 2003. Temperature index melt modeling in mountain areas. *J. Hydrol.*, **282**(1-4), 104–115 (doi: 10.1016/S0022-1694(03)00257-9).

Hoffman, M., G. Catania, T. Neumann, L. Andrews and J. Rumrill, 2011. Links between acceleration, melting, and supraglacial lake drainage of the western Greenland Ice Sheet. *J. Geophys. Res.*, **116**(F4), F04035 (doi: 10.1029/2010JF001934).

Holland, D., R. Thomas, B. de Young, M. Ribergaard and B. Lyberth, 2008. Acceleration of Jakobshavn Isbræ triggered by warm subsurface ocean waters. *Nature Geosci.*, **1**(10), 659–664 (doi: 10.1038/ngeo316).

Iken, A., H. Röthlisberger, A. Flotron and W. Haeberli, 1983. The uplift of Unteraargletscher at the beginning of the melt season—a consequence of water storage at the bed? *J. Glaciol.*, **29**(101), 28–47.

Joughin, I., W. Abdalati and M. Fahnestock, 2004. Large fluctuations in speed on Greenland's Jakobshavn Isbræ glacier. *Nature*, **432**(7017), 608–610 (doi: 10.1038/nature03130).

Joughin, I., I. Howat, M. Fahnestock, B. Smith, W. Krabill, R. Alley, H. Stern and M. Truffer, 2008a. Continued evolution of Jakobshavn Isbræ following its rapid speedup. *J. Geophys. Res.*, **113**(F4), F04006 (doi: 10.1029/2008JF001023).

Joughin, I., S. Das, M. King, B. Smith, I. Howat and T. Moon, 2008b. Seasonal speedup along the western flank of the Greenland Ice Sheet. *Science*, **320**(5877), 781–784 (doi: 10.1126/science.1153288).

Joughin, I., B. Smith, I. Howat, D. Floricioiu, R. Alley, M. Truffer and M. Fahnestock, 2012.Seasonal to decadal scale variations in the surface velocity of Jakobshavn Isbrae, Greenland: Observation and model-based analysis, *J. Geophys. Res.*, **117**(F2), F02030 (doi: 10.1029/2011JF002110).

Kamb, B., H. Engelhardt, M. Fahnestock, N. Humphrey, M. Meier and D. Stone, 1994. Mechanical and hydrologic basis for the rapid motion of a large tidewater glacier 2. Interpretation. *J. Geophys. Res.*, **99**(B8), 15231–15244 (doi: 10.1029/94JB00467).

Krabill, W., E. Hanna, P. Huybrechts, W. Abdalati, J. Cappelen, B. Csatho, E. Frederick, S. Manizade, C. Martin, J. Sonntag, R. Swift, R. Thomas and J. Yungel, 2004. Greenland Ice Sheet: Increased coastal thinning. *Geophys. Res. Lett.*, **31**(24), L24402 (doi: 10.1029/2004GL021533).

Luckman, A. and T. Murray, 2005. Seasonal variation in velocity before retreat of Jakobshavn Isbræ, Greenland. *Geophys. Res. Lett.*, **32**(8), L08501 (doi: 10.1029/2005GL022519).

Meier, M. and A. Post, 1987. Fast Tidewater Glaciers. *J. Geophys. Res.*, **92**(B9), 9051–9058.

Meier, M., S. Lundstrom, D. Stone, B. Kamb, H. Engelhardt, N. Humphrey, W. Dunlap, M. Fahnestock, R. Krimmel and R. Walters, 1994. Mechanical and hydrologic basis for the rapid motion of a large tidewater glacier 1. Observations. *J. Geophys. Res.*, **99**(B8) 15219–15229.

Mernild, S., G. Liston, K. Steffen and P. Chylek, 2010. Meltwater flux and runoff modeling in the ablation area of Jakobshavn Isbræ, West Greenland. *J. Glaciol.*, **56**(195), 20–32 (doi: 10.3189/002214310791190794).

Moon, T. and I. Joughin, 2008. Changes in ice front position on Greenland's outlet glaciers from 1992 to 2007. *J. Geophys. Res.*, **113**(F2), F02022 (doi: 10.1029/2007JF000927).

Mote, T., 2007. Greenland surface melt trends 1973–2007: Evidence of a large increase in 2007. *Geophys. Res. Lett.*, **34**(22), L22507 (doi: 10.1029/2007GL031976).

Motyka, R., M. Truffer, M. Fahnestock, J. Mortensen, S. Rysgaard and I. Howat, 2011. Submarine melting of the 1985 Jakobshavn Isbræ floating tongue and the triggering of the current retreat. *J. Geophys. Res.*, **116**(F1), F01007 (doi: 10.1029/2009JF001632).

Nick, F., A. Vieli, I. Howat and I. Joughin, 2009. Large-scale changes in Greenland outlet glacier dynamics triggered at the terminus. *Nature Geosci.*, **2**(2), 110–114 (doi: 10.1038/ngeo394).

Nye, J., 1953. The flow law of ice from measurements in glacier tunnels, laboratory experiments and the Jungfraufirn borehole experiment. *Proc. R. Soc.*, **219**(1139), 477–489.

Parizek, B. and R. Alley, 2004. Implications of increased Greenland surface melt under global-warming scenarios: ice-sheet simulations. *Quat. Sci. Rev.*, **23**(9-10), 1013–1027 (doi: 10.1016/j.quascirev.2003.12.024).

Pfeffer, W., 2007. A simple mechanism for irreversible tidewater glacier retreat. *J. Geophys. Res.*, **112**(F3), F03S25 (doi: 10.1029/2006JF000590).

Plummer, J., S. Gogineni, C. van der Veen, C. Leuschen and J. Li, 2008. Ice thickness and bed map for Jakobshavn Isbræ. *CReSIS Tech. Report*, **2008-1**, (2008).

Podlech, S. and A. Weidick, 2004. A catastrophic break-up of the front of Jakobshavn Isbræ, West Greenland, 2002/03. *J. Glaciol.*, **50**(168), 153–154 (doi: 10.3189/172756504781830231).

Podrasky, D., M. Truffer, M. Fahnestock, M. Lüthi, 2010. Short period velocity response to tides and calving near the terminus of Jakobshavn Isbræ. Abstract C23C-0636 Poster presented at 2010 Fall Meeting, AGU, San Francisco, Calif., 13-17 Dec.

Rignot, E. and P. Kanagaratnam, 2006. Changes in the velocity structure of the Greenland Ice Sheet. *Science*, **311**(5763), 986–90 (doi: 10.1126/science.1121381).

Röthlisberger, H., 1972. Water pressure in intra- and subglacial channels. *J. Glaciol.*, **11**(62), 7–13.

Schoof, C., 2007. Ice sheet grounding line dynamics: Steady states, stability, and hysteresis. *J. Geophys. Res.*, **112**(F3), F03S28 (doi: 10.1029/2006JF000664).

Schoof, C., 2010. Ice-sheet acceleration driven by melt supply variability. *Nature*, **468**(7325), 803–806 (doi: 10.1038/nature09618).

Sohn, H., K. Jezek and C. van der Veen, 1998. Jakobshavn Glacier, west Greenland: 30 years of spaceborne observations. *Geophys. Res. Lett.*, **25**(14), 2699–2702 (doi: 10.1029/98GL01973).

Sole, A., D. Mair, P. Nienow, I. Bartholomew, M. King, M. Burke and I. Joughin, 2011. Seasonal speedup of a Greenland marine-terminating outlet glacier forced by surface melt-induced changes in subglacial hydrology. *J. Geophys. Res.*, **116**(F3), F03014 (doi: 10.1029/2010JF001948).

Sundal, A., A. Shepherd, P. Nienow, E. Hanna, S. Palmer and P. Huybrechts, 2011. Melt-induced speed-up of Greenland Ice Sheet offset by efficient subglacial drainage. *Nature*, **469**(7331), 521–524 (doi: 10.1038/nature09740).

Thomas, R., E. Frederick, W. Krabill, S. Manizade and C. Martin, 2009. Recent changes on Greenland outlet glaciers. *J. Glaciol.*, **55**(189), 147–162 (doi: 10.3189/002214309788608958).

Truffer, M., W. Harrison and R. March, 2005. Record negative glacier balances and low velocities during the 2004 heatwave in Alaska, USA: implications for the interpretation of observations by Zwally. *J. Glaciol.*, **51**(175), 663–664 (doi: 10.3189/172756501781831747).

Vieli, A., M. Funk and H. Blatter, 2001. Flow dynamics of tidewater glaciers: A numerical modelling approach. *J. Glaciol.*, **47**(159), 595–606.

van de Wal, R., W. Boot, M. van den Broeke, C. Smeets, C. Reijmer, J. Donker and J. Oerlemans, 2008. Large and rapid melt-induced velocity changes in the ablation zone of the Greenland Ice Sheet. *Science*, **321**(5885), 111–113 (doi: 10.1126/science.1158540).

Zwally, H., W. Abdalati, T. Herring, K. Larson, J. Saba and K. Steffen, 2002. Surface melt-induced acceleration of Greenland Ice-Sheet flow. *Science*, **297**(5579), 218–222 (doi: 10.1126/science.1072708).

Appendix 2.A

Beginning with the total derivative for a vector field of velocity, υ,

$$\frac{d\upsilon}{dt} = \frac{\partial \upsilon}{\partial t} + \upsilon \cdot (\nabla \upsilon) \tag{2.A.1}$$

the total derivative of the longitudinal (along flow) component, u, of the velocity is

$$\frac{du}{dt} = \frac{\partial u}{\partial t} + u\frac{\partial u}{\partial \xi}. \tag{2.A.2}$$

The acceleration of Jakobshavn Isbræ has been observed to scale with surface speeds. In other words, acceleration is greatest in fast flowing regions. A reasonable way to describe this type of acceleration is to treat it as a percent acceleration, where all points on the glacier speed up by the same constant amount proportional to speed. For a constant relative acceleration, α, the acceleration is related to the velocity by

$$\alpha = \frac{1}{u}\frac{\partial u}{\partial t}. \tag{2.A.3}$$

While the relative acceleration does not vary with position, the time rate of change of velocity does change. In the case of Jakobshavn Isbræ it will be greatest near the terminus and decrease upstream. Such a distribution of acceleration imposes a time-dependent strain rate. To find the strain rate as a function of time we start by integrating Equation (2.A.3):

$$u(\xi, t) = u_0 e^{\alpha(t-t_0)} \tag{2.A.4}$$

and then differentiate Equation (2.A.4) once with respect to ξ,

$$\frac{\partial u}{\partial \xi} = \frac{\partial u_0}{\partial \xi} e^{\alpha(t-t_0)}. \tag{2.A.5}$$

Since α is a constant with respect to ξ and the gradient of velocity defines the strain rate, the time-dependent strain rate is

$$\dot{\varepsilon}_\xi(t) = \dot{\varepsilon}_{\xi,0} e^{\alpha(t-t_0)}. \tag{2.A.6}$$

Substituting Equations (2.A.5) and (2.A.3) into Equation (A.37) results in the following for the total derivative:

$$\frac{du}{dt} = \left(\alpha + \dot{\varepsilon}_{\xi,0} e^{\alpha(t-t_0)}\right) u, \tag{2.A.7}$$

which is separable and can be integrated to find the time-dependent velocity,

$$\ln \frac{u(t)}{u_0} = \alpha(t-t_0) + \frac{\dot{\varepsilon}_{\xi,0}}{\alpha}\left(e^{\alpha(t-t_0)} - 1\right). \tag{2.A.8}$$

Here we argue that where values of α are small—and time intervals are not greater than a year—then Equation (2.A.6) will be approximately linear, even for fast-flowing Jakobshavn Isbræ. Expanding the exponential and integrating Equation (2.A.8) we find an expression for the expected position as a function of time:

$$\xi_{\text{exp}}(t) \approx \xi_0 + \frac{u_0}{\alpha + \dot{\varepsilon}_{\xi,0}} \left(e^{(\alpha + \dot{\varepsilon}_{\xi,0})(t - t_0)} - 1 \right). \tag{2.A.9}$$

Defining γ as the sum of α and $\dot{\varepsilon}_{\xi,0}$ the expected position is

$$\xi_{\text{exp}}(t) \approx \xi_0 + \frac{u_0}{\gamma} \left(e^{\gamma(t - t_0)} - 1 \right). \tag{2.A.10}$$

While this treatment does not allow for discrimination between the acceleration and strain rate, the primary purpose of Equation (2.A.10) is to remove most of the signal associated with the effects of large strain rates and inter-annual acceleration from the GPS position time series.

Chapter 3
Quantifying velocity response to ocean tides and calving near the terminus of Jakobshavn Isbræ, Greenland [1]

Abstract

Dynamic changes on Greenland outlet glaciers are a primary driver for increases in ice sheet mass loss and contribution to sea level rise. One dramatic example of such change has been observed at Jakobshavn Isbræ, which has thinned, retreated and doubled in speed since the early 2000s. Complementary to large changes on decadal scales, we document the glacier response on shorter time scales, driven by tidal forcing and calving events. During a fourteen-day period in August 2009, we documented changes in geometry and speed near the terminus. On this timescale ice flow responds to forcing at the front from iceberg calving and ocean tides. We note a step increase in velocity near the terminus during a large calving event with transient deceleration in the days following the event. A simple calving response model explains from 94 % to 99 % of variations in detrended positions at four sites considered. During each day, variability due to tidal forcing explains from 10 % to 90 % of the remaining variability after removing the effects of the calving response model. The influence of the tidal forcing on flow decays upstream with a characteristic length scale of 2 km, comparable to about two ice thicknesses.

3.1 Introduction

In the first decade of the 21st century the majority of tidewater outlet glaciers of the Greenland Ice Sheet steadily retreated at a rate in excess of 100 $\mathrm{m\,a^{-1}}$, on average [Moon and Joughin, 2008]. In most cases, this pattern of retreat has been coincident with a trend of increasing surface speeds [Moon and others, 2012]. In addition, higher rates of frontal ablation have resulted in rapid thinning on many of Greenland's largest outlet glaciers [Thomas and others, 2009]. As mass losses at the calving fronts of outlet glaciers make up a large fraction of observed mass loss of the Greenland Ice Sheet [Rignot and Kanagaratnam, 2006; van den Broeke and others, 2009], such widespread changes on outlet glaciers have the potential to increase rates of mass wastage and contribution to global sea level.

[1] In review in *Journal of Glaciology* as Podrasky, D., M. Truffer, M. Luthi, and M. Fahnestock, 2013. Quantifying velocity response to ocean tides and calving near the terminus of Jakobshavn Isbræ, Greenland

There is a growing body of evidence showing that the rapid changes seen at Greenland outlet glaciers are primarily driven by changes at the glacier front [Joughin and others, 2008; Nick and others, 2009, 2013]. The forcing which drives changes at the glacier termini seems to be, at least partially, related to climate through warmer ocean waters along the coast of Greenland [Holland and others, 2008; Howat and others, 2008]. Changes initiated at the terminus are then propagated inland as changes in ice thickness and surface slope [Joughin and others, 2012]. Such rapid, dynamic changes in geometry have allowed the Greenland Ice Sheet to respond to climate perturbations at a rate much faster than predicted by the response to surface mass balance forcing alone [Nye, 1960].

Constraining the response of outlet glaciers to climate forcing on decadal timescales demands a solid understanding of dynamic processes occurring over short timescales. These include perturbations to glacier motion from iceberg calving, ocean tides and surface meltwater forcing with the potential for altering outlet glacier geometries. While changes in the length and thickness of oulet glaciers are most pronounced near glacier terminii, making in-situ measurements in the near-terminus region of tidewater glaciers is notoriously challenging due to rapid flow speeds, heavy surface crevassing and iceberg calving. While remote sensing methods have improved a great deal, repeat cycles of a week or more limit investigations of glacier processes on short timescales.

Outlet glacier response to large-scale calving events and, where applicable, ice shelf retreat has been documented in Greenland [Nick and others, 2012; Luckman and Murray, 2005] and Antarctica [Scambos, 2004]. These results demonstrate a pattern of glacier acceleration and thinning following the catastrophic collapse of ice shelves or floating tongues, consistent with ice shelf buttressing hypotheses [Dupont and Alley, 2005]. While reduced in magnitude and reach, the response to smaller (non-catastrophic) calving events is of a similar nature displaying increases in speed and extension and/or thinning [Amundson and others, 2008; Nettles and others, 2008; Rosenau and others, 2013]. A predictable response to calving events over a continuum of magnitudes illustrates that, while response to smaller calving events is limited in spatial and temporal scope compared with catastrophic retreats, such events play an important role in outlet glacier dynamics by controlling glacier geometry near the terminus.

Modeling glacier calving has proven to be a challenging problem, but the periodic forcing applied to tidewater glaciers by ocean tides is easily predicted. However, the wide range of glacier response to the consistent forcing provided by tides demonstrates the di-

versity of tidewater glacier systems: In Antarctica, evidence of ice stream response to tidal forcing has been observed as far as 80 km inland of the grounding zone [Anandakrishnan and others, 2003], while results from Alaskan tidewater glaciers indicate a far less extensive response of a few kilometers or less [Walters, 1989; O'Neel and others, 2001]. In Greenland, the behavior in response to tidal forcing falls between Antarctic and Alaskan end members; results from Helheim Glacier [De Juan and others, 2010] show tidal response extending up to ~ 10 km from the terminus.

In addition to spatial patterns of response, glacier response to tides can be classified based on the phase difference between the tidal forcing and glacier response. Results from the majority of studies indicate that ocean tides and modulated glacier speeds are roughly out of phase, so that speeds are greatest when tidal height is at a minimum or during periods of falling tide. This type of response suggests that tides are providing periodic variations in back-stress at the glacier front [Thomas, 2007]. In a limited number of cases tidal height and modulated glacier speed have been observed to be in phase, particularly for low-frequency tidal constituents [Gudmundsson, 2006; Murray and others, 2007]. Correlation between tidal forcing and glacier motion has been explained in terms of a buoyant force exerted by ocean tides and a reduction in friction at pinning points on the glacier bed [Heinert and Riedel, 2007]. Alternatively, Gudmundsson [2007] proposed a non-linear relation between tidal height and basal rheology to explain the in-phase response to tides on Rutford Ice Stream. Differences in the strength, phase and spatial pattern of response to tidal forcing demonstrate the utility of investigations of short-term variations in flow of tidewater glaciers as a tool for evaluating the sensitivity of marine-terminating systems to various modes of forcing at the ice front and/or grounding zone.

Despite the emphasis on variations, overall the flow of tidewater glaciers tends to be more steady than other glacier systems [Clarke, 1987]. This has been particularly true of Greenland's fastest tidewater outlet, Jakobshavn Isbræ [Bindschadler, 1984], where speeds have been very steady over intra-annual timescales [Echelmeyer and Harrison, 1990; Luckman and Murray, 2005; Podrasky and others, 2012]. Velocity variations occurring on sub-seasonal time scales are obscured by the exceptionally high flow speeds, as much as 12 km a^{-1} [Joughin and others, 2012], along the main channel of the glacier.

This study aims to identify and quantify short-term flow variations at Jakobshavn Isbræ by decomposing time series of glacier motion with a suite of simple models to identify the relative influence of the sources responsible for forcing short-term variations. We

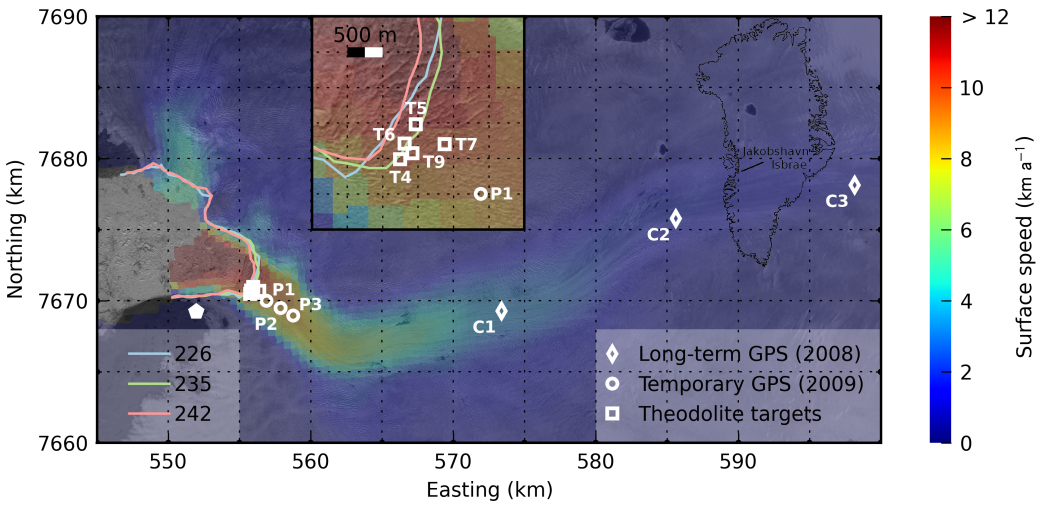

Figure 3.1: Day 218, 2009 SPOT scene showing the Jakobshavn Isbræ study area. The image is overlaid with surface speeds from a 2008 SAR mosaic of Greenland [Joughin and others, 2010]. White symbols mark the locations of long-term GPS (2008 data), temporary GPS, and theodolite optical targets. The location of the GPS base station and automatic theodolite is marked by the white pentagon. Terminus outlines digitized from Landsat 7 scenes acquired on days 226, 235 and 242 are shown in blue, green and red.

examine 14 days of high-rate motion data recorded in the near-terminus region of Jakobshavn Isbræ during August 2009. Two simple models for explaining glacier response to ocean tidal forcing and iceberg calving are used to estimate the strength of variations attributable to these two modes of forcing at the terminus. Once quantified, the responses to a single large calving event and periodic tidal forcing are then compared with background motion, described by a linear model for glacier motion time series during the two-week study period.

3.2 Data and Methods

3.2.1 Ice motion

Three temporary GPS sites were occupied during a 12 day period in August 2009. Dual frequency receivers were used at all GPS sites with a 15 s sampling interval. GPS data were processed kinematically with *Track* (v. 1.22), part of the GAMIT/GLOBK GPS processing package [Chen, 1999] with typical baseline distances of 5–50 km. Five optical markers were

Table 3.1: Data coverage for near-terminus glacier sites given in day of year in 2009. T sites indicate positions measured with an automatic theodolite, P site positions were measured with GPS receivers and C site positions (year 2008) were measured with long-deployment campaign GPS receivers.

Site	Days
T4	228–233
T5	228–233
T6	228–233
T7	228–241
T9	233–241
P1	228–239
P2	228–239
P3	228–239
C1	131–205 (2008)
C2	131–219 (2008)
C3	133–207 (2008)

deployed at sites 1–2 km from the terminus (Fig. 3.1). The optical targets were surveyed with a Leica 1610 automatic theodolite and DI3000S distomat. Two additional reference targets were placed on bedrock in the forefield to correct for small amounts of motion due to thermal expansion of the steel theodolite stand. The known distances to the reference targets combined with measurements of ambient air temperatures were used to correct for refractive errors in distance measurements to the optical targets located on the glacier. Measurements of optical marker positions were repeated approximately every 10–15 min during the 14 day study period (Tab. 3.1). However, the record of theodolite positions was interrupted during certain time periods due to windy conditions (Fig. 3.2). Horizontal position data of each site were rotated into a local flow-parallel direction.

Due to large baseline distances, the theodolite data are subject to large errors relative to the GPS measurements. Some of these errors are obvious outliers, far removed from the rest of the data. More often, theodolite errors are smaller and can be attributed to instrumental error and atmospheric delays. The theodolite data were detrended with a best-fit

linear model and data points more than one standard deviation away from the trend were identified as outliers and excluded from the analysis. Once outliers were removed the position data were smoothed to reduce the influence of measurement error. A local quadratic regression filter (LOWESS), implemented with Matlab (v. 7.14), was used for smoothing the theodolite data. The size of the smoothing window was 8 data points, or approximately 2 hr. Position data from GPS were down-sampled, using an interval-averaging routine, to a rate of 15 min. Position time series of GPS sites were not smoothed after re-sampling. We include results of GPS data in 2008 from a previous study [Podrasky and others, 2012] to provide estimates of surface speed and constrain the response to ocean tides at positions 20–50 km upstream from the terminus, however as these data are from the previous year, we do not include them in the calving and tidal response analyses of this study.

3.2.2 Iceberg calving

During the study period, one large calving event occured on day 233 and was the only calving activity over the 14 days of interest. The precise timing of calving onset was constrained with passive seismic data [Amundson and others, 2012] acquired near the GPS base station. The magnitude of calving event can be qualified with time lapse photography near the terminus and tide data measured in the inner fjord. It is difficult to estimate the volume of ice calved from these data sets, but we can constrain the change in terminus position due to calving and glacier motion using satellite remote sensing data. Terminus positions were determined for three days in August with available Landsat scenes. The calving front was digitized from scenes on days 226, 235 and 242. The distance from each site to the terminus was estimated by integrating the length of a flow line from each site to the terminus. Flow lines passing through GPS and theodolite markers were derived from 2008 SAR data [Joughin and others, 2010].

Amundson and others [2008] describe response to calving as a step-change in glacier speed. We model the horizontal position response to calving, ξ_{calv}, with a piecewise, second-order polynomial

$$\xi_{\mathrm{calv}}(t) = \begin{cases} \frac{1}{2}a_1(t_\mathrm{c}-t)^2 + v_1(t_\mathrm{c}-t) + \xi_0 & t < t_\mathrm{c} \\ \frac{1}{2}a_2(t-t_\mathrm{c})^2 + v_2(t-t_\mathrm{c}) + \xi_0 & t \geq t_\mathrm{c} \end{cases} \tag{3.1}$$

with two intervals and an interior knot, t_c, at the time of the calving event on day 233. The best-fitting kinematic parameters, a_i, v_i and ξ_0, where $i = 1,2$, are determined using a

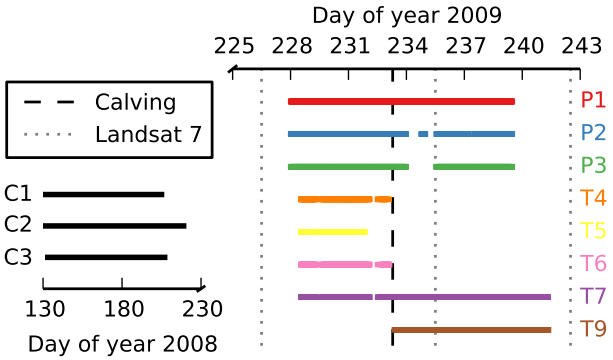

Figure 3.2: Coverage of GPS and theodolite data for the 2009 and 2008 data sets. The dashed line marks the timing of the calving event on day233 and dotted lines indicate the timing of Landsat 7 scenes used to digitize the ice front.

linear least-squares optimization. To ensure continuity of modeled positions for both time intervals, ξ_0 is constrained to the same value before and after the calving event. We apply the calving model to six days of position data centered about t_c.

As a consequence of extraordinarily large longitudinal strain rates in the terminus region of Jakobshavn Isbræ, the second order terms a_1 and a_2 encompass the effects of motion through a velocity gradient as well as acceleration. It is necessary to separate the combined effects in order to estimate values of pre- and post-calving acceleration at the GPS and optical markers. Here we use methods similar to those described by Amundson and others [2008] and Podrasky and others [2012]. Equation (4) from Podrasky and others [2012] reads

$$\xi_{\mathrm{exp}}(t) = \xi_0 + \frac{u_0}{\gamma}\left(e^{\gamma(t-t_0)} - 1\right), \tag{3.2}$$

where ξ_{exp} is the horizontal position, u_0 is the along-flow velocity at initial time, t_0. The combined acceleration term,

$$\gamma = \frac{1}{u}\frac{\partial u}{\partial t} + \dot{\varepsilon}_{\xi,0}, \tag{3.3}$$

is the sum of longitudinal strain rate, $\dot{\varepsilon}_{\xi,0}$, and a constant, relative acceleration term, where the acceleration is assumed to be proportional to velocity, u. Expanding Eqn (3.2) gives

$$\xi_{\mathrm{exp}}(t) \approx \xi_0 + u_0(t-t_0) + \frac{u_0\gamma}{2}(t-t_0)^2, \tag{3.4}$$

which has the same form as Eqn (3.1). Equating ξ_{calv} with ξ_{exp} implies $v_i = u_0$ and

$$a_i = u_0\left(\frac{1}{u}\frac{\partial u}{\partial t} + \dot{\varepsilon}_{\xi,0}\right). \tag{3.5}$$

Table 3.2: Strongest constituents of tidal record in Ilulissat.

Constituent	Frequency (d^{-1})	Period (h)	Amplitude (m)
MSF	0.0677	354.3671	0.0415
O_1	0.9295	25.8193	0.1176
K_1	1.0027	23.9345	0.3268
M_2	1.9323	12.4206	0.6726
S_2	2.0000	12.0000	0.3187

Over small time intervals, $u \approx u_0$ and

$$\frac{\partial u}{\partial t} = a_\mathrm{i} - u_0 \dot{\varepsilon}_{\xi,0}. \tag{3.6}$$

Using strain rates estimated from GPS and theodolite data along with parameters a_i and v_i we use Eqn (3.6) to solve for accelerations in the days before and after large calving events.

3.2.3 Tidal analysis

Tides were measured with a pressure transducer in the ice fjord within 5 km of the calving front concurrent with the 14 days of ice motion measurements and a longer record from Ilulissat shows close agreement with tides in the ice fjord. The Ilulissat tide record was analyzed with the T_TIDE package [Pawlowicz and others, 2002] in order to identify the strongest tidal constituents.

The amplitude and frequency of significant tidal constituents are listed in Table 3.2. The tides measured in the inner fjord incorporate noise including surface waves generated by calving events and other sources, as well as small instrument error. While the measured tides provide valuable information, such as the timing of major calving events, the record of tidal stage in the inner fjord does not fully cover the time span of glacier motion data. We use the longer record of tides recorded in Ilulissat harbor to analyze the tidal response of the glacier. The two tidal data sets are in close agreement, with no measurable delay in time and maximum difference in stage < 10 cm. While the Ilulissat record has much less noise than the fjord measurements, some sources of noise are still present. Sources of noise include instrumental error and waves generated by major calving events in the inner

fjord. To eliminate the noise in the Ilulissat tide data, we solved for the amplitude, A, and phase, ϕ, of known frequencies, f, of the major tidal constituents identified with T_TIDE. The smooth, noiseless ocean tide model,

$$H(t) = \mathrm{Re} \sum_{k=1}^{n} A_k e^{2\pi i f_k t + \phi_k} \tag{3.7}$$

is used in subsequent steps of the tidal analysis.

We calculate daily values of tidal admittance, the ratio between tidal response and tidal height, in horizontal (along flow) and vertical tidal repsonse components at each glacier site for each day of data. Day-long records of position data were first detrended to remove the background signal associated with rapid, constant-speed motion. The method we employ for calculating tidal admittance uses position data, not speeds. By using position data directly, the calculations are subject to less noise than would be introduced by differentiating to produce velocity time series. However, assuming ocean tides modulate ice flow the tidal response will be expressed in the slope of glacier position time series and it is not possible to directly compare horizontal glacier positions with tidal height.

To determine the influence of tides on glacier motion we propose a simple model based on reconstructed tides to explain the variability of detrended positions. Tide data are modified using two parameters to best fit position data: phase difference between tides and detrended position, and an amplitude multiplier (admittance). A grid search method is used to find the optimal parameters (phase and admittance) for modeling tidal response each day.

There are three plausible hypotheses to explain the relation of horizontal motion to tides: 1. Tides may modulate glacier flow through an elastic response to changing pressure on the vertical calving face, in which case glacier position and tides will be anti-correlated. 2. Ocean tides could affect basal water pressure in the terminus region, thereby influencing basal motion and surface speeds will be correlated with tidal height. 3. The glacier may respond viscously to perturbations in horizontal compressive stress exerted by tides resulting in variations of along flow strain rate and surface speed will be anti-correlated with tidal height. Additionally, tidal height and glacier position will experience a phase difference of 90°. To allow for these possible modes of tidal response we search over both positive and negative values of tidal admittance. However, when modeling vertical admittance we only optimize for positive values of tidal admittance. We search over an m- by n-size grid of these two parameters for tidal admittance, Λ, and time delay, δt, to

find the best fitting model for tidal response which minimizes the χ^2 difference between measured, detrended positions, ξ_{lin}, and modeled positions, while accounting for position uncertainty (σ_ξ):

$$\chi^2_{m,n} = \frac{(\xi_{lin} - \Lambda_m H(t - \delta t_n))^2}{{\sigma_\xi}^2}. \tag{3.8}$$

We use two criteria for evaluating the physical and statistical validity of each day's model results. Results for horizontal tidal admittance with positive phase differences between modeled positions and tides are excluded on the basis that the response to tides cannot precede the tidal forcing. F-tests were performed for the results of each day to validate the significance of the model. Results without a statistically significant model are excluded from further analysis.

Tidal analysis of the 2008 GPS data at sites C1, C2 and C3 was performed using a different method. To calculate admittances at these sites we take the ratio of the amplitude at the M_2 frequency, from analysis of position data using T_TIDE, and the amplitude of the M_2 ocean tide constituent in Tab. 3.2. This method is similar to the approach used by O'Neel and others [2001] and assumes that the only source of modulation at the M_2 frequency is due to ocean tides.

3.3 Results

3.3.1 Ice motion

Processing of GPS observations resulted in position time series for the three P-sites spanning days 228 to 239 (in 2009). Power failures resulted in limited periods of missing data at sites P2 and P3. At these temporary GPS sites, we estimate a 10 mm uncertainty in horizontal positions and a 20 mm uncertainty in vertical positions by examining the level of noise present in brief spans of data. GPS observations at the long-deployment C-sites were processed over a longer time span during 2008, a year prior to the measurements acquired for the current study. At these continuous sites, we estimate a 6 mm uncertainty in horizontal positions and 20 mm in vertical positions. Theodolite-measured horizontal positions have an estimated uncertainty of 70 mm; for vertical positions we estimate an uncertainty of 100 mm. Some of the optical targets were placed very near the terminus and during a large calving event on day 233 three of the targets were destroyed. Subsequently, one optical target that was not visible at the time of deployment, could be measured following the calving event.

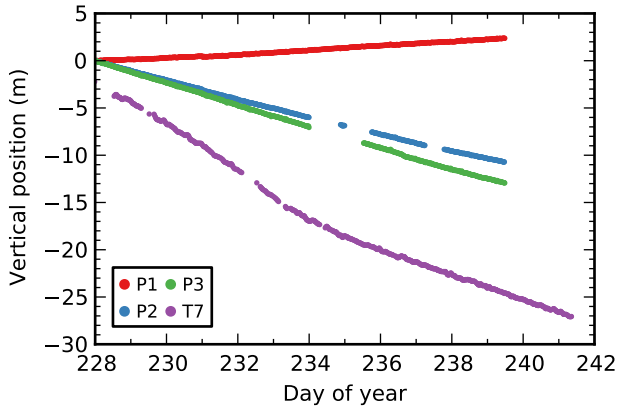

Figure 3.3: Vertical trajectories of the three temporary GPS markers (P1, P2 and P3) and optical marker T7. The lower most GPS site, P1 (red), experienced steady upward motion totaling ~ 3 m over 12 days.

Time series of vertical positions at the GPS indicate very steady rates of vertical motion, however, vertical positions of the optical markers display a greater degree of variability with time (Fig. 3.3). Curiously, the vertical time series for site P1 shows steadily increasing vertical position over the study period. The total upward motion at P1 was ~ 3 m over a period of 12 days. This upward vertical trajectory was only observed at P1.

Ice surface speeds are greatest near the calving front and rapidly decay with distance upstream. A maximum speed of 48 m d^{-1} was recorded after the calving event on day 233 at an optical target located $\sim$1 km from the front. Surface speeds decrease to ~ 10 m d^{-1} at a distance of 20 km and decrease more gradually at greater distances (Fig. 3.4). We find that our surface speeds agree well with other observations [Joughin and others, 2012].

The distribution of speeds over the lower glacier is consistent with the large longitudinal strain rates in the terminus region (Fig. 3.5). The greatest strain rates are found between the lower-most pair of sites, P1 to T7, with typical values of 2–4 a^{-1}, decreasing to ~ 0.25 a^{-1} 2 km upstream.

Glacier surface speeds at sites nearest the terminus experience the greatest degree of variability, with variations more muted upstream. Ice surface speeds in the near-terminus region exhibit variability at diurnal and semi-diurnal frequencies. They also display transient velocity features and sudden changes in speed (Fig. 3.6). Short-term variability at long-deployment GPS sites is primarily diurnal, but also includes episodic changes in

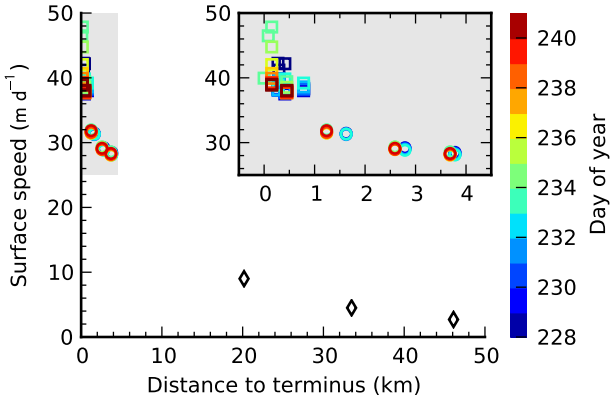

Figure 3.4: Daily-average surface speeds, at GPS and optical marker locations, used to detrend each day's position data prior to performing the tidal analysis. Points are color-coded by day of year. Black markers indicate mean speeds from the 2008 data set for reference. The gray shaded region indicates the range of the inset figure.

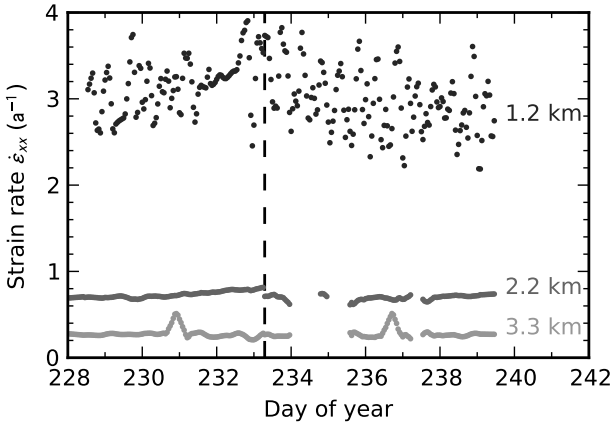

Figure 3.5: Longitudinal strain rates between one optical target and temporary GPS sites. Strain rates between P1 and T7 (black), P2 and P1 (gray), and P3 and P2 (light gray). Curves are annotated with the mean distance to the terminus. The timing of a large calving event on August 12 is marked by a vertical dashed line.

speed on the order of 10% of average speed [Podrasky and others, 2012]. In all cases, the amplitude of these variations is small in proportion with the magnitude of background speeds. The magnitudes of short-term variations amount to 5–10% of background at all sites.

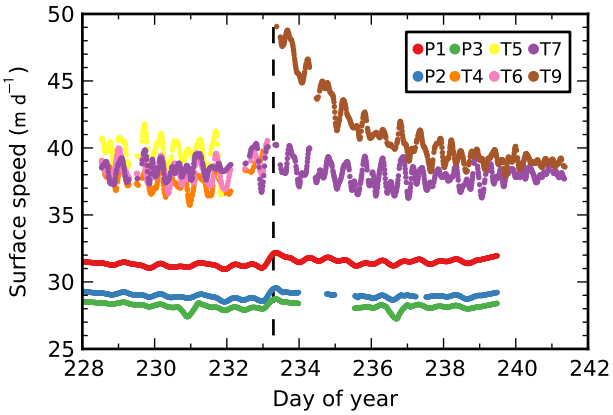

Figure 3.6: Time series of surface speeds at optical target and temporary GPS sites (T- and P-sites). The timing of a large calving event on August 12 is marked by a vertical dashed line.

3.3.2 Iceberg calving

A major calving event was documented with time lapse photography on day 233, and the precise timing of onset, 06:56 UTC, was identified in the seismographic record. This was the only major calving event recorded during the study. The loss of calved ice resulted in a significant change in terminus position and shortened the distance from the ice front to the GPS and optical targets by approximately 500 m (Fig. 3.1). The change in distance to the calving front was quantified as described in the methods section, and distance values were updated at the time of the calving event on day 233. While the calving event occurred two days before the position of the terminus was digitized, on day 235, we assume that distance to the terminus did not change significantly from day 233 to 235. We examine the error from this assumption by estimating the change in length of the lower glacier due to longitudinal strain. Applying a strain rate of 3 a^{-1} to the two days of motion results in a strain of $\sim$2 % or a length change of only 20 m.

Following the large calving event, the near-terminus region experienced a step increase in speed (Tab. 3.3), as previously described [Amundson and others, 2008; Nettles and others, 2008]. This type of response is observed at the temporary GPS locations, but was not seen at the continuous GPS sites located further upstream.

Results from the constant-acceleration model for glacier response to calving at the near-terminus sites indicate that there was little to no acceleration (or deceleration) in the days

preceding the event. However, there was a consistent pattern of deceleration in the days following calving (Tab. 3.3, Fig. 3.7), though glacier speeds were greater in the days after the calving event than before (Fig. 3.6). The calving model was only applied to sites with data both before and after the calving event on day 233 (P1, P2, P3 and T7), but the surface speeds at site T9 suggest a post calving deceleration greater than recorded at the other sites (Fig. 3.6). The deceleration at T9 is estimated to be as much as 2–3 $\mathrm{m\,d^{-2}}$.

Table 3.3: Change in speed and acceleration in response to iceberg calving.

	Pre-calving		Post-calving	
Site	Speed ($\mathrm{m\,d^{-1}}$)	Acceleration ($\mathrm{m\,d^{-2}}$)	Speed ($\mathrm{m\,d^{-1}}$)	Acceleration ($\mathrm{m\,d^{-2}}$)
T7	39.358 ± 0.006	0.01 ± 0.04	39.176 ± 0.005	-0.99 ± 0.04
P1	31.3972 ± 0.0005	-0.01 ± 0.02	32.0251 ± 0.0005	-0.33 ± 0.02
P2	28.7887 ± 0.0005	-0.067 ± 0.003	29.5096 ± 0.0005	-0.287 ± 0.003
P3	28.1683 ± 0.0005	0.042 ± 0.003	28.7018 ± 0.0005	-0.242 ± 0.003

The sharp breaks in slope of the calving models for the P-sites echo the findings of Amundson and others [2008] who identified a step-increase in speeds following a series of large calving events in 2007. However, the calving model for site T7, $\sim 0.5\,\mathrm{km}$ from the terminus, transitions from decelerating to accelerating with a minimal change in speed (Fig. 3.7).

3.3.3 Tidal analysis

Horizontal and vertical tidal admittances are calculated at each site for each day of data with a statistically significant tidal response model. Figure 3.8 shows the time series of daily tidal admittances for the temporary GPS sites. In the near-terminus region of Jakobshavn Isbræ we find that tidal height and glacier speed are anti-correlated and higher surface speeds occur during low tide while speeds are lower at high tide. Because tidal height and surface speed are anti-correlated, the extrema of horizontal position are concurrent with the inflection points of tidal height, when the tide is changing most rapidly (Fig. 3.9). This implies a phase difference between extrema of detrended horizontal position and tidal height where maxima in detrended position lag maxima in speed by 3 hr

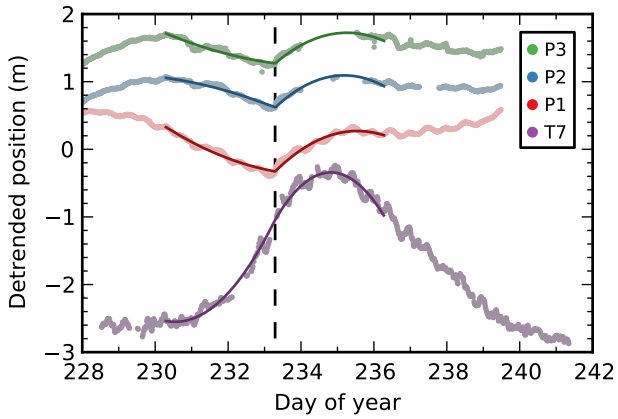

Figure 3.7: Detrended position and calving response models for sites P1, P2, P3 and T7. The timing of a large calving event on August 12 is marked by a vertical dashed line.

when forced by tidal frequencies of approximately 2 d^{-1}.

Within the limits of uncertainty, tide-induced vertical motion is in phase with ocean tides. For both horizontal and vertical admittance the degree of phase uncertainty between tides and glacier response limits our ability to identify any time delay between forcing and response or propagation times of response between measurement sites. Any such delays, if present, are shorter than ~ 1 hr.

Error bounds on tidal admittances at the optical markers are significantly greater than at the GPS sites. This is a result of the lower sampling rate at the optical markers in addition to greater uncertainty of individual position measurements at these sites.

By calculating a tidal admittance for each day of position data, we are able to examine changes in tidal response as a function of time. Time series of tidal admittance at GPS sites show a trend of decreasing admittance leading up to the day 233 calving event (Fig. 3.8). Tidal admittance at these sites is more variable in the days following calving but suggest a trend of increasing tidal response after the calving event.

Time series of tidal admittance at optical markers are less informative because only one marker bridged the time spans before and after the calving event on day 233. In addition, the admittance uncertainties of optical marker data are much larger than those for the GPS data.

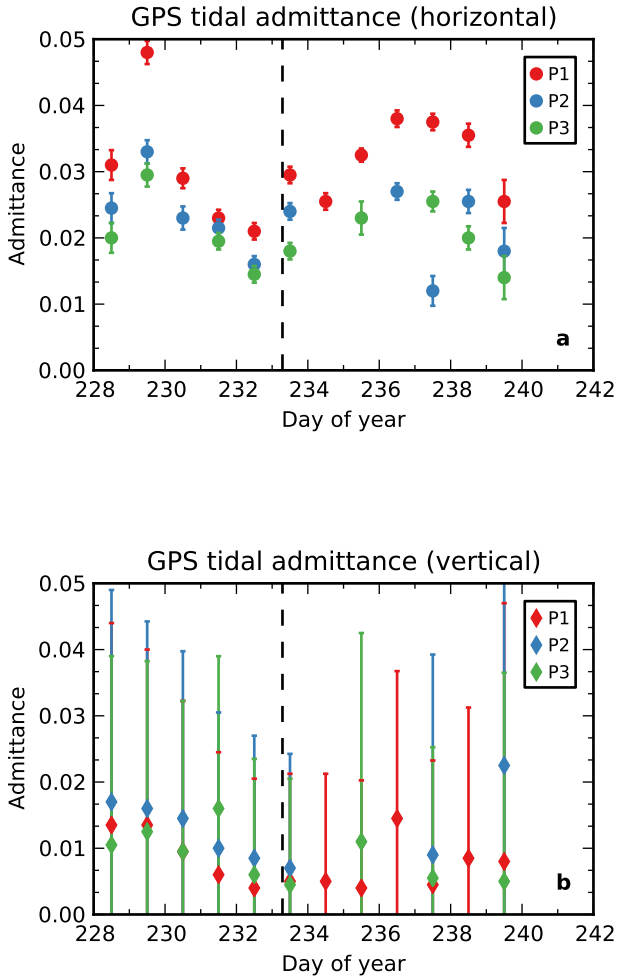

Figure 3.8: Daily tidal admittance for 12 days of measurements at temporary GPS sites. The timing of a large calving event on August 12 is marked by a vertical dashed line.

3.4 Discussion

3.4.1 Temporal changes in response to forcing

We attempt to describe surface speeds in the near-terminus region of Jakobshavn Isbræ by decomposing horizontal position time series with three models: a linear fit to positions, a calving response model and a tidal response model.

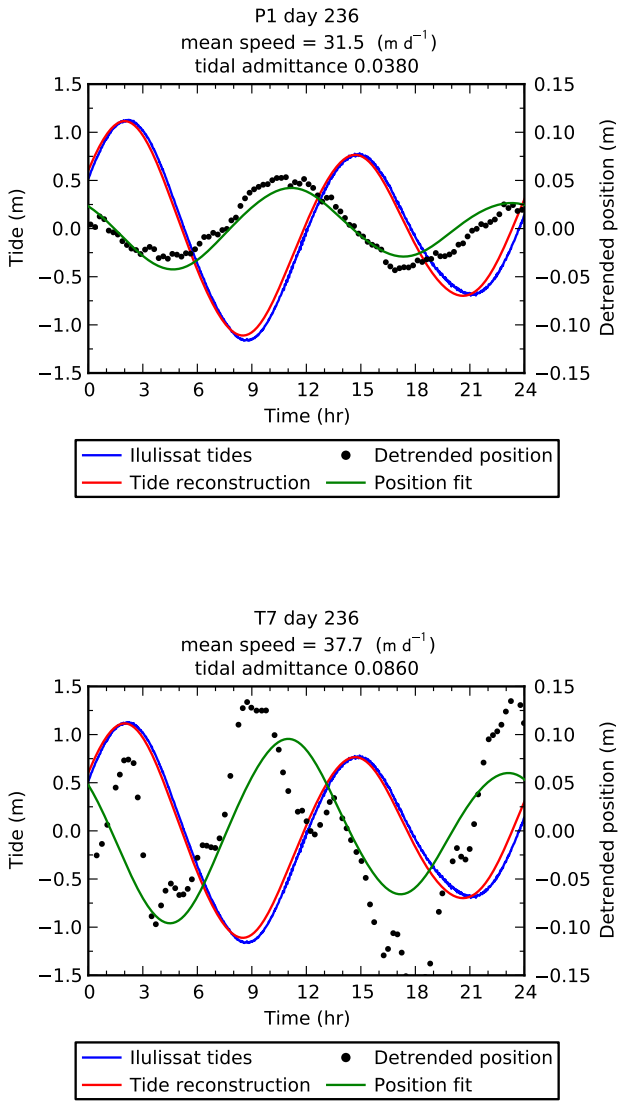

Figure 3.9: Results of tidal analysis at sites P1 (a) and T7 (b), day 236. Measured tides are shown in blue. The red curve shows the tidal model used in the analysis. Black points show measured positions and the green curve is the best fitting model of tidal response.

Linear model

By far the dominant signal over the two-week study period is explained by the first model. At all study sites, more than 99.9 % of the variance in positions can be accounted for by a linear fit to position data. This implies that, while on inter-annual time scales the surface

speed of Jakobshavn Isbræ has more than doubled [Joughin and others, 2004] since the late 1990s, variations over shorter time scales are much smaller.

Calving response model

The greatest deviations from the linear model are explained by the calving response model. The calving response model assumes simple, constant-acceleration motion for two three-day periods before and after the calving event on day 233. This model explains from 93.8 % to 99.4 % of the variance remaining after detrending the motion data with the linear model. Results from the calving model show that the glacier responds to the calving event with a step-change in speed as previously described by Amundson and others [2008] and Nettles and others [2008]. Additionally, we observed a transient deceleration following calving similar to results on Jakobshavn Isbræ reported by Rosenau and others [2013] using photogrammetric techniques in 2010.

The response to calving seen at Jakobshavn Isbræ could be explained by a number of mechanisms. First, the nature of iceberg calving observed at Jakobshavn Isbræ results in a sudden, large loss of ice and a rearrangement of the glacier geometry in the near-terminus region. Following such calving events, the fresh ice front has a greater vertical freeboard and the stress state is altered, favoring large extensional and shear stresses at the newly formed vertical face. Second, the evacuation of massive, loosely connected icebergs, as described by Amundson and Truffer [2010], could reduce the friction provided by partially rotated icebergs dragging along the bed and allow the ice to flow more freely at the freshly calved ice front. Third, large calving events temporarily disrupt the cohesion of proglacial ice mélange and could result in a reduction of back stress provided by a stiffer, pre-calving mélange.

It is difficult to quantify the direct influence of proglacial mélange via back stress exerted on the ice front, but this phenomenon is likely less important during summer months due to a lack of sea ice binding loose icebergs together. More likely the influence of the mélange is affected through an indirect process controlling the style of iceberg calving [Amundson and Truffer, 2010] and would therefore not affect ice velocity directly.

Tidal response model

The smallest variations modeled are attributed to tidal forcing at the calving front. On a given day, the tidal response model explains from 10 % to 90 % of the variability remaining after accounting for the calving response and constant-speed motion. This means that, while measurable, the response to tidal forcing accounts for only 0.1–500 ppm of the deviation from steady flow. The tidal response model for horizontal positions is used to derive models for velocity response to tidal forcing and we find that tidally modulated variations in surface speed are from 0.4 % to 2.9 % of background speeds. This level of modulation falls below the level capable of being resolved, ± 5 % of background, by the application of photogrammetric techniques employed by Rosenau and others [2013] at Jakobshavn Isbræ in 2004, 2007 and 2010. While the response to tidal forcing is small relative to high background speeds, the magnitude of the variations is significant, representing an absolute velocity variation in excess of $\pm 1\ \mathrm{m\,d^{-1}}$ about mean flow estimated from derivatives of the tidal response models.

To illustrate the reduction in variability after applying the various motion models, Figure 3.10 shows position data from site P1 along with the linear fit to positions and the models for calving response and tidal response. Residual position data display less variability following the application of each subsequent model. Residual positions at P1 on day 232 vary by ± 3 cm after accounting for the three motion models. In this particular case, the linear model explained 99.9994 % of the variance over 12 days, the calving response model accounted for 97 % of the remaining variance during the 6 days surrounding the calving event and the tidal response model contributed 60 % of the remaining variance during day 232.

While small in magnitude compared with background flow, the tidal response of Jakobshavn Isbræ agrees well with the findings from other glacier systems in Greenland and Alaska. At Helheim Glacier, in East Greenland, ocean tides are responsible for a velocity modulation of $\sim 0.5\ \mathrm{m\,d^{-1}}$ about a mean of roughly $25\ \mathrm{m\,d^{-1}}$, corresponding to 2 % of background [De Juan and others, 2010]. In Alaska, O'Neel and others [2001] report a modulation of ~ 3 % away from the mean $27\ \mathrm{m\,d^{-1}}$, or $\pm 0.75\ \mathrm{m\,d^{-1}}$, at Le Conte Glacier. Similarly, results from Columbia Glacier [Walters, 1989] show a tide induced variation of $1\ \mathrm{m\,d^{-1}}$ but with a larger relative variation of 10 % about a mean speed of $\sim 10\ \mathrm{m\,d^{-1}}$. The close agreement of the absolute tidal variations among the Greenland and Alaskan studies

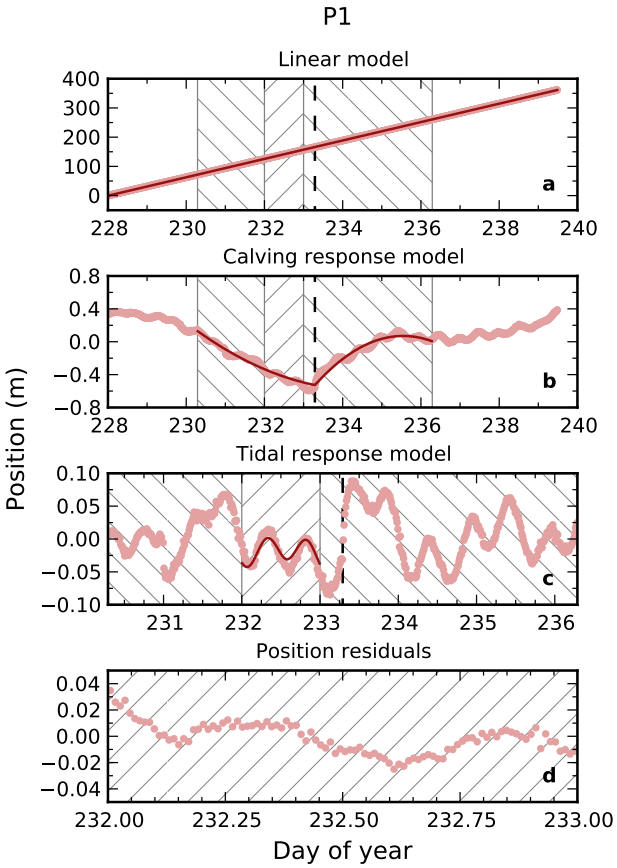

Figure 3.10: P1 residual positions after subtracting modeled motion due to the linear model (b), calving response model (c) and tidal response model (d) are plotted as light red points. Position predicted by the linear (a), calving response (b) and tidal response (c) models are shown as solid red lines. The hatched regions indicate time spans over which the calving response and tidal response models are applied; note the reduction in time interval from a to d. The timing of a large calving event on August 12 is marked by a vertical dashed line.

shows that the 0.4 % to 2.9 % tidal variations at Jakobshavn Isbræ, while significant, are obscured by large background flow speeds.

We also draw a comparison between the background motion and tidal response of the sites in this study. Tidal admittance and daily-average surface speed of all GPS and optical marker sites seem to be related, with a correlation coefficient of 0.87 (Pearson's r). We do not argue that this correlation implies any causality between speeds and tidal response; however, it does suggest a common mechanism responsible for high sensitivity to tidal

forcing and large surface speeds: Basal drag and related basal motion is the most likely candidate for such a common physical mechanism. De Juan and others [2010] found a correlation between changes in both tidal admittance and surface speed at Helheim Glacier and argue that the observed relation is the result of a temporary decrease in basal drag immediately following iceberg calving.

Other sources of forcing

In addition to ocean tides and iceberg calving, sources of short-term variations in motion that are not accounted for by the analysis above include diurnal (surface meltwater) and episodic (supra-glacial lake drainage) forcing of the subglacial hydrology, and changes in resistive stress of the pro-glacial mélange not accounted for by the calving model. Results from Helheim Glacier [Andersen and others, 2010] and Jakobshavn Isbræ [Podrasky and others, 2012] indicate velocity variations due to surface meltwater forcing are typically from 2 % to 5 % of background.

To investigate the influence of diurnal meltwater forcing, or other quasi-periodic signals, in the near-terminus region of Jakobshavn Isbræ we search over a range of likely frequencies with the Lomb-Scargle periodogram [Scargle, 1982]. This algorithm is particularly suited to time series with unevenly sampled data. We calculate the periodogram for position residuals of sites P1, P2, P3, and T7 over frequencies of 3 d^{-1} or less. Results of the un-normalized periodogram show a significant response at a period of 24 h at all four sites, with the largest magnitude response at T7 (Fig. 3.11). At all sites, the peak at 24 h is the largest signal over the range of frequencies tested. Encouragingly, there is very little response at the frequency of the M_2 tidal constituent, with period 12.4 h, indicating that the influence of tides is being adequately modeled while not aliasing non-tidal sources of diurnal variation. The rather large widths of the peaks at 24 h periods are not surprising given the quasi-periodic nature of surface meltwater forcing and that the nature of this forcing is not perfectly captured by the sinusoids employed by the Lomb-Scargle method. We are not able to explain the peaks at periods of $\sim$ 16 h, but the high-frequency response (periods below 12 h) in the T7 periodogram is likely due to noise of an atmospheric nature in the theodolite-measured positions. The amplitudes of the four periodograms at frequencies of 24 h are from one-half to one times the amplitude of tidally forced variations. Despite the shortcomings of modeling diurnal meltwater forcing with a simple sinusoid, this tentative result indicates that near the terminus of Jakobshavn Isbræ the responses to tidal forcing

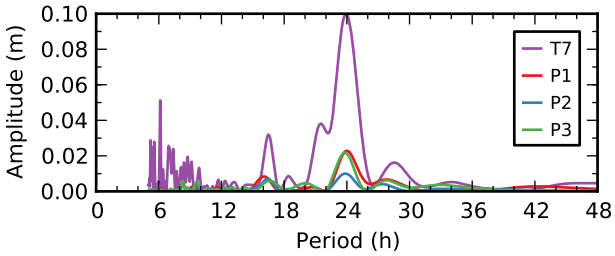

Figure 3.11: Frequency analysis of residual positions after removing signals due to the linear model and calving and tidal responses applied to sites P1, P2, P3 and T7. The largest signal remaining in residual positions has a period of $\sim$24 h.

and surface meltwater forcing are of approximately equal magnitude. This is only true, of course, during the melt season and excludes a comparison with a hypothetical non-linear response to longer period tidal constituents [Gudmundsson, 2007].

It is possible that the diurnal variability identified in the Lomb-Scargle periodogram is the result of some physical process other than surface meltwater forcing. To rule out other processes occuring over a diurnal frequency we attempt to measure the phase of the diurnal signal present in the positions residuals. A least-squares optimization is employed to find the sine curve with frequency 1 d^{-1} that best fits the residual position time series of P1, P2, P3 (with no significant fit achieved for T7). The optimization includes parameters for amplitude and phase. A simple analytical derivative of the best-fitting sine curve approximating residual positions gives the timing of the maxima of residual speeds. Maxima at site P1 occur 11.7 h after local noon and at P2 and P3 maxima occur 10.9 h after local noon. Results from a previous study on Jakobshavn Isbræ [Podrasky and others, 2012] indicate that diurnal surface speed maxima at sites 20–50 km upstream of the terminus occur $\sim$6 h after local noon. For comparison, longer delays of up to 24 h were found at Helheim Glacier in 2007 and 2008 by Andersen and others [2010]. The difference in phase delay between the terminus region and areas further upstream gives a sense of propagation times for perturbations to the subglacial/englacial hydrology.

In 2007 a series of lakes south of the main channel of Jakobshavn Isbræ drained within a period of four days and, in conjunction with enhanced surface melt, may have resulted in a drop in surface speed of more than 12 % of background [Podrasky and others, 2012]. The current study does not document supra-glacial lake drainage and we find no evidence for a similar lake drainage event during the 14 days of the current study; the only sudden

velocity change approaching 12 % is an abrupt increase in speed and is concurrent with the calving event on day 233.

3.4.2 Spatial pattern of repsonse to tides

Interpreting the pattern of tidal response

To examine the spatial variation of tidal response, we propose a simple, analytical model adapted from Walters [1989] for tidal admittance, Λ, as a function of distance, D, from the terminus. We assume that the influence of tides on glacier motion decays exponentially with distance from the terminus

$$\Lambda(D) = \Lambda_0 e^{-\beta D} \tag{3.9}$$

with the rate of decay given by β. We apply Eqn (3.9) to solve for the best fitting horizontal tidal admittance model for each day during the study period with values for tidal admittance from at least three sites, requiring that at least one of these is from an optical marker site. The same procedure is used for generating vertical tidal admittance models.

Each of the daily tidal admittance models (horizontal and vertical) are shown in Fig. 3.12 along with tidal admittances calculated at GPS and optical marker sites. Horizontal tidal admittances decay with increasing distance from the calving front in a predictable manner (Fig. 3.12a), but the vertical admittance at GPS site P1 is anomalously low compared to sites up- and downstream (Fig. 3.12c). In addition, P1 experienced a positive vertical trajectory totaling 3 m over 12 days of measurements; all of the other GPS and optical markers followed negative vertical trajectories (Fig. 3.3).

Two plausible mechanisms could explain the positive vertical motion at this site: 1. The shape of a constricting bed trough in addition to possible convergent ice flow would result in vertical straining consistent with positive vertical motion. 2. At the location of P1, the glacier could be flowing out of an over-deepened feature in the glacier bed and up a reverse bed slope. The effect of either hypothesis is in opposition to the large rates of along-flow extension and thinning, and would need to overcome the associated downward surface displacements in order to result in the observed 3 m of vertical motion. We favor the second explanation based on an examination of surface and bed topography [Plummer and others, 2008] along the trajectory traced by the marker at P1. The bed topography data show that at site P1 the glacier is flowing out of an over deepening and up a reverse bed slope with an increase of $\sim$ 30 m in bed elevation over the 350 m traversed by

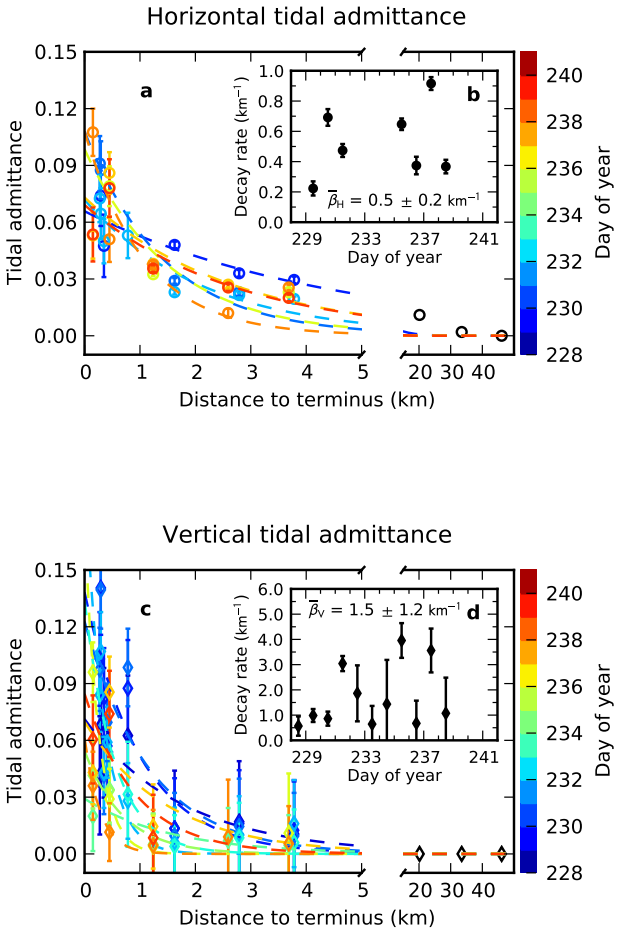

Figure 3.12: Daily horizontal (a) and vertical (c) tidal admittances plotted as a function of distance from the calving front. Data points are color-coded for day of year. Unfilled black markers show the tidal response estimated from the 2008 data set. Inset figures show the length-rates of decay from daily horizontal (b) and vertical (d) tidal admittance models based on eqn. (3.9).

P1. Furthermore, the surface elevation data, from 2008, show an upward sloping ice surface with an elevation increase of 5 m over the same distance. Considering the information about the bed topography in the vicinity of P1, the vertical motion recorded at that site is best explained by a feature in the glacier bed topography.

With the exception of the anomolous behaviour observed at P1, tidal admittance falls steadily with increasing distance from the glacier terminus. Generally, the influence of

tides on horizontal motion extends farther up-glacier than the vertical response. The distance over which tides influence glacier motion can be characterized by the length-rate of decay, β, from the tidal admittance models. The average horizontal length-rate of decay is $0.5 \pm 0.2\ \mathrm{km}^{-1}$ and the average vertical length-rate of decay is $1.5 \pm 1.2\ \mathrm{km}^{-1}$ (Fig. 3.12). This means that the horizontal and vertical responses to tidal forcing have *e*-folding lengths of ~ 2 km and ~ 0.7 km, respectively.

Comparison of tidal response to other glaciers

The reach of tidal influence on Jakobshavn Isbræ agrees well with results from similar glacier systems in Greenland and Alaska, but is substantially shorter in length compared with studies involving Antarctic ice streams. The stated length-rate of decay for along-flow tidal modulation on Helheim Glacier ranges from $0.24\ \mathrm{km}^{-1}$ in 2006 and 2007 to $0.48\ \mathrm{km}^{-1}$ in 2008 [De Juan Verger, 2011]. These rates correspond to *e*-folding lengths of 4 km in 2006/7 and 2 km in 2008 and the author attributes the difference to a change in flotation where the glacier was, at least partially, floating in the years preceding 2008, but grounded during 2008. The year 2008 *e*-folding length for grounded ice at Helheim Glacier agrees with our results on Jakobshavn Isbræ which, during summer months, is very nearly grounded throughout the terminus region. Rosenau and others [2013] have shown that during the summer of 2010 Jakobshavn Isbræ advected ephemeral portions of floating ice limited to 0.5 km in length. Good agreement is also found when comparing results with findings from Columbia Glacier at the beginning of its 20-year retreat. Walters [1989] reports a length-scale for tidal response of 2 km based on measurements at 1 km to 5 km from the terminus collected in 1984, 1985 and 1986. This agreement is surprising considering the large difference in terminal ice thickness for Jakobshavn Isbræ (~ 1000 m [Rosenau and others, 2013]) and Columbia Glacier (~ 150 m [McNabb and others, 2012]). The only other estimate of along-flow tidal response length in the northern hemisphere is from Le Conte Glacier (~ 300 m thick) where O'Neel and others [2001] find an *e*-folding length of 0.5 km.

Theoretical estimates for the tidal response length scale of Alaskan tidewater glaciers have been proposed for Columbia and Le Conte Glaciers. Walters [1989] estimates a theoretical response length scale, derived from a model for the coupling of longitudinal stresses, of 2.7 km for Columbia Glacier applicable to the years 1984 to 1986. Thomas [2007] presents a detailed analysis for the problem of damping of tidal forcing and estimates the

length over which response to tidal forcing becomes negligible. This framework is applied to Le Conte Glacier resulting in an estimate for tidal response length scale of 2.6 km. When we apply the theory to Jakobshavn Isbræ using assumed parameters for glacier geometry and rheology it indicates that beyond 7 km the response to tidal forcing would be zero.

Tidal response has also been studied on several West Antarctic ice streams with significantly different results. On ice streams where high-rate position data have been collected, the length of the glacier influenced by tidal forcing is as much as two orders of magnitude greater than the response length of Alaskan and Greenland tidewater glaciers. Results from GPS measurements on Bindschadler Ice Stream (Ice Stream D) identified tidal modulation of flow speed as far as 80 km upstream from the grounding zone [Anandakrishnan and others, 2003]. GPS and seismic records show a response to tidal forcing 40 km upstream of the grounding zone of Rutford Ice Stream [Aðalgeirsdóttir and others, 2008] and the ice stream responds to forcing from a range of tidal constituents including semi-diurnal, diurnal, fortnightly and annual. In the case of Rutford Ice Stream, the response to ocean tides is approximately in phase with the forcing [Murray and others, 2007], which distinguishes the response mechanism of this glacier from most other systems where similar measurements have been made. It has been shown that at Rutford Ice Stream the response to tides is non-linear with frequency and Gudmundsson [2010] proposes a model to explain the observed response as a non-linear relation between water depth and basal drag. A consequence of the non-linear response is higher mean speed resulting from tidal forcing; the deviation above mean flow at high tide is greater than the drop below mean flow at low tide [Gudmundsson, 2007]. The enhancement of mean flow speed was estimated at 5 %, based on the results of the model. It is unlikely that such an enhancement of mean flow speed is occurring at Jakobshavn Isbræ as speeds are not in phase with tidal height and tidal modulation is attributed to changes in backstress exerted by ocean tides [Thomas, 2007].

A passive seismic investigation on Kamb Ice Stream (Ice Stream C) demonstrates glacier response to ocean tides as far as 160 km from the grounding zone [Anandakrishnan and Alley, 1997]. Basal seismicity of Kamb Ice Stream is roughly anti-correlated with tidal height. The authors argue for seismicity as a proxy for basal motion and conclude that low tidal height results in faster ice stream flow. Other results from studies of Siple Coast ice streams demonstrate more complex interaction between ice flow and ocean tides. Harrison and Echelmeyer [1993] measured diurnal fluctuations in measured strain and seismicity

at a location 300 km upstream of the grounding zone that may be due to Ross Sea tides, which are strongly diurnal. However, measurements of surface speed did not resolve any short-term variations greater than 3 % of mean flow. Bindschadler and others [2003] later measured the tidal response of Whillans Ice Stream (Ice Stream B) using GPS to identify stick-slip motion characterized by short lived displacements occurring during rising and falling tides. Such long coupling distances and phenomena demonstrating high sensitivity to basal conditions point to fundamental differences between Antarctic ice streams and topographically confined tidewater glaciers.

Topographically confined Greenland outlet glaciers, such as Helheim Glacier and Jakobshavn Isbræ, are characterized by thick ice, steep surface slopes and narrow fjords; all favoring high driving stresses. Under such conditions internal deformation through vertical shearing is capable of contributing a large proportion to observed surface speeds [Truffer and Echelmeyer, 2003; Lüthi and others, 2002]. Though thinner at the terminus, Le Conte Glacier flows into Le Conte Bay with a steep surface gradient through an over-deepened bed and driving stresses are large. While Columbia Glacier had a response to tidal forcing similar to Le Conte Glacier and Greenland outlets, it did not have the ice thickness or steep surface slope to match. However, when the study examining Columbia Glacier's response to tides [Walters, 1989] was conducted, the glacier had recently begun its retreat from a terminal push moraine in the vicinity of Heather Island [Meier and others, 1994]. The presence of the submarine moraine may have acted to insulate the glacier from the influence of tidal forcing. The various conditions of the glacier systems listed above all have the effect of localizing the stress balance, thereby reducing the transmission of variations in longitudinal stress.

In contrast with Alaskan and Greenland tidewater glaciers, Antarctic ice streams demonstrate extremely long coupling lengths, often 100s of ice thicknesses. A large portion of observed surface speeds on Siple Coast ice streams is due to basal motion over and/or within a weak bed of unlithified sediments [Alley and others, 1986]. Large width-to-thickness ratios, flat surface profiles, and low basal yield stresses result in limited vertical shear increasing the ratio of driving stress to resistive forces. In addition, Antarctic ice streams are exceptionally cold, often with temperate conditions limited to ice near the bed. This results in a high ice viscosity, limiting internal deformation and further increasing the relative importance of basal motion, where applicable. Large rates of basal motion in proportion to depth-averaged speed and weak resistive stresses point to a highly non-localized stress

balance on Antarctic ice streams and provide a satisfactory explanation for the influence of tidal forcing over such long distances.

By assessing response to tidal forcing it is possible to qualify glacier sensitivity to basal conditions. For example, the steady rates of rapid flow of Greenland outlet glaciers, despite the well known mode of forcing from tides, suggest that the large speeds observed at systems such as Jakobshavn Isbræ are primarily due to the large driving stresses found there. Indeed, the flow of Jakobshavn Isbræ is quite stable in response to perturbations to the force balance at the front due to ocean tides and iceberg calving, measured in this study, and forcing of the subglacial hydrology due to surface meltwater input and supraglacial lake drainage [Podrasky and others, 2012]. By contrast, the Siple Coast ice streams are extremely sensitive to changes in basal rheology as demonstrated by the phenomenon of ice stream stagnation [Bennett, 2003]. On Jakobshavn Isbræ, and other similar Greenland outlet glaciers, high driving stresses imply significant basal traction and other resistive forces resulting in a localized stress balance. Localized compensation of the driving stress mutes the response to tidal forcing and iceberg calving upstream of the terminus.

3.5 Conclusions

We measured high-rate surface positions at discrete locations in the terminal region of Jakobshavn Isbræ during a two-week period in August, 2009. During this time we identified variations in ice flow near the terminus in response to tides, surface melt water and a singe, large calving event. However, these variations are exceptionally small compared to the background of steady motion observed over two weeks. A constant-speed model for ice motion is able to explain well over 99 % of motion during the study period. A large calving event occurring during the middle of the observation period resulted in additional variability in glacier motion and the simple calving response model explained ~ 95 % of the variance remaining after subtracting the signal due to constant speed motion. Each day, 10–90 % of the remaining variance is attributed to tidal forcing at the ice front. We estimate that variations due to surface meltwater forcing near the terminus are similar in magnitude to the response to tides, varying within a few percent of the mean surface speed.

Significant response to tidal forcing and calving events is restricted to the very lowest reaches of the glacier, within 10 km of the terminus. The influence of ocean tides on horizontal motion decays at a rate of ~ 0.5 km^{-1} or a characteristic length scale of 2 km

and the vertical response decays at a rate of $\sim 1.5\ \mathrm{km}^{-1}$ or within ~ 0.7 km. These results show good agreement with findings from similar studies of other tidewater glaciers in Greenland and Alaska. The spatial extent of the influence of ocean tides is much longer at Antarctic ice streams, by as much as 1–2 orders of magnitude. This disparity reflects a difference in the spatial distribution of the stress balance: Antarctic ice streams have a highly non-localized stress balance while on Jakobshavn Isbræ driving stress is more locally compensated. An analysis of a tidewater glacier's response to easily predicted, periodic ocean tides is a useful tool for assessing sensitivity to changes in backstress at the grounding zone. From the measurements in this study, we conclude that the current configuration of Jakobshavn Isbræ is less sensitive than Antarctic ice streams to stress perturbations at the grounding zone.

The response to a single, large calving event is characterized by a step-increase in flow speed coincident with the event, followed by a period of deceleration lasting a few days after the calving event. We note a response to calving as far as 4 km upstream of the terminus, and results from data collected the previous year (2008) indicate no evidence of short-term response to single calving events at sites located 20 km or more from the terminus [Podrasky and others, 2012].

The rapid decay of vertical tidal admittance with increasing distance from the terminus provides independent confirmation of the findings of Rosenau and others [2013] that during the melt season, regions of floating ice are temporary and limited to areas less than 1 km from the calving front. However, it is unlikely that this behavior will continue indefinitely and if the glacier continues to retreat into deeper bed topography the extent of floating ice will be subject to change. Similarly, the limited extent of horizontal motion response to tides and calving indicate that, for the most part, the ice flow of Jakobshavn Isbræ is not sensitive to these short term forcings. Large dynamic changes have been documented at Jakobshavn Isbræ, but are the result of much stronger mechanisms of forcing: the loss of the floating tongue in the 2000s, rapid terminus retreat and thinning of over 100 m, and seasonal variations in terminus position of ~ 6 km.

Acknowledgments

Support for this project was provided by NASA's Cryospheric Sciences Program (NNG06GB49G) and the Swiss National Science Foundation (SNF) grants 200021-113503 and 200020-129898. Logistical support was provided by CH2M Hill Polar Field Services.

The staff and pilots of Air Greenland made the field measurements possible and we thank them for skillful and safe flying. We thank R.J. Motyka for his help in the field. Thanks to E. Boyce and S. White at UNAVCO for technical assistance. J.M. Amundson provided expert advice and helpful comments. Thank you to I. Silis for sharing his knowledge of Greenland. UNESCO site manager, N. Habermann facilitated our work in the Iulissat Icefjord world heritage site.

References

Alley, R. B., D. D. Blankenship, C. R. Bentley and S. T. Rooney, 1986. Deformation of till beneath ice stream B, West Antarctica, *Nature*, **322**(6074), 57–59.

Amundson, J. M. and M. Truffer, 2010. A unifying framework for iceberg-calving models, *J. Glaciol.*, **56**(199), 822–830.

Amundson, J. M., J. F. Clinton, M. A. Fahnestock, M. Truffer, R. J. Motyka and M. P. Lüthi, 2012. Observing calving-generated ocean waves with coastal broadband seismometers, Jakobshavn Isbræ, Greenland, *Ann. Glaciol.*, **53**(60), 79–84.

Amundson, J. M., M. Truffer, M. P. Lüthi, M. A. Fahnestock, M. West and R. J. Motyka, 2008. Glacier, fjord, and seismic response to recent large calving events, Jakobshavn Isbræ, Greenland, *Geophys. Res. Lett.*, **35**(22), L22501.

Anandakrishnan, S. and R. B. Alley, 1997. Tidal forcing of basal seismicity of ice stream C, West Antarctica, observed far inland, *J. Geophys. Res.*, **102**(15), 183–196.

Anandakrishnan, S., D. E. Voigt and R. B. Alley, 2003. Ice stream D flow speed is strongly modulated by the tide beneath the Ross Ice Shelf, *Geophys. Res. Lett.*, **30**(7), 1–4.

Andersen, M. L., T. B. Larsen, M. Nettles, P. Elosegui, D. van As, G. S. Hamilton, L. A. Stearns, J. L. Davis, A. P. Ahlstrøm, J. de Juan, G. Ekström, L. Stenseng, S. A. Khan, R. Forsberg and D. Dahl-Jensen, 2010. Spatial and temporal melt variability at Helheim Glacier, East Greenland, and its effect on ice dynamics, *J. Geophys. Res.*, **115**(F4), 1–18.

Aðalgeirsdóttir, G., A. M. Smith, T. Murray, M. A. King, K. Makinson, K. W. Nicholls and A. E. Behar, 2008. Tidal influence on Rutford Ice Stream, West Antarctica: observations of surface flow and basal processes from closely spaced GPS and passive seismic stations, *J. Glaciol.*, **54**(187), 715–724.

Bennett, M. R., 2003. Ice streams as the arteries of an ice sheet: their mechanics, stability and significance, *Earth-Sci. Rev.*, **61**(3-4), 309–339.

Bindschadler, R. A., 1984. Jakobshavns Glacier drainage basin: A balance assessment, *J. Geophys. Res.*, **89**(C2), 2066.

Bindschadler, R. A., R. B. Alley, M. A. King, S. Anandakrishnan and L. Padman, 2003. Tidally controlled stick-slip discharge of a West Antarctic ice., *Science*, **301**(5636), 1087–9.

van den Broeke, M., J. Bamber, J. Ettema, E. Rignot, E. Schrama, W. J. van de Berg, E. van Meijgaard, I. Velicogna and B. Wouters, 2009. Partitioning recent Greenland mass loss., *Science*, **326**(5955), 984–6.

Chen, G, 1999. GPS kinematic positioning for the airborne laser altimetry at Long Valley, California. (PhD thesis, Massachussets Institute of Technology)

Clarke, G. K. C., 1987. Fast Glacier Flow: Ice Streams, Surging, and Tidewater Glaciers, *J. Geophys. Res.*, **92**(21), 8835–8841.

De Juan, J., P. Elósegui, M. Nettles, T. B. Larsen, J. L. Davis, G. S. Hamilton, L. A. Stearns, M. L. Andersen, G. Ekström, A. P. Ahlstrøm, L. Stenseng, S. A. Khan and R. Forsberg, 2010. Sudden increase in tidal response linked to calving and acceleration at a large Greenland outlet glacier, *Geophys. Res. Lett.*, **37**(12), 1–5.

De Juan Verger, Julia, 2011. Tidewater glacier flow of Helheim Glacier, Greenland, 2006-2008, using high-rate GPS. (PhD thesis, University of Barcelona)

Dupont, T. and R. B. Alley, 2005. Assessment of the importance of ice-shelf buttressing to ice-sheet flow, *Geophys. Res. Lett.*, **32**(4), 1–4.

Echelmeyer, K. A. and W. D. Harrison, 1990. Jakobshavn Isbræ, West Greenland: Seasonal variations in velocity—or lack thereof, *J. Glaciol.*, **36**(122), 82–88.

Gudmundsson, G. H., 2006. Fortnightly variations in the flow velocity of Rutford Ice Stream, West Antarctica., *Nature*, **444**(7122), 1063–4.

Gudmundsson, G. H., 2007. Tides and the flow of Rutford Ice Stream, West Antarctica, *J. Geophys. Res.*, **112**(F4), 1–8.

Gudmundsson, G. H., 2010. Ice-stream response to ocean tides and the form of the basal sliding law, *Cryosph.*, **4**(4), 2523–2555.

Harrison, W. D. and K. A. Echelmeyer, 1993. Short-period observations of speed, strain and seismicity on Ice Stream B, Antarctica, *J. Glaciol.*, **39**(133).

Heinert, M. and B. Riedel, 2007. Parametric modelling of the geometrical ice-ocean interaction in the Ekströmisen grounding zone based on short time-series, *Geophys. J. Intl.*, **169**(2), 407–420.

Holland, D. M., R. H. Thomas, B. de Young, M. H. Ribergaard and B. Lyberth, 2008. Acceleration of Jakobshavn Isbræ triggered by warm subsurface ocean waters, *Nature Geosci.*, **1**(10), 659–664.

Howat, I. M., I. Joughin, M. A. Fahnestock, B. E. Smith and T. A. Scambos, 2008. Synchronous retreat and acceleration of southeast Greenland outlet glaciers 2000–06: ice dynamics and coupling to climate, *J. Glaciol.*, **54**(187), 646–660.

Joughin, I., W. Abdalati and M. A. Fahnestock, 2004. Large fluctuations in speed on Greenland's Jakobshavn Isbræ glacier, *Nature*, **432**(7017), 608–10.

Joughin, I., B. E. Smith, I. M. Howat, D. Floricioiu, R. B. Alley, M. Truffer and M. A. Fahnestock, 2012. Seasonal to decadal scale variations in the surface velocity of Jakobshavn Isbræ, Greenland: Observation and model-based analysis, *J. Geophys. Res.*, **117**(F2), 1–20.

Joughin, I., I. M. Howat, M. A. Fahnestock, B. E. Smith, W. Krabill, R. B. Alley, H. Stern and M. Truffer, 2008. Continued evolution of Jakobshavn Isbræ following its rapid speedup, *J. Geophys. Res.*, **113**(F4).

Joughin, I., B. E. Smith, I. M. Howat and T. A. Scambos, 2010. MEaSUREs Greenland ice velocity map from InSAR data.

Luckman, A. and T. Murray, 2005. Seasonal variation in velocity before retreat of Jakobshavn Isbræ, Greenland, *Geophys. Res. Lett.*, **32**(8), 1–4.

Lüthi, M. P., M. Funk, A. Iken, P. Gogineni and M. Truffer, 2002. Mechanisms of fast flow in Jakobshavn Isbræ, West Greenland: Part III, *J. Glaciol.*, **48**(162), 369–385.

McNabb, R. W., R. Hock, S. O'Neel, L. A. Rasmussen, Y. Ahn, M. Braun, H. Conway, S. Herreid, I. Joughin, W. T. Pfeffer, B. E. Smith and M. Truffer, 2012. Using surface velocities to calculate ice thickness and bed topography: a case study at Columbia Glacier, Alaska, USA, *J. Glaciol.*, **58**(212), 1451–1464.

Meier, M., S. Lundstrom, D. Stone, B. Kamb, H. Engelhardt, N. Humphrey, W. W. Dunlap, M. A. Fahnestock, R. M. Krimmel and R. Walters, 1994. Mechanical and hydrologic basis for the rapid motion of a large tidewater glacier 1. Observations, *J. Geophys. Res.*, **99**(B8), 219–15229.

Moon, T. and I. Joughin, 2008. Changes in ice front position on Greenland's outlet glaciers from 1992 to 2007, *J. Geophys. Res.*, **113**(F2), 1–10.

Moon, T., I. Joughin, B. E. Smith and I. M. Howat, 2012. 21st-Century Evolution of Greenland Outlet Glacier Velocities, *Science*, **693**, 576–578.

Murray, T., A. M. Smith, M. A. King and G. P. Weedon, 2007. Ice flow modulated by tides at up to annual periods at Rutford Ice Stream, West Antarctica, *Geophys. Res. Lett.*, **34**(18), 6–11.

Nettles, M., T. B. Larsen, P. Elósegui, G. S. Hamilton, L. A. Stearns, A. P. Ahlstrøm, J. L. Davis, M. L. Andersen, J. de Juan, S. A. Khan, L. Stenseng, G. Ekström and R. Forsberg, 2008. Step-wise changes in glacier flow speed coincide with calving and glacial earthquakes at Helheim Glacier, Greenland, *Geophys. Res. Lett.*, **35**(24), 1–5.

Nick, F. M., A. Luckman, A. Vieli, C. J. Van der Veen, D. van As, R. S. W. van de Wal, F. Pattyn, A. L. Hubbard and D. Floricioiu, 2012. The response of Petermann Glacier, Greenland, to large calving events, and its future stability in the context of atmospheric and oceanic warming, *J. Glaciol.*, **58**(208), 229–239.

Nick, F. M., A. Vieli, M. L. Andersen, I. Joughin, A. Payne, T. L. Edwards, F. Pattyn and R. S. W. van de Wal, 2013. Future sea-level rise from Greenland's main outlet glaciers in a warming climate, *Nature*, **497**(7448), 235–238.

Nick, F. M., A. Vieli, I. M. Howat and I. Joughin, 2009. Large-scale changes in Greenland outlet glacier dynamics triggered at the terminus, *Nature Geosci.*, **2**(2), 110–114.

Nye, J. F., 1960. The response of glaciers and ice-sheets to seasonal and climatic changes, *Proc. R. Soc. London, Ser. A*, **256**(1287), 559–584.

O'Neel, S., K. A. Echelmeyer and R. J. Motyka, 2001. Short-term flow dynamics of a retreating tidewater glacier: Le Conte Glacier, Alaska, USA, *J. Glaciol.*, **47**(159), 567–578.

Pawlowicz, R., B. Beardsley and S. Lentz, 2002. Classical tidal harmonic analysis including error estimates in MATLAB using T_TIDE, *Comp. & Geosc.*, **28**(8), 929–937.

Plummer, J., S. Gogineni, C. Van der Veen, C. Leuschen and J. Li, 2008. Ice thickness and bed map for Jakobshavn Isbræ *CReSIS Tech. Report*, **2008-1**, (2008).

Podrasky, D. B., M. Truffer, M. A. Fahnestock, J. M. Amundson, R. Cassotto and I. Joughin, 2012. Outlet glacier response to forcing over hourly to interannual timescales, Jakobshavn Isbræ, Greenland, *J. Glaciol.*, **58**(212), 1212–1226.

Rignot, E. and P. Kanagaratnam, 2006. Changes in the velocity structure of the Greenland Ice Sheet, *Science*, **311**(5763), 986–90.

Rosenau, R., E. Schwalbe, H. G. Maas, M. Baessler and R. Dietrich, 2013. Grounding line migration and high-resolution calving dynamics of Jakobshavn Isbræ, West Greenland, *J. Geophys. Res.*, **118**

Scambos, T. A., 2004. Glacier acceleration and thinning after ice shelf collapse in the Larsen B embayment, Antarctica, *Geophys. Res. Lett.*, **31**(18), L18402.

Scargle, J. D., 1982. Studies in astronomical time series analysis. II—Statistical aspects of spectral analysis of unevenly spaced data, *Astrophys. J.*, **263**, 835.

Thomas, R., E. Frederick, W. Krabill, S. Manizade and C. Martin, 2009. Recent changes on Greenland outlet glaciers, *J. Glaciol.*, **55**(189), 147–162.

Thomas, R. H., 2007. Tide-induced perturbations of glacier velocities, *Glob. Planet. Change*, **59**(1-4), 217–224.

Truffer, M. and K. A. Echelmeyer, 2003. Of isbræ and ice streams, *Ann. Glaciol.*, **36**(1), 66–72.

Walters, R. A., 1989. Small-amplitude, short-period variations in the speed of a tide-water glacier in south-central Alaska, USA, *Ann. Glaciol.*, **2**, 187–191.

Chapter 4
Channelization of ice flow inland of Jakobshavn Isbræ, Greenland [1]

Abstract

The tidewater retreat of Jakobshavn Isbræ has been well documented with remote sensing and in-situ measurements of ice surface speed and terminus position. The main fast-flowing channel has doubled in speed since the early 2000s. The increases in speed have been attributed to steepening of the ice surface resulting in higher driving stresses. We examine changes in the velocity of slower-flowing ice adjacent to the main channel and along a transect 120 km inland. From velocity data in 1985, 2000 and 2008 we identify changes in the direction of ice flow in addition to increases in speed. Analysis of ice surface elevation data from 1985 and 2008 reveals that evolution of ice surface velocity over the past two decades is the result of changes in the ice surface gradient, with steeper slopes driving higher speeds and rotation of slope aspect responsible for the rotation of velocities in the surrounding ice toward the main channel.

4.1 Introduction

Currently observed rates of mass loss, -140 $\pm$ 50 Gt a^{-1} (0.39 $\pm$ 0.1 mm a^{-1}), from the Greenland Ice Sheet [Shepherd and others, 2012] are the result of changes in ice sheet surface mass budget combined with increases in outlet glacier calving flux of approximately equal proportion [van den Broeke and others, 2009]. Ice sheet thinning due to negative surface mass balance and calving flux is strongest around the periphery of the ice sheet with the highest rates of dynamic thinning found at fast flowing outlet glaciers [Pritchard and others, 2009]. Cumulative thinning at some locations has exceeded 100 m from 1997 to 2007 [Motyka and others, 2010] with thinning rates of 15 m a^{-1} [Thomas and others, 2011]. Concurrent with observed acceleration and thinning, Greenland outlet glaciers are retreating inland at an average rate of more than 100 m a^{-1} [Moon and others, 2012]. Projections of ice loss from four of Greenland's oulet glaciers comprising 22 % of the ice-sheet wide drainage basin indicate continued losses through the next two centuries [Nick and others,

[1] In preparation for submition to *Geophysical Review Letters* as Podrasky, D., M. Truffer, R. Motyka, M. Fahnestock and I. Joughin. Channelization of ice flow inland of Jakobshavn Isbræ, Greenland.

2013], albeit at modest rates below the upper bounds on calving flux proposed by Pfeffer and others [2008].

It is now clear that the outlet glaciers draining the polar ice sheets are capable of responding to changes in forcing—leading to both increases and decreases in flow speed—over timescales drastically shorter than previously thought [Truffer and Fahnestock, 2007]. Therefore, changes in climate forcing over the next century are of immediate relevance for eustatic sea level rise. Changes occuring along the peripheral regions of the Greenland Ice Sheet have been well documented. Here we examine what effect changes originating at an outlet glacier have had on the interior of the ice sheet. We present an assembly of geodetic data sets, covering portions of the Jakobshavn Isbræ drainage basin, combined with precise point-measurements of velocity located > 100 km inland of the ice sheet margin. The point measurements in our study are colocated with points approximately following the 1800 m elevation contour measured from 1993 to 1995 by Thomas and others [2000]. We attempt to reconcile changes in velocity magnitude and direction with measurements of elevation change from the ice sheet margin far inland, above the location of the equilibrium line altitude.

4.2 Background

Jakobshavn Isbræ, situated on Greenland's west coast to the east of Disko Bay, is one of the ice sheet's largest outlet glaciers with a drainage basin encompassing nearly 10 000 km^2 [Rignot and Kanagaratnam, 2006]. Observations of terminus positions dating back more than 100 years document a retreat from the Little Ice Age maximum extent that lasted until about 1950 [Weidick and others, 1990]. From approximately 1950 to the end of the 1990s the yearly-mean terminus position was stable with a seasonal variation of ~ 2.5 km [Sohn and others, 1998]. However, while the terminus position remained stable up to 2000, the floating glacier tongue had begun steadily thinning by 1997 [Thomas and others, 2003]. Thinning on the floating tongue has been attributed to high rates of subshelf melting [Motyka and others, 2011] driven by unusually warm ocean temperatures entering Kangia Icefjord [Holland and others, 2008]. By the early 2000s cumulative thinning resulted in the break up of the floating tongue and a retreat of > 12 km in less than 3 years [Podlech and Weidick, 2004].

The retreat and thinning in the lower regions of Jakobshavn Isbræ preceeded a doubling of flow speeds [Joughin and others, 2004] and a drawdown of upstream ice and in-

creased rates of thinning to in excess of 10 m a^{-1} [Thomas, 2004]. Additionally, the glacier lacked a year-round floating tongue after retreating, and only re-formed a smaller portion of floating ice each winter [Amundson and others, 2010]. The seasonal formation of the floating tongue of Jakobshavn Isbræ has been suggested as a primary control on seasonal velocity variations [Joughin and others, 2008] while the continued retreat and thinning are driving interannual acceleration along the main glacier channel [Joughin and others, 2012].

The speedup of Jakobshavn Isbræ, initiated by changes in glacier geometry near the terminus [Nick and others, 2009], have propagated upstream along the main channel of fast-flowing ice [Joughin and others, 2012]. The velocity response in the slower-flowing regions of ice adjacent to the glacier and at points well inland of the terminus is much smaller [Joughin and others, 2010]. While the magintude of velocity changes at points far inland are small, the affected area is proportionally large and such small changes over a wide area have important implications for changes in ice flux.

4.3 Data and Methods

To examine the spatial evolution of velocities in the Jakobshavn Isbræ drainage we use two Digital Elevation Model (DEM) datasets from 1985 and 2008 to quantify changes in surface elevation and slope. Changes in surface velocities are analyzed with a combination of remote sensing and GPS measurements. We include spatially-distributed velocity data sets from years 1985, 2000 and 2008 and point measurements of surface velocity from 2010/11.

4.3.1 Digital elevation models

1985 DEM

We use the 1985 DEM from Motyka and others [2010] which was formed from a pair of digitized aerial photo mosaics imaged on July 10 and 24, 1985. From the digitized mosaics, a 40 m spatial resolution DEM was derived. Further details regarding the method for creating the 1985 DEM can be found in Motyka and others [2010]. For the purposes of this study, the 40 m DEM has been down-sampled to 500 m resolution.

2008 DEM

The 2008 DEM is derived from a pair of SPOT-5 images acquired on August 2, 2008. This data access was granted under the SPIRIT (stereoscopic survey of Polar Ice: Reference

Images and Topographies) Polar Dali Program. A detailed description of this data set is provided by Korona and others [2009]. The resolution of the original DEM is 40 m and was down-sampled to 500 m. Heights described by the SPIRIT DEM are in reference to a geoid datum (EGM96). Prior to any analysis it was necessary to convert the 2008 SPOT DEM to an ellipsoidal datum (WGS84) common to the other data sets.

4.3.2 Ice surface velocities

In this study we incorporate ice surface velocity data sets derived from vertical aerial photos, Synthetic Aperture Radar (SAR) and GPS-measured position data. We refer to the first two data sets as spatially distributed to distinguish them from the GPS point measurements.

2000 and 2008 velocities

Velocity data sets for years 2000 and 2008 were obtained from Greenland SAR winter velocity mosaics [Joughin and others, 2010]. SAR velocities are posted at a ground resolution of 500 m. Estimates of uncertainty in SAR velocity components result in a combined error in surface speed on the order of 10 $\mathrm{m\,a^{-1}}$. Errors in velocity directions are $\sim 1^\circ$ for the 2000 data set and $\sim 0.5^\circ$ in 2008.

1985 velocities

We derive surface velocities from the same pair of 1985 orthophoto mosaics used in the creating of the 1985 DEM. Year 1985 velocities were determined using feature tracking techniques applied to the optical orthophoto mosaics [Scambos and others, 1992]. Velocities were calculated at a spacing of 25 m but are resampled to the same 500 m resolution as the SAR velocity data. While ice surface velocities are calculated at a 25 m spacing, the 5 m ground-resolution and the aquisition times of the digitized mosaics impose an uncertainty of $20\,\mathrm{m\,a^{-1}}$ for speeds, with a 0.5° uncertainty in velocity directions.

4.3.3 GPS measurements

During years 1993 to 1995 a surveying campaign was conducted at ice stakes positioned approximately 30 km apart around the ice sheet at the 1800 m elevation contour [Thomas

and others, 2000]. The same stakes were resurveyed one or two years later and the GPS-derived position differences were used to estimate, among other quantities, ice surface speed. We reproduced the measurements of the original survey for points falling in or near the Jakobshavn Isbræ drainage basin in 2010 and 2011. Following the original naming convention of Thomas and others [2000], these sites are CD-08, CD38, CD-87, CD-107 and CD-136. New stakes were placed and surveyed in April 2010 and re-surveyed in April 2011. Ice stakes were surveyed using GPS receivers for no less than one half-hour, and survey durations usually lasted more than an hour or two. GPS observations were processed against a GPS base station adjacent to the 2006 terminus with baseline distances of 100–150 km. All positions were processed using *Track*, part of the GAMIT/GLOBK software suite [Chen, 1999].

After GPS processing, additional corrections were applied to compensate for tilting of some of the stakes during the year-long occupation. The amount and direction of the tilt were measured during the April 2011 campaign and positions were corrected for the effect of stake tilt where necessary. We estimate errors in GPS positions to be 0.015 m based on the standard deviation of the point cloud of positions at each site. Combined with the independent error introduced by tilting of the survey stakes the total uncertainty in velocity magnitudes is 0.1 $\mathrm{m\,a^{-1}}$. The uncertainty in the angular change in velocity directions is estimated by propagating uncertainties in the horizontal components of surface velocities using standard methods of propagation of error.

4.4 Results

4.4.1 DEM differencing 1985 to 2008

Differencing the 2008 and 1985 DEMs reveals a pattern of extreme thinning, in excess of 150 m, on the main trunk of the glacier within 10–20 km of the 2008 terminus. Rates of thinning are lower in the marginal regions and at points on the main trunk farther upstream of the terminus; however, these regions still experienced significant thinning of 25–75 m. The results of our DEM differencing agree well with the 1985 to 2007 DEM difference in figure 6 of Motyka and others [2010].

Estimates of the uncertainties in vertical positions provided with the SPOT DEM product are 5.0 m. The uncertainties in vertical positions of the 1985 DEM range from 2.8 m in the terminus region to 5.6 m in the region of the snowline [Motyka and others, 2010]. Therefore, uncertainties of 1985 to 2008 elevation differences range from 5.7 m to 7.5 m in

the terminus region and near the 1985 snowline, respectively.

4.4.2 Velocity differencing

The spatially distributed ice surface velocity datasets used for velocity differencing are shown in Fig. 4.1. We difference the spatially distributed velocity data over two distinct time intervals, 1985 to 2000 and 2000 to 2008. The coverage of the 1985 to 2000 difference region is smaller than the 2000 to 2008 difference data due to limited coverage in the orthophoto mosaics. In addition to the smaller region of coverage, the 1985 velocity data does not have velocity values at every grid point within the region due to the presence of surface features not compatible with the optical image correlation routine.

Percent velocity change

In order to illustrate the changes in surface speed of both the main glacier and marginal regions, we present velocity magnitude differences as percent changes in speed from 1985 to 2000, and 2000 to 2008 and 1985 to 2008 (Fig. 4.2). From 1985 to 2008 the lower reaches of the main glacier channel more than doubled in speed (Fig. 4.2c). The progression of the 1985 to 2008 speedup of the main channel is approximately equally divided between the time period preceding and following 2000 (Fig. 4.2a and b). During the earlier time period (1985 to 2000) the percent speedup was more concentrated near the terminus while from 2000 to 2008 the percent speedup is nearly uniform along the length of the main channel as far as 50 km from the 2008 terminus.

Both before and after 2000 the percent speedups were greater in the region south of the main glacier channel compared to the region north of the channel (Fig. 4.2a and b). In all time periods considered, the regions of ice near the land-terminating ice sheet margins north and south of the Kangia Icefjord experienced percent slowdowns in excess of 50 %. The slowdown of land-terminating ice is particularly strong during the period from 1985 to 2000 (Fig. 4.2a).

Far inland, at the 1800 m GPS sites we see evidence of changes in surface velocity, though changes at these sites are much less dramatic than those observed closer to the terminus. Among the GPS sites, the greatest changes in velocity magnitude occurred at CD-87 where speed increased by $17.1 \pm 0.1\,\mathrm{m\,a^{-1}}$, a relative increase of 8.83 ± 0.05 %. The other GPS sites experienced speed increases of 2–5 $\mathrm{m\,a^{-1}}$ from 1995/96 to 2010/11 (Fig. 4.2

Table 4.1: Change in velocity directions and magnitudes at 1800 m GPS sites. Values of percent speedup of referenced to 2000 speeds.

Site	1995/96 speed ($m\,a^{-1}$)	Angular change (deg.)	Magnitude change ($m\,a^{-1}$)	Percent speedup
CD-08	106.9	0.386 ± 0.005	2.0 ± 0.1	1.87 ± 0.09
CD-38	117.8	0.01 ± 0.01	5.4 ± 0.1	4.58 ± 0.09
CD-87	193.6	-0.24 ± 0.06	17.1 ± 0.1	8.83 ± 0.05
CD-107	91.3	-0.41 ± 0.04	5.0 ± 0.1	5.5 ± 0.1
CD-136	108.3	-0.28 ± 0.01	2.7 ± 0.1	2.49 ± 0.09

and Tab. 4.1).

Changes in ice velocity direction

Differences in velocity direction are calculated from the spatially distributed data sets for the time periods 1985 to 2000, 2000 to 2008 and 1985 to 2008 and from the 1800 m GPS data over the period 1995/96 to 2010/11 (Fig. 4.3). At the inland GPS sites there is a consistent pattern of velocity deflection toward the main glacier channel. At the two sites north of the main channel the velocities have rotated south, while at the three sites south of the main channel the velocities have rotated northward toward the main channel (Fig. 4.3c and Tab. 4.1).

In regions closer to the terminus we find a velocity response similar to changes measured inland. From 2000 to 2008 velocities in the region of the marginal ice south of the main channel have been deflected northward, toward the main channel and velocities of ice north of the main channel have rotated southward, toward the main channel (Fig. 4.3b). The change in direction of velocities from 2000 to 2008 in the marginal regions is greater than 10°.

4.5 Discussion

A close analysis of velocity changes in slow-flowing regions outside the main glacier channel reveals evidence that the surrounding ice sheet is responding to forcing initiated at the terminus on decadal timescales. Below, we examine changes in both velocity magnitude

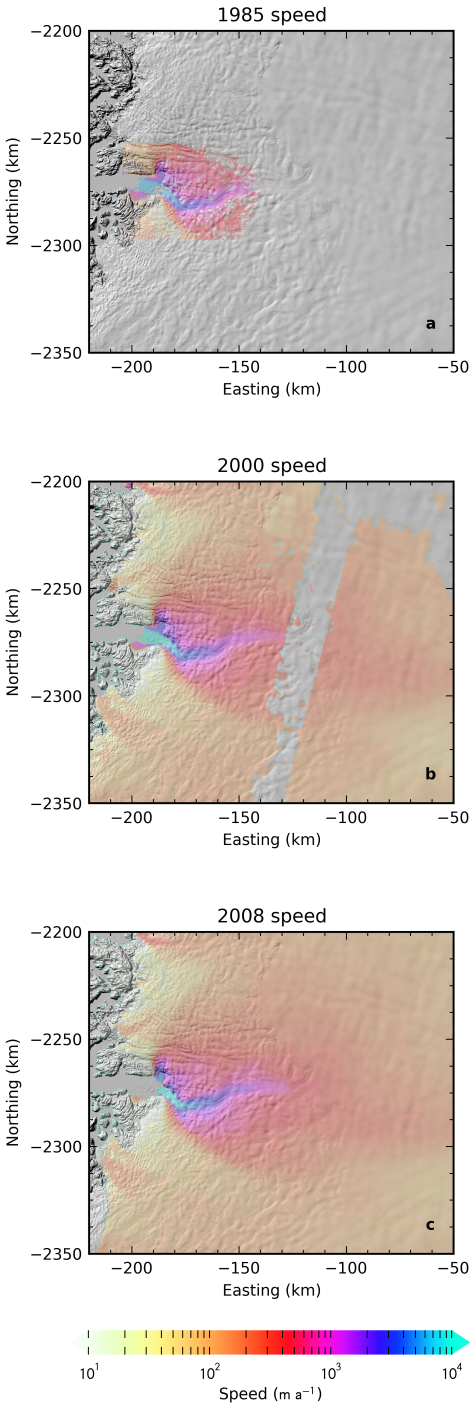

Figure 4.1: Surface speed maps for 1985, 2000 and 2008. 1985 (a) surface velocities are derived by applying feature tracking methods to orthophoto mosaics imaged in July 1985. 2000 (b) and 2008 (c) surface velocities are from ice-sheet wide SAR mosaics.

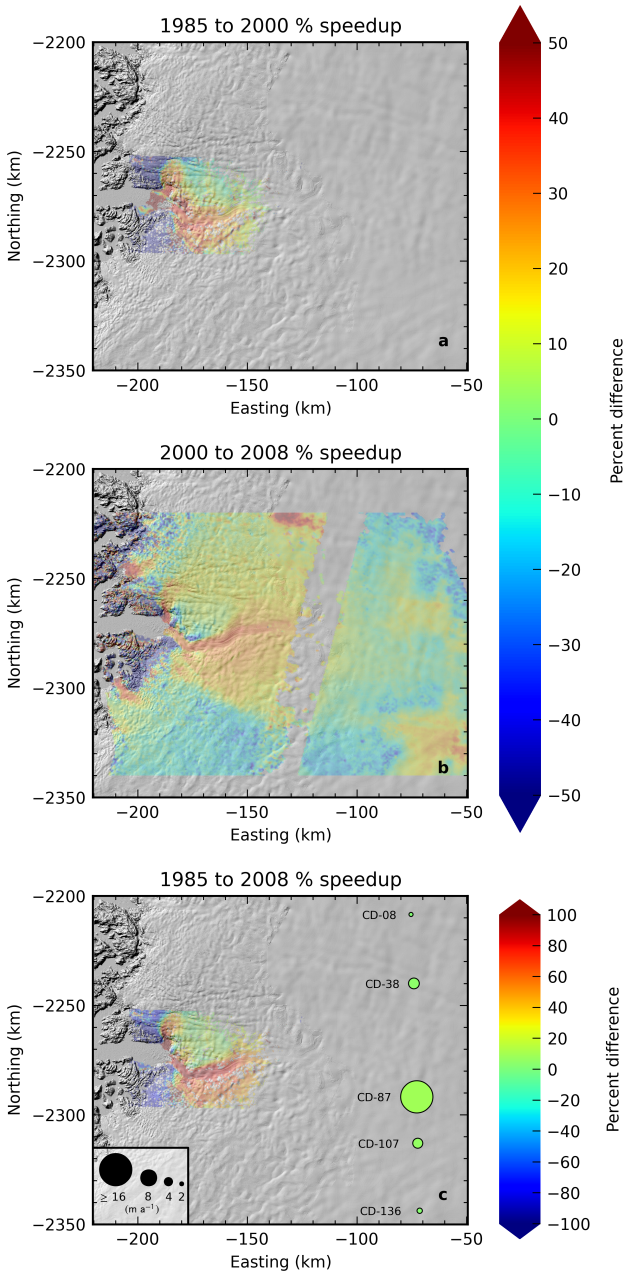

Figure 4.2: Velocity magnitude difference maps. Changes in surface velocity magnitude are expressed as percent change during periods 1985 to 2000 (a), 2000 to 2008 (b) and 1985 to 2008 (c). Speed changes at 1800 m GPS sites over the interval 1995/96 to 2010/11 (c) are plotted as circles color-coded to show percent change and the while marker diameter scales with absolute change in speed.

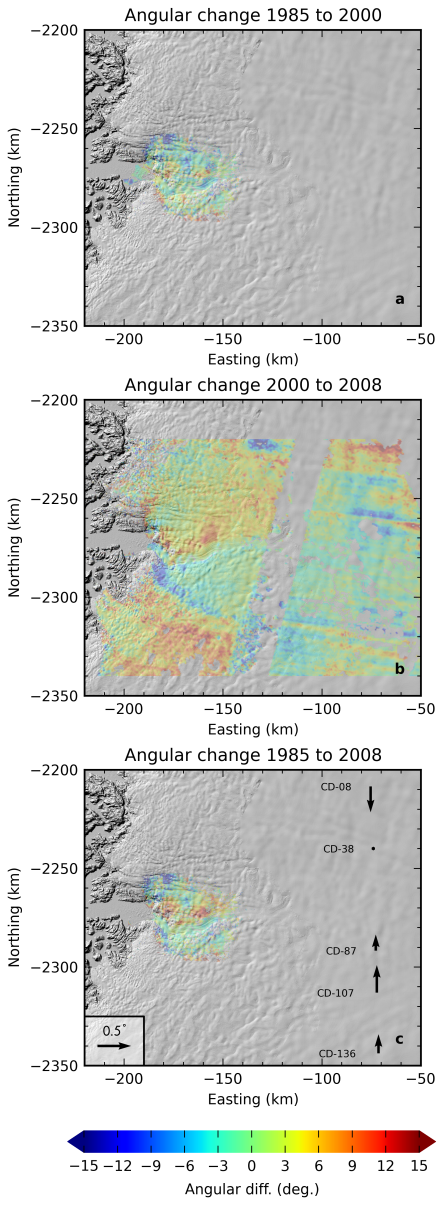

Figure 4.3: Angular change in velocity direction. Changes in surface velocity direction are shown for time periods 1985 to 2000 (a), 2000 to 2008 (b) and 1985 to 2008 (c). Velocity directional changes at the 1800 m GPS sites are indicated with black arrows. Arrows pointing downward indicate clockwise (north of east) rotation while arrow pointing upward indicate counter-clockwise (south of east) rotation. In regions south of the main glacier channel negative angular change indicates velocity rotation toward the main channel and in regions north of the main glacier channel positive angular change indicates rotation toward the main channel.

and direction.

4.5.1 Velocity response

Percent velocity change

The magnitude of velocity change on Jakobshavn Isbræ in the region of fast flow along the main glacier channel has been described in the literature by Joughin and others [2004]. These changes have been attributed to forcing at the terminus [Holland and others, 2008] resulting in the thinning [Motyka and others, 2011] and breakup of the floating tongue and an initial retreat of $> 12\,\mathrm{km}$ [Podlech and Weidick, 2004] that continues at a rate of approximately $500\,\mathrm{m\,a^{-1}}$ [Podrasky and others, 2012]. Though smaller in magnitude, significant changes in speed have occured in the slower-flowing regions adjacent to the main channel, as much as a 50 % increase from 1985 to 2008.

Between 1985 and 2000 ice adjacent to the main channel experienced speedups of 20–40 %. These percent changes are similar to increases that occurred along the main channel, but are less than the speedup of the floating tongue prior to retreat. We note that, with the exception of land-terminating margins, the percent change in speed over this time period is uniformly-positive. Speedup of the main channel, beginning in the late 1990s [Luckman and Murray, 2005], coincided with increased rates of thinning within 20 km of the terminus beginning in 1997 [Thomas, 2004]. Up to 2000 the floating tongue had not yet fully retreated and the velocity responses in regions north and south of the main glacier channel likely coincided with the timing of increased surface slopes between the thinning, accelerating main channel and adjacent ice.

The contrasting behavior of the land-terminating margins indicates that these regions have not been directly influenced by changes along the main channel of Jakobshavn Isbræ. Motyka and others [2010] compare the 1985 DEM with 1997 NASA Airborne Topographic Mapper (ATM) ice elevations and find that the land-terminating ice-sheet margins thinned between years 1985 and 1997. The slowdown of land-terminating margins from 1985 to 2000 is likely a direct result of the thinning, creating lower driving stresses in these regions.

After 2000, the main glacier channel continued to steadily accelerate [Joughin and others, 2008], but the change in surface speeds in regions of ice adjacent to the main channel was not uniformly positive. While the region south of the main channel sped up 20–30 % from 2000 to 2008, there was a significant slowing of ice between the north and south

tributaries. The slower speeds in this region can be explained by thinning of ~ 100 m of ice that was less than 500 m thick to begin with, similar to the velocity response seen at land-terminating margins.

At the locations of the inland GPS measurements we expect ice sheet flow to be well described by the shallow ice approximation

$$u = \frac{2A}{n+1}\left(\rho g S\right)^n H^{n+1}. \tag{4.1}$$

We define u as the surface speed, g is the acceleration due to gravity, ρ is ice density, H is the ice thickness and S is the ice surface slope. Ice rheology is described by an appropriately depth-averaged flow rate factor A and the flow law exponent, n. Differentiating Eqn (4.1) with respect to ice thickness gives the change in speed due to a change in thickness

$$\Delta u = \frac{2A}{n+1}(n+1)\Delta H\left(\rho g S\right)^n H^n. \tag{4.2}$$

We divide Eqn (4.2) by Eqn (4.1) to find the relative change in speed

$$\frac{\Delta u}{u} = (n+1)\frac{\Delta H}{H}. \tag{4.3}$$

For a flow law exponent of 3 we would expect to see a 4 % change in speed in response to a 1 % change in ice thickness. This relation does not completely describe changes in speed in regions where the glacier is bedded well below sea level, where small changes in effective pressure have a large effect on the rate of basal motion. Large thickness changes in proportion to the original ice thickness greatly reduce the driving stress and can have a strong influence on the surface speed of regions outside of the deep glacier channel.

Drawing on results from the GPS measurements, we see evidence of a velocity response at sites far inland of the ice-sheet margin. The magnitude of speed changes are on the order of the uncertainties in the SAR velocities (~ 10 m a^{-1}) and are not evident in the record of remote sensed velocities at Jakobshavn Isbræ. The changes at these sites are small in both absolute change in speed and percent speedup, but they are distributed over a wide portion of the drainage basin.

Using the change in velocities at the 1800 m a.s.l GPS sites, we are able to estimate a change in ice flux across a transect passing through the five GPS sites far inland of the changes that have occured near the terminus. We assume that changes in ice thickness are small along the transect, confirmed by ATM meausurements, and use estimates of ice thickness from [Bamber and others, 2001]. Changes in ice surface velocity are distributed

using a linear spline interpolant of the data at the five GPS sites. In this region of the ice sheet, we assume that the shallow ice approximation adequately describes ice flow. This implies that for isothermal ice the ratio of depth-averaged speed to surface speed is no less than 0.8. To allow for warmer ice near the bed in addition to possible basal motion we apply a ratio of 0.9. Integrating the change in ice flux due to velocity changes from 1995/96 to 2010/11 along the transect results in a change of 1.9 $km^3 a^{-1}$. While the interior of the ice sheet has demonstrated a response to the changes near the margin, the increase in flux is too small to compensate for the increase in discharge across the grounding line over the same period.

Changes in velocity direction

In addition to changes in velocity magnitude, the slower-flowing ice adjacent to the fast, main channel of Jakobshavn Isbræ is responding to thinning, retreat and speedup with a deflection in velocity direction toward the main channel. The change in flow direction is especially evident from 2000 to 2008 in regions within 50 km of the ice sheet margin, where velocities have rotated by $> 15^\circ$. The deflection of velocities suggests that the ice adjacent to the main channel is not only flowing faster, but is also converging toward the main channel at a greater rate than before initiation of the tidewater retreat, independent of any change in speed.

The ability to resolve changes in velocity direction in the slower-flowing interior of the ice sheet are limited by uncertainties in SAR velocity measurements. Based on stated errors in the SAR velocity components, we estimate angular uncertainties in SAR velocities for the 2000 and 2008 datasets of 1° and 0.5° respectively. At this level of precision, only the larger angular changes nearer the ice-sheet margin are resolvable. Though sparsely distributed, the GPS measured velocities have a greater angular precision, from 0.005° to 0.06° depending on measurement location. Velocities of the 1800 m GPS sites show a pattern similar to, but more subtle than, the pattern of flow redirection toward the main channel occuring in regions covered by the spatially distributed data sets. GPS sites closer to the centerline of the drainage basin show a proportionally larger angular change. This pattern may indicate that the velocities are changing in response to perturbations propagating up the main channel and also from the center of the main channel into the adjacent slower-flowing ice.

Results from measurements and modeling of ice flow along the main channel of Jakob-

shavn Isbræ identified changes in ice surface slope, propagated upstream from the terminus, as the primary driver of the continuing interannual acceleration [Joughin and others, 2012]. In the next section we investigate evidence for changes in surface slope driving the observed speedup and flow redirection of ice adjacent to the main channel.

4.5.2 Evolution of ice surface slope

Changes in degree of surface slope

In addition to thickness changes, changes in ice surface slope have an influence on surface speeds by changing the driving stress. Again assuming shallow ice flow for the ice surrounding the main glacier channel, we derive a relation between changes in slope and surface speed

$$\frac{\Delta u}{u} = n\frac{\Delta S}{S}. \tag{4.4}$$

and for a flow law exponent of 3 we would expect to see a 3 % change in speed in response to a 1 % change in surface slope. Figure 4.4 shows the relative change in ice surface slopes derived from smoothed 1985 and 2008 DEMs resampled to 5 km resolution (to reduce the influence of noise). Comparing the percent speed up from 1985 to 2008 (Fig. 4.2) with the relative change in surface slope (Fig. 4.4) over the same time period, we find that Eqn (4.4) provides a satisfactory explanation for the observed increase of speeds in the slower-flowing ice adjacent to the main glacier channel. Particularly in the region south of the main channel, widespread slope changes from 10–20 % indicate that the pattern of thinning has increased surface slopes, which are directly responsible for the speedup south of the main channel.

Changes in slope aspect

The pattern of thinning has also driven the change in velocity directions from 1985 to 2008. To examine the importance of changes in the direction of ice surface gradients (or slope aspect), we calculate slope aspect from the same smoothed, resampled DEMs used to determine changes in slope magnitude. Changes in ice surface slope aspect (Fig. 4.5) closely match the pattern of velocity direction change from 2000 to 2008 (Fig. 4.3b). The aspect data show that the regions of ice adjacent to the main channel have not only steepened, but surface gradients have rotated toward the fast-flowing main channel by as much as 15°.

Assuming locally-compensated shallow-ice flow, changes in velocity direction vary in direct proportion to the change in slope aspect. To a large degree, this holds true for the data considered, but there is little evidence for changes in velocity direction prior to 2000 (Fig. 4.3a). We hypothesize that this is due to a time delay between the onset of ice surface thinning and rotation of ice surface gradients rather than a delay between gradient rotation and velocity direction; there should be no delay between changes in driving stress and ice flow.

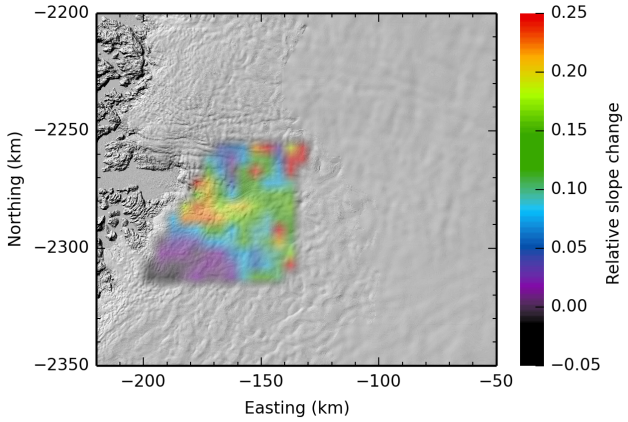

Figure 4.4: Relative difference in surface slope, 1985 to 2008. Typical slopes in the lower reaches of the main glacier channel are 1.5–3.0 °.

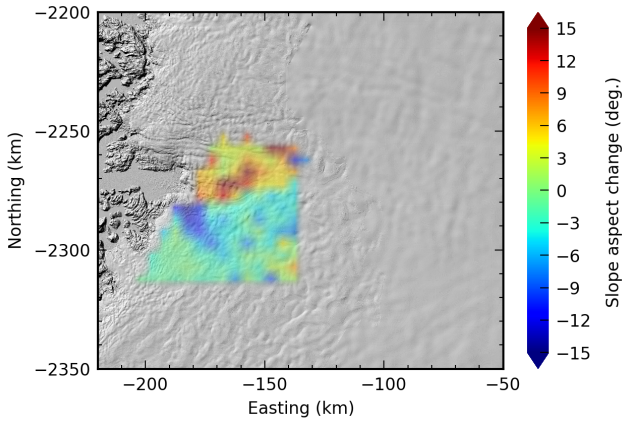

Figure 4.5: Difference in surface slope aspect, 1985 to 2008. Change in surface slope aspect is indicated in degrees. Negative change in aspect indicates a rotation north of east and positive change in apsect is a rotation south of east.

Changes in the ice surface gradient (slope magnitude and aspect) account for the majority of the observed changes in ice flow in the slower-flowing regions of ice adjacent to the main channel of Jakobshavn Isbræ. This suggests that coupling of stresses over distances of more than a few ice thicknesses have little influence on the evolution of the ice surface velocities throughout the drainage basin. One exception occured in the region between the north and south tributaries of Jakobshavn Isbræ where large amounts of thinning have reduced the driving stress. A similar evolution of ice thickness and surface gradients driven by changes along the main fast-flowing channel have propagated far inland and have influenced surface velocities as far as 120 km from the ice-sheet margin.

4.6 Conclusions

The findings of our study quantify additional, basin-wide consequences of the continued speedup and retreat of Jakobshavn Isbræ, initiated in the early 2000s. We measure speedups from 1995/96 to 2010/11 at sites far inland of the ice sheet margin. The magnitude of speedups ranges from 2–17 $\mathrm{m\,a^{-1}}$ or 2–9 %.

In addition to changes in velocity magnitude we document deflections in velocity direction toward the fast-flowing ice across the entire width of the Jakobshavn Isbræ drainage basin. The velocity changes can be explained by an evolution of ice surface gradients; where increases in slope magnitude have driven increases in speed and rotations of slope aspect have resulted in the deflection of velocities toward the main channel.

While there is a measurable response at the inland GPS sites, it is not enough to compensate for the change in flux near the terminus. The change in flux near the terminus is an order of magnitude greater than at the 1800 m GPS sites. However, the velocity changes at sites far inland of the terminus, in a region > 120 km from the calving front and situated above the equilibrium line altitude, indicate a response within two decades to changes initiated at the terminus.

4.7 Acknowledgments

Support for this project was provided by NASA's Cryospheric Sciences Program (NNG06GB49G). Logistical support was provided by CH2M Hill Polar Field Services. We thank R. Cassotto and D. Dellagiustina for their help with the GPS survey.

References

Amundson, J. M., M. A. Fahnestock, M. Truffer, J. Brown, M. P. Lüthi and R. J. Motyka, 2010. Ice mélange dynamics and implications for terminus stability, Jakobshavn Isbræ, Greenland, *J. Geophys. Res.*, **115**(F1).

Bamber, J. L., R. L. Layberry and S. P. Gogineni, 2001. A new ice thickness and bed data set for the Greenland ice sheet 1. Measurement, data reduction, and errors, *J. Geophys. Res.*, **106**(D24), 33773–33780.

van den Broeke, M., J. L. Bamber, J. Ettema, E. Rignot, E. Schrama, W. J. van de Berg, E. van Meijgaard, I. Velicogna and B. Wouters, 2009. Partitioning recent Greenland mass loss., *Science*, **326**(5955), 984–6.

Chen, G., 1999. GPS kinematic positioning for the airborne laser altimetry at Long Valley, California, (Phd thesis, Massachussets Institute of Technology).

Holland, D. M., R. H. Thomas, B. de Young, M. H. Ribergaard and B. Lyberth, 2008. Acceleration of Jakobshavn Isbræ triggered by warm subsurface ocean waters, *Nature Geosci.*, **1**(10), 659–664.

Joughin, I., W. Abdalati and M. A. Fahnestock, 2004. Large fluctuations in speed on Greenland's Jakobshavn Isbræ glacier, *Nature*, **432**(7017), 608–610.

Joughin, I., B. E. Smith, I. M. Howat, D. Floricioiu, R. B. Alley, M. Truffer and M. A. Fahnestock, 2012. Seasonal to decadal scale variations in the surface velocity of Jakobshavn Isbræ, Greenland: Observation and model-based analysis, *J. Geophys. Res.*, **117**(F2), 1–20.

Joughin, I., B. E. Smith, I. M. Howat, T. A. Scambos and T. Moon, 2010. Greenland flow variability from ice-sheet-wide velocity mapping, *J. Glaciol.*, **56**(197), 415–430.

Joughin, I., I. M. Howat, M. A. Fahnestock, B. E. Smith, W. Krabill, R. B. Alley, H. Stern and M. Truffer, 2008. Continued evolution of Jakobshavn Isbræ following its rapid speedup, *J. Geophys. Res.*, **113**(F4).

Joughin, I., B. E. Smith, I. M. Howat and T. A. Scambos, 2010. MEaSUREs Greenland ice velocity map from InSAR data.

Korona, J., E. Berthier, M. Bernard, F. Rémy and E. Thouvenot, 2009. SPIRIT. SPOT 5 stereoscopic survey of Polar Ice: reference images and topographies during the fourth International Polar Year (2007–2009), *ISPRS J. Photogramm. Rem. Sens.*, **64**(2), 204–212.

Luckman, A. and T. Murray, 2005. Seasonal variation in velocity before retreat of Jakobshavn Isbræ, Greenland, *Geophys. Res. Lett.*, **32**(8), 1–4.

Moon, T., I. Joughin, B. E. Smith and I. M. Howat, 2012. 21st-Century evolution of Greenland outlet glacier velocities, *Science*, **693**, 576–578.

Motyka, R. J., M. A. Fahnestock and M. Truffer, 2010. Volume change of Jakobshavn Isbræ, West Greenland 1985–1997–2007, *J. Glaciol.*, **56**(198), 635–646.

Motyka, R. J., M. Truffer, M. A. Fahnestock, J. Mortensen, S. Rysgaard and I. M. Howat, 2011. Submarine melting of the 1985 Jakobshavn Isbræ floating tongue and the triggering of the current retreat, *J. Geophys. Res.*, **116**(F1), 1–17.

Nick, F. M., A. Vieli, M. L. Andersen, I. Joughin, A. Payne, T. L. Edwards, F. Pattyn and R. S. W. van de Wal, 2013. Future sea-level rise from GreenlandÕs main outlet glaciers in a warming climate, *Nature*, **497**(7448), 235–238.

Nick, F. M., A. Vieli, I. M. Howat and I. Joughin, 2009. Large-scale changes in Greenland outlet glacier dynamics triggered at the terminus, *Nature Geosci.*, **2**(2), 110–114.

Pfeffer, W. T., J. T. Harper and S. O'Neel, 2008. Kinematic constraints on glacier contributions to 21st-century sea-level rise., *Science*, **321**(5894), 1340–3.

Podlech, S. and A. Weidick, 2004. A catastrophic break-up of the front of Jakobshavn Isbræ, West Greenland, 2002/03, *J. Glaciol.*, **50**(168), 153–154.

Podrasky, D. B., M. Truffer, M. A. Fahnestock, J. M. Amundson, R. K. Cassotto and I. Joughin, 2012. Outlet glacier response to forcing over hourly to interannual timescales, Jakobshavn Isbræ, Greenland, *J. Glaciol.*, **58**(212), 1212–1226.

Pritchard, H. D., R. J. Arthern, D. G. Vaughan and L. A. Edwards, 2009. Extensive dynamic thinning on the margins of the Greenland and Antarctic ice sheets., *Nature*, **461**(7266), 971–5.

Rignot, E. J. and P. Kanagaratnam, 2006. Changes in the velocity structure of the Greenland Ice Sheet., *Science*, **311**(5763), 986–90.

Scambos, T. A., M. J. Dutkiewicz, J. C. Wilson and R. A. Bindschadler, 1992. Application of image cross-correlation to the measurement of glacier velocity using satellite image data, *Remote Sens. of Environ.*, **42**(3), 177–186.

Shepherd, A., and 46 others, 2012. A reconciled estimate of ice-sheet mass balance., *Science*, **338**(6111), 1183–9.

Sohn, H. G., K. C. Jezek and C. J. van der Veen, 1998. Jakobshavn Glacier, west Greenland: 30 years of spaceborne observations, *Geophys. Res. Lett.*, **25**(14), 2699.

Thomas, R., T. Akins, B. Csatho, M. A. Fahnestock, S. P. Gogineni, C. Kim and J. Sonntag, 2000. Mass Balance of the Greenland Ice Sheet at high elevations, *Science*, **289**(5478), 426–428.

Thomas, R., E. Frederick, J. Li, W. Krabill, S. Manizade, J. Paden, J. Sonntag, R. Swift and J. Yungel, 2011. Accelerating ice loss from the fastest Greenland and Antarctic glaciers, *Geophys. Res. Lett.*, **38**(10), 1–6.

Thomas, R. H., 2004. Force-perturbation analysis of recent thinning and acceleration of Jakobshavn Isbræ , Greenland, *J. Glaciol.*, **50**(168), 57–66.

Thomas, R. H., W. Abdalati, E. Frederick, W. B. Krabill, S. Manizade, K. Steffen, 2003. Investigation of surface melting and dynamic thinning on Jakobshavn Isbræ, Greenland, *J. Glaciol.*, **49**(165), 231–239.

Truffer, M. and M. A. Fahnestock, 2007. Climate change. Rethinking ice sheet time scales., *Science*, **315**(5818), 1508–10.

Weidick, A., H. Oerter, N. Reeh, H. H. Thomson and L. Thorning, 1990. The recession of the Inland Ice margin during the Holocene climatic optimum in the Jakobshavn Isfjord area of West Greenland, *Palaeogeogr. Palaeocl.*, **82**, 389–399.

Chapter 5
Conclusions

From the late 1990s to present, the ice flow of Jakobshavn Isbræ, in West Greenland, has been documented with remote sensing techniques. These previous studies have revealed more than a two-fold increase in speed as a result of a rapid tidewater retreat initiated in the early 2000s. The rate of acceleration is closely tied to the mean rate of terminus retreat and speeds have increased at a rate of 4–8 % a^{-1}. Continuing interannual acceleration along the fast-flowing southern tributary is driven by increases in ice surface slope propagated upstream from the terminus.

Higher time resolution measurements of glacier motion presented here show details of glacier motion not resolvable in the remote sensing record, and reveal details about velocity variations on seasonal to hourly timescales. Superimposed on the year to year trend of increasing speed are seasonal velocity variations amounting to 10 % of yearly mean speed or less. Seasonal advance and retreat of the terminus is the primary driver of the seasonal velocity variations along the fast-flowing southern tributary. However, surface meltwater forcing during summer months has an influence on the seasonal evolution of glacier speeds as well. Each spring the steady speed-up, initiated by the start of calving and ensuing terminus retreat, is interrupted by more variable glacier flow resulting from fluctuations in surface melt. The relationship between rates of surface meltwater input and glacier motion is not simple and results in pairs of speed-ups and slowdowns. Often the slowdowns are of longer duration than the preceding speed-ups causing an overall reduction in flow speed due to a variable supply of surface meltwater. High-rate GPS measurements of glacier motion reveal that the interannual acceleration was interrupted in 2007 by a series of slow-down events which cancelled the expected acceleration between 2007 and 2008. These results show that proposed mechanisms for a positive feedback between outlet glacier speed and increased surface melt are dubious at best.

In addition to changes occurring at the glacier terminus on decadal and seasonal timescales, there are sources of forcing at the front which take place over much shorter timescales. Ocean tidal forcing and the effects of iceberg calving influence glacier flow over timescales of hours to days. Findings from a two-week campaign to record the motion of the lower 5 km of the glacier using GPS and automatic theodolite measurements constrains the length of the glacier region that responds instantaneously to changes in stress near the ice front. The influence of tidal forcing on Jakobshavn Isbræ decays rapidly with distance

from the terminus, with an *e*-folding length of 2 km. Significant response to iceberg calving and ocean tides is limited to the lower 10 km of the glacier. These results suggest that the length scale of longitudinal stress coupling is on the order of a few ice thicknesses. Therefore, the observed changes in flow speed at locations further upstream can only be due to local changes in basal lubrication or driving stress.

An examination of ice surface velocities in the Jakobshavn Isbræ drainage basin from 1985 to 2011 reveals that the ice adjacent to the southern tributary has not only increased in speed but the direction of velocities have consistently rotated toward the channel of fast flow. The pattern of increasing speeds and converging ice flow are observed more than 100 km inland of the ice-sheet margin. Basin-wide changes in ice surface velocities are reconciled with the evolution of the ice surface, both elevation and slope. Using a pair of DEMs, changes in ice thickness and surface gradient were computed between 1985 and 2008. The effects of dynamic thinning on the southern tributary in excess of 100 m and commensurate increases in flow speed have propagated to the surrounding, slower-flowing regions of the drainage basin where surface slopes have steepened. Increases in ice surface slope have increased the driving stress, explaining the observed increases in surface speed in affected regions. Furthermore, results of the DEM analysis show that ice surface slope aspect has consistently rotated toward the southern tributary, providing a mechanism for the observed rotation of velocities toward the fast-flowing channel.

Wide spread changes in velocity magnitude and direction in regions far from the fast-flowing main channel show that the ice sheet is responding to the retreat of Jakobshavn Isbræ on a timescale that is far shorter than traditionally thought possible. A measured increase in ice flux along a transect $\sim$120 km inland of the ice-sheet margin along with more convergent flow of slower-flowing ice adjacent to the southern tributary demonstrate that the ice sheet has quickly reacted to the changes initiated at the glacier terminus by feeding more ice to the main channel within the time of two decades.

Outlook

It remains to be seen how far the tidewater retreat of Jakobshavn Isbræ will proceed, but the progression will be controlled by glacier geometry, the shape of the deep glacier channel beneath the southern tributary and the maximum rate at which ice can be evacuated past the grounding line. Due to the complex relationship between surface meltwater forcing and glacier surface speed, projected increases in ice-sheet surface melt are unlikely to

have a significant effect on rates of ice discharge during the continuing retreat. Rather, the velocity response of inland ice to the initiation of the large-scale tidewater retreat is being driven by changes in glacier geometry propagated upstream from the terminus. The stready rate of glacier retreat from the 2000s to present suggests that the currently observed rate of ice discharge from Jakobshavn Isbræ will almost certainly persist into the next decade or longer.

Appendix A
Error estimates and propagation

A.1 Tidal analysis error analysis

The χ^2 difference between measured and modeled (tidal response model) positions is given by

$$\chi^2 = \sum_{i=1}^{n} \frac{(y_i - f_i)^2}{\sigma_i{}^2}, \tag{A.1}$$

where y_i are measured positions and

$$f_i(t) = \Lambda H(t - \tau) \tag{A.2}$$

are modeled positions based on a tidal admittance, Λ, and time offset, τ, modifying tidal heights, H. The 1σ contour of χ^2 is given by

$$\chi^2 = \chi^2{}_{\min} + 1. \tag{A.3}$$

Values of model parameters Λ and τ satisfying the condition

$$\chi^2 < \chi^2{}_{\min} + 1 \tag{A.4}$$

define a range of admittances and time offsets within a 1σ confidence interval.

A.2 Tidal decay model error analysis

Begin with the equation modeling the decay of tidal admittance with distance from the glacier terminus,

$$\Lambda(D) = \Lambda_0 e^{-\beta D}. \tag{A.5}$$

Equation (A.5) can be linearized and rewritten as

$$\ln \Lambda = \ln \Lambda_0 - \beta D, \tag{A.6}$$

The χ^2 difference between calculated and modeled admittances is given by

$$\chi^2 = \sum_{i=1}^{n} \frac{(y_i - (A - \beta D_i))^2}{\sigma_i{}^2}, \tag{A.7}$$

where we write $\ln\Lambda$ as y_i and $\ln\Lambda_0$ as A. Differentiating eqn. (A.7) w.r.t. A and b, setting the result to zero and assuming $\sigma_i = \sigma$ gives

$$\frac{\partial\chi^2}{\partial A} = -\frac{2}{\sigma}\sum_{i=1}^{n} y_i - (\hat{A} - \hat{\beta}D_i) = 0, \tag{A.8}$$

$$\frac{\partial\chi^2}{\partial \beta} = \frac{2}{\sigma}\sum_{i=1}^{n} D_i(y_i - (\hat{A} - \hat{\beta}D_i)) = 0; \tag{A.9}$$

where

$$\bar{D} = \frac{1}{n}\sum_{i=1}^{n} D_i \tag{A.10}$$

and

$$\bar{y} = \frac{1}{n}\sum_{i=1}^{n} y_i. \tag{A.11}$$

From eqn. (A.8)

$$\bar{y} = \hat{A} - \hat{\beta}\bar{D} \tag{A.12}$$

and from eqn. (A.9)

$$\overline{yD} = \hat{A}\bar{D} - \hat{\beta}\overline{D^2}. \tag{A.13}$$

Solve eqn. (A.12) and substitute into eqn. (A.13) to solve for $\hat{b}$,

$$\hat{\beta} = \sum_{i=1}^{n} \frac{y_i\bar{D} - y_i D_i}{n(\overline{D^2} - \bar{D}^2)}. \tag{A.14}$$

Differentiate eqn. (A.15)

$$\frac{\partial\hat{\beta}}{\partial y_i} = \frac{\bar{D} - D_i}{n(\overline{D^2} - \bar{D}^2)}. \tag{A.15}$$

and apply the rules of standard error propagation

$$\delta_{\hat{\beta}}{}^2 = \sum_{i=1}^{n} \left(\frac{\bar{D} - D_i}{n(\overline{D^2} - \bar{D}^2)}\right)^2 \delta_{D_i}{}^2, \tag{A.16}$$

or

$$\delta_{\hat{\beta}}{}^2 = \frac{\delta_{D_i}{}^2}{n(\overline{D^2} - \bar{D}^2)}. \tag{A.17}$$

A.3 Calving model error analysis

Chi-squared of 2nd order polynomial fit:

$$\chi^2 = \sum_{i=1}^{n} \frac{(y_i - (ax_i{}^2 + bx_i + c))^2}{\sigma_i{}^2}. \tag{A.18}$$

Differentiating w.r.t. a, b, and c, setting results to zero and assuming $\sigma_i = \sigma$ gives

$$\frac{\partial \chi^2}{\partial a} = -\frac{2}{\sigma}\sum_{i=1}^{n} {x_i}^2(y_i - (\hat{a}{x_i}^2 + \hat{b}x_i + \hat{c})) = 0, \tag{A.19}$$

$$\frac{\partial \chi^2}{\partial b} = -\frac{2}{\sigma}\sum_{i=1}^{n} x_i(y_i - (\hat{a}{x_i}^2 + \hat{b}x_i + \hat{c})) = 0, \tag{A.20}$$

$$\frac{\partial \chi^2}{\partial c} = -\frac{2}{\sigma}\sum_{i=1}^{n} y_i - (\hat{a}{x_i}^2 + \hat{b}x_i + \hat{c}) = 0; \tag{A.21}$$

where

$$\bar{x} = \frac{1}{n}\sum_{i=1}^{n} x_i \tag{A.22}$$

and

$$\bar{y} = \frac{1}{n}\sum_{i=1}^{n} y_i. \tag{A.23}$$

A.3.1 Acceleration uncertainty

Solve eqn. (A.19) for $\hat{c}$

$$\hat{c} = \frac{\overline{x^2 y}}{\overline{x^2}} - \hat{a}\frac{\overline{x^4}}{\overline{x^2}} - \hat{b}\frac{\overline{x^3}}{\overline{x^2}} \tag{A.24}$$

and substitute into eqn. (A.21)

$$\hat{b} = \frac{\bar{y} - \hat{a}\overline{x^2} - \hat{a}\frac{\overline{x^4}}{\overline{x^2}} - \frac{\overline{x^2 y}}{\overline{x^2}}}{\bar{x} + \frac{\overline{x^3}}{\overline{x^2}}}. \tag{A.25}$$

Now substitute eqns. (A.24) and (A.25) into eqn. (A.20)

$$\overline{xy} - \frac{\overline{x^2}\bar{y} - \overline{x^2 y}}{\bar{x} + \frac{\overline{x^3}}{\overline{x^2}}} + \frac{\bar{x}\bar{y} - \overline{x^2 y}\frac{\bar{x}}{\overline{x^2}}}{\bar{x} + \frac{\overline{x^3}}{\overline{x^2}}}\left(\frac{\overline{x^3}}{\overline{x^2}}\right) = \hat{a}\overline{x^3} - \hat{a}\bar{x}\frac{\overline{x^4}}{\overline{x^2}} + \hat{a}\frac{\overline{x^2} + \frac{\overline{x^4}}{\overline{x^2}}}{\bar{x} + \frac{\overline{x^3}}{\overline{x^2}}}\left(\overline{x^2} + \bar{x}\frac{\overline{x^3}}{\overline{x^2}}\right) \tag{A.26}$$

and write as a function of y_i,

$$\hat{a} = \sum_{i=1}^{n} \frac{x_i y_i - \frac{\overline{x^2}y_i - {x_i}^2 y_i + \bar{x}\frac{\overline{x^3}}{\overline{x^2}}y_i - \frac{\bar{x}\overline{x^3}}{(\overline{x^2})^2}{x_i}^2 y_i}{\bar{x} + \frac{\overline{x^3}}{\overline{x^2}}}}{n\left[\overline{x^3} - \bar{x}\frac{\overline{x^4}}{\overline{x^2}} + \frac{\overline{x^2} + \frac{\overline{x^4}}{\overline{x^2}}}{\bar{x} + \frac{\overline{x^3}}{\overline{x^2}}}\left(\overline{x^2} + \bar{x}\frac{\overline{x^3}}{\overline{x^2}}\right)\right]}. \tag{A.27}$$

Differentiate eqn. (A.27) w.r.t. y_i

$$\frac{\partial \hat{a}}{\partial y_i} = \frac{x_i - \frac{\overline{x^2} - {x_i}^2 + \bar{x}\frac{\overline{x^3}}{\overline{x^2}}\left(1 - \frac{{x_i}^2}{\overline{x^2}}\right)}{\bar{x} + \frac{\overline{x^3}}{\overline{x^2}}}}{n\left[\overline{x^3} - \bar{x}\frac{\overline{x^4}}{\overline{x^2}} + \frac{\overline{x^2} + \frac{\overline{x^4}}{\overline{x^2}}}{\bar{x} + \frac{\overline{x^3}}{\overline{x^2}}}\left(\overline{x^2} + \bar{x}\frac{\overline{x^3}}{\overline{x^2}}\right)\right]}, \tag{A.28}$$

and applying standard propagation of errors based on error, δ_{y_i}, in y_i gives:

$$\delta_{\hat{a}}{}^2 = \sum_{i=1}^{n} \frac{\left[x_i - \frac{\overline{x^2} - {x_i}^2 + \bar{x}\frac{\overline{x^3}}{\overline{x^2}}\left(1 - \frac{{x_i}^2}{\overline{x^2}}\right)}{\bar{x} + \frac{\overline{x^3}}{\overline{x^2}}} \right]^2}{n^2 \left[\overline{x^3} - \bar{x}\frac{\overline{x^4}}{\overline{x^2}} + \frac{\overline{x^2} + \frac{\overline{x^4}}{\overline{x^2}}}{\bar{x} + \frac{\overline{x^3}}{\overline{x^2}}} \left(\overline{x^2} + \bar{x}\frac{\overline{x^3}}{\overline{x^2}} \right) \right]^2} \delta_{y_i}{}^2, \tag{A.29}$$

or,

$$\delta_{\hat{a}}{}^2 = \frac{\overline{x^4} + 2\bar{x}\overline{x^3} - \bar{x}^2\overline{x^2} - (\overline{x^2})^2 + 2\frac{(\overline{x^3})^2}{\overline{x^2}} + \bar{x}^2\frac{(\overline{x^3})^2}{(\overline{x^2})^2}\left(\frac{\overline{x^4}}{(\overline{x^2})^2} - 1\right)}{n\left[\left(\bar{x} + \frac{\overline{x^3}}{\overline{x^2}}\right)\left(\overline{x^3} - \bar{x}\frac{\overline{x^4}}{\overline{x^2}} + \frac{\overline{x^2} + \frac{\overline{x^4}}{\overline{x^2}}}{\bar{x} + \frac{\overline{x^3}}{\overline{x^2}}}\left(\overline{x^2} + \bar{x}\frac{\overline{x^3}}{\overline{x^2}}\right)\right)\right]^2} \delta_{y_i}{}^2. \tag{A.30}$$

A.3.2 Speed uncertainty

Solve eqn. (A.25) for $\hat{a}$,

$$\hat{a} = \frac{\bar{y} + \hat{b}\left(\frac{\overline{x^3}}{\overline{x^2}} - \bar{x}\right)}{\overline{x^2} - \frac{\overline{x^4}}{\overline{x^2}}}, \tag{A.31}$$

and substitute into eqn. (A.21) along with eqn. (A.24),

$$\frac{\overline{x^2 y}}{\overline{x^2}} = \hat{b}\left(\bar{x} - \frac{\overline{x^3}}{\overline{x^2}}\right) + \hat{b}\frac{\overline{x^3} - \bar{x}\overline{x^2} - \left(\frac{\overline{x^3}}{\overline{x^2}} - \bar{x}\right)\frac{\overline{x^4}}{\overline{x^2}}}{\frac{\overline{x^4}}{\overline{x^2}} - \overline{x^2}} \tag{A.32}$$

Solve eqn. (A.32) for $\hat{b}$ and write as a function of y_i:

$$\hat{b} = \sum_{i=1}^{n} \frac{\frac{{x_i}^2 y_i}{\overline{x^2}}}{n\left[\bar{x} - \frac{\overline{x^3}}{\overline{x^2}} + \frac{\overline{x^3} - \bar{x}\overline{x^2} - \left(\frac{\overline{x^3}}{\overline{x^2}} - \bar{x}\right)\frac{\overline{x^4}}{\overline{x^2}}}{\frac{\overline{x^4}}{\overline{x^2}} - \overline{x^2}}\right]} \tag{A.33}$$

Differentiate eqn. (A.33) w.r.t. y_i

$$\frac{\partial \hat{b}}{\partial y_i} = \frac{\frac{{x_i}^2}{\overline{x^2}}}{n\left[\bar{x} - \frac{\overline{x^3}}{\overline{x^2}} + \frac{\overline{x^3} - \bar{x}\overline{x^2} - \left(\frac{\overline{x^3}}{\overline{x^2}} - \bar{x}\right)\frac{\overline{x^4}}{\overline{x^2}}}{\frac{\overline{x^4}}{\overline{x^2}} - \overline{x^2}}\right]}, \tag{A.34}$$

and applying standard propagation of errors based on error, δ_{y_i}, in y_i gives:

$$\delta_{\hat{b}}{}^2 = \sum_{i=1}^{n} \frac{\left(\frac{{x_i}^2}{\overline{x^2}}\right)^2}{n^2\left[\bar{x} - \frac{\overline{x^3}}{\overline{x^2}} + \frac{\overline{x^3} - \bar{x}\overline{x^2} - \left(\frac{\overline{x^3}}{\overline{x^2}} - \bar{x}\right)\frac{\overline{x^4}}{\overline{x^2}}}{\frac{\overline{x^4}}{\overline{x^2}} - \overline{x^2}}\right]^2} \delta_{y_i}{}^2, \tag{A.35}$$

or

$$\delta_{\hat{b}}^2 = \frac{\overline{x^4}\delta_{y_i}{}^2}{n\left[\bar{x}\overline{x^2} - \overline{x^3} + \frac{\overline{x^2}\,\overline{x^3} - \bar{x}(\overline{x^2})^2 - \left(\frac{\overline{x^3}}{\overline{x^2}} - \bar{x}\right)\overline{x^4}}{\frac{\overline{x^4}}{\overline{x^2}} - \overline{x^2}}\right]^2}. \tag{A.36}$$

A.3.3 Error propagation through strain rate correction

$$\frac{\partial u}{\partial t} = 2a - u_0\dot{\varepsilon}_{\xi,0} \tag{A.37}$$

Applying standard propagation of error to eqn. (A.37) gives an uncertainty in the estimate of acceleration based on the errors in strain rate, $\dot{\varepsilon}_{\xi,0}$, and the term a and the initial speed, u_0, from the calving model:

$$\delta\left(\frac{\partial u}{\partial t}\right) = \sqrt{(2\delta a)^2 + (\dot{\varepsilon}_{\xi,0}\delta u_0)^2 + (u_0\delta\dot{\varepsilon}_{\xi,0})^2} \tag{A.38}$$